Anna-Louise Meyer Wangen

A case study of rotor sails for electric pendulum ferries

Master's thesis in Marine Technology
Supervisor: Sverre Steen
Co-supervisor: Jarle V. Kramer
February 2024

Master's thesis

NTNU
Norwegian University of
Science and Technology

Anna-Louise Meyer Wangen

A case study of rotor sails for electric pendulum ferries

Master's thesis in Marine Technology
Supervisor: Sverre Steen
Co-supervisor: Jarle V. Kramer
February 2024

Norwegian University of Science and Technology
Faculty of Engineering
Department of Marine Technology

NTNU
Norwegian University of
Science and Technology

NTNU
Kunnskap for en bedre verden

A case study of rotor sails for electric pendulum ferries

Author:
Anna-Louise M. Wangen

19th February 2024

NTNU Trondheim
Norwegian University of Science and Technology
Department of Marine Technology

MASTER THESIS IN MARINE TECHNOLOGY

AUTUMN 2023

FOR

Anna-Louise Meyer Wangen

A case study of rotor sails for electric pendulum ferries

Due to government regulations, double-ended road ferries in Norway are quickly switching from fossil fuels to batteries as their primary energy storage. This is mainly possible due to relatively short crossing distances and high-power charging on each end of the route. On one hand, an electric-powered ferry has low energy-related costs, as electric energy can be bought at a lower price than chemical fuels such as diesel or hydrogen. On the other hand, this solution requires the investment in large battery packs, which is expensive. The battery needs more energy capacity than required for a single trip, even if it can be recharged at both ends. This is, in part, to ensure a long lifetime. Every charging cycle reduces the battery's total capacity by a small amount due to some irreversible chemical reactions. One solution to this problem is to let the battery's full capacity be significantly larger than the energy required between each charge cycle, as this reduces chemical wear and tear during charging. This is, however, an expensive solution.

Suppose the total energy during one trip can be reduced. In that case, this can lead to smaller and cheaper battery packs with the same lifetime or a longer lifetime with the same battery capacity. In addition, although electric energy is more affordable than many other alternatives, it can still represent a significant cost for ship operators. Therefore, finding ways to reduce the energy requirement for an electric ferry is essential.

Wind-assisted propulsion – also known as modern sail technologies – is actively being explored for both deep- and short-sea shipping to reduce fuel costs and emissions. Several technologies are available on the market, but rotor sails are currently the dominating type. This project will explore whether wind propulsion technology can make economic sense for pendulum ferries. This should be done through a case study that explores the potential benefits of rotor sails on a pendulum ferry route in Norway, assuming it is operated with battery power. A hypothesis is that many ferry routes will have good wind conditions, as they typically are fjord crossings, where the wind tend to blow along the fjord. If this is the case, side wind conditions will have a high probability for the road ferries, which is ideal for wind propulsion in general and in particular for rotor sails.

The overall objective of the thesis is to investigate the potential energy saving that can be obtained by mounting wind propulsion devices on a typically road ferry crossing a Norwegian fjord. It is suggested to address the objective through a case study. The candidate should make the necessary choices and assumptions to implement the case study.

The following should be included in the master thesis:
- A literature review that describes the state of the art concerning methods for estimating energy savings due to modern wind propulsion systems for commercial ships.

- A description of the ferry route, operational profile, and ship used in the case study. This should be based on an existing ferry crossing as much as possible. The candidate should make reasonable assumptions in cases where there is a lack of technical data for the specific case chosen for the project.
- An exploration of data sources that can give accurate information about the wind conditions locally in a Norwegian fjord.
- A software implementation of a route simulation for an electric ferry partly powered by rotor sails. This might very well be based on existing theory and tools. The underlying theory and method shall be adequately described in the thesis. Simplifications and assumptions in the analysis should be argued based on the details of the specific case.
- An interpretation of the energy savings due to rotor sails in the context of the ferry operation. This will require a high-level analysis of the overall energy consumption of the ferry.
- A high-level evaluation of how the battery's lifetime will change with lower energy consumption during regular operation due to the rotor sails.
- A high-level evaluation of the total economic savings due to rotor sails, including savings in energy cost and savings due to the (potentially) longer lifetime of the battery.

The master thesis shall describe the theories applied, approximations and assumptions made, the implementation, the tuning and validation, and the candidate's contribution to resolving the problems within the scope of the thesis work. Theories and conclusions should be based on mathematical derivations and logical reasoning identifying the various steps in the deduction. The candidate should utilize the existing possibilities for obtaining relevant literature and is recommended to use the library actively.

The thesis should be organized rationally to expose results, assessments, and conclusions. The text should be brief and to the point, with clear language. Telegraphic language should be avoided.

The following elements should be included: A text defining the scope, a preface, a list of contents, a summary, the main body of the thesis, the conclusions with recommendations for further work, a list of symbols and acronyms, references, and (optional) appendices. All figures, tables, and equations shall be enumerated.

The original contribution of the candidate and material taken from other sources shall be clearly defined. Work from other sources shall be properly referenced using an acknowledged referencing system.

The thesis shall be submitted electronically in pdf in Inspera:

- Signed by the candidate

- The text defining the scope included, signed by the supervisor (this text)

- Other electronic appendages, such as source code or input files, might be included in the submission. Separately submitted appendices (files) must be referred to in the main text to be considered in the evaluation.

- In case computer programs have been made as part of the thesis work, the source code shall be included. In case of experimental work, the experimental results shall be included in a suitable electronic format.

NTNU Trondheim
Norwegian University of Science and Technology
Department of Marine Technology

Supervisor   : Professor Sverre Steen
Co-supervisor : Jarle V. Kramer
Start   : 15.09.2023
Deadline   : 19.02.2024 at 23:59

Trondheim, 15.09.2023

Sverre Steen, Supervisor

Abstract

As the global shipping industry attempts to limit its environmental impact, the norwegian government has set the goal of limiting the emissions of greenhouse gases by 50% by 2030 for domestic shipping and fishing. In response to this imperative, various energy-efficient technologies are being explored, including Flettner rotors. To evaluate the potential of Flettner rotors as a sustainable solution, this thesis conducts a case study analysis on a battery-electric ferry operating along the Flakk-Rørvik route in Trondheimsfjorden, Norway.

The study investigated two main objectives 1) savings in propeller power and 2) reductions in Depth of Discharge (DoD), by changing the rotor size configurations. The ferry was equipped with two Flettner rotors, and three rotor size configurations were examined based on technical information from Norsepower (2022).The objectives were investigated through a case analysis using weather data measured from sensors located at each side of the ferry connection. The case was conducted based on wind data measured during a timeframe of one year. During this period, one of the sensors had significant downtime. The timeframe for the dowtime was filtered out from both sensors to ensure equivalent data basis when analysing the results. However, to investigate the potential of the Flettner rotors also during the timeframe of the downtime, a second analysis was performed using all available data from the sensor that did not have any downtime.

The resistance of the ferry used in the case study was derived through a speed-power curve, with the assumption of $\eta_D = 0.7$, from a CFD analysis performed on the hull provided by the ship operator of the ferry. The thrust and power from the Flettner rotors were calculated based on semi-empirical polynomials for the lift-, drag- and power coefficients from Tillig and Ringsberg (2020).

The analysis of different rotor size configurations revealed an interesting trend in power generation efficiency. Based on the wind data that did not have any downtime it was seen that increasing rotor size led to significant power generation gains, with an $\approx 19\%$ increase observed when transitioning from the smallest (4m×18m) to the medium-sized rotor (4m×24m). However, the incremental gain diminished as rotor size further increased, suggesting a point of diminishing returns.

The study also demonstrated reductions in DoD across all rotor size configurations, resulting in notable battery cycle savings. Based on the wind data from the sensor that did not have any downtime, the maximum change of DoD for the rotor of size 4m×24m was -1.460%, i.e., by equipping the ferry with two 4m×24m Flettner rotors, the DoD diminished from 11.17% to 9.71%. This saves $\approx$12 415 cycles of the battery's cycle life. This further means that the battery can complete $\approx$12 415 full charge-discharge cycles more when equipped with with the Flettner rotors than without.

Sammendrag

Ettersom den globale skipsfartsindustrien forsøker å begrense sin miljøpåvirkning, har den norske regjeringen satt et mål om å redusere utslipp av klimagasser med 50 % innen 2030 for innenriks sjøfart og fiske. Som svar på dette imperativet utforskes ulike energieffektive teknologier, inkludert Flettner-rotorer. For å evaluere potensialet til Flettner-rotorer som en bærekraftig løsning, gjennomfører denne avhandlingen et case studie på en batterielektrisk ferge som opererer langs ruten Flakk-Rørvik i Trondheimsfjorden, Norge.

Studiet har hatt to hovedmål som fokus: 1) besparelser i propellkraft og 2) reduksjon i batteriets utladningsdybde (DoD), ved å endre rotorstørrelseskonfigurasjoner. Fergen i case studiet var utstyrt med to Flettner-rotorer, og tre ulike rotorstørrelseskonfigurasjoner ble undersøkt basert på teknisk informasjon fra Norsepower (2022). De to hovedmålene ble undersøkt gjennom en analyse av case studie der hovedberegningene ble utført ved bruk av værdata målt fra sensorer plassert på hver side av fergeforbindelsen. Vindmålingene brukt i caset hadde en tidsramme på 1 år. I løpet av denne perioden hadde en av sensorene betydelig nedetid. Tidsrammen for nedetiden ble filtrert ut fra begge sensorer for å sikre ekvivalent datagrunnlag når resultatene ble analysert. Imidlertid, for å undersøke potensialet til Flettner-rotorene også i løpet av nedetidsperioden, ble en ytterligere analyse utført ved bruk av all tilgjengelig data fra sensoren som ikke hadde noen nedetid.

Motstanden til fergen som ble brukt i case studiet ble utledet gjennom en speed-power kurve fra en CFD-analyse utført på skroget levert av fergens operatør, med antagelsen $\eta_D = 0.7$. Skyvekraften og effekten fra Flettner-rotorene ble beregnet basert på semi-empiriske polynomer for løft-, drag- og effekt-koeffisienter fra Tillig and Ringsberg (2020).

Analysen av forskjellige rotorstørrelseskonfigurasjoner avdekket en interessant trend for effekten generert fra Flettner rotorene. Basert på vinddata fra sensoren som ikke hadde noen nedetid, ble det observert at økning av rotorstørrelse førte til betydelige gevinster i effekten generert, med en økning på ca. 19% ved overgang fra den minste (4m x 18m) til den mellomstore rotoren (4m x 24m). Imidlertid avtok den inkrementelle gevinsten etter hvert som rotorstørrelsen økte ytterligere, noe som antyder et punkt med avtagende avkastning i forhold til Flettner rotorenes evne til generering av effekt.

Studien viste også reduksjoner i DoD over alle rotorstørrelseskonfigurasjoner, noe som resulterte i bemerkelsesverdige besparelser i batterisyklus. Basert på vinddata fra sensoren som ikke hadde noen nedetid, var den maksimale endringen av DoD for rotoren av størrelse 4m x 24m -1,460%, dvs. ved å utstyre fergen med to 4m x 24m Flettner-rotorer, ble DoD redusert fra 11,17% til 9,71%. Dette sparer ca. 12 415 sykluser av batteriets syklusliv. Dette betyr videre at batteriet kan fullføre ca. 12 415 fullstendige lade-utladningssykluser mer når fergen er utstyrt med de to Flettner-rotorene enn uten.

Preface

This thesis marks the completion of my Master of Science in Marine Technology, with a specialization in Marine Hydrodynamics. The research was conducted during the fall/winter semester of 2022 and 2023 at the Norwegian University of Science and Technology (NTNU) in Trondheim.

First off, I want to say a huge thank you to my supervisors, Professor Sverre Steen and Jarle V. Kramer from the Department of Marine Technology. Their constant support and advice were crucial, especially when I had to switch my thesis topic. I'm truly thankful for their patience and for all the meetings we had that helped steer this work in the right direction.

Diving into marine hydrodynamics, aerodynamics, and programming has been a challenging but incredibly rewarding part of my final semester. This work pushed me to expand my knowledge and fueled my curiosity in a wide range of engineering fields.

I would like to express my gratitude to Emlyn John Davies at SINTEF OceanLab for his indispensable assistance with wind data measurements and his insightful explanations regarding sensor interpretation and downtime analysis. A profound thank you is also due to Fabian Thies (also known as Fabian Tillig) for his help in validation of the Flettner rotor model. Their expertise and generous support played a pivotal role in the success of my research.

Going through a challenging study program really shows you how much you need good friends to keep you going. I can't thank my friends at Marin Teknikk enough for all the great times and laughs throughout the five years. Especially my office mates Maria Voldsund, Marie Kongshaug, and Hanna Bjørshol. They made the hard days easier and the good days great. I wouldn't have made it through without them.

Last but not least, a huge thank you to my family and parents, Mona E. Meyer and Magnus Wangen, for everything. I especially want to thank my dad for his endless support and advice throughout my five years at NTNU. Your wisdom and encouragement have been incredibly important to me.

Anna-Louise Meyer Wangen
19.02.2024, Trondheim

Nomenclature

ρ_{air} Air density

ρ_w Water density

τ Shear stress

Nomenclature

ΔC_F Coefficient for added resistance due to hull roughness

A Projected area

A_F Frontal projected area

A_L Lateral projected area

A_{sail} Projected sail area

B Vessel breadth

C_B Block coefficient

C_D Drag coefficient

c_D Sail drag coefficient

C_F Frictional resistance coefficient

C_H Hull-shape factor

C_L Lift force coefficient

C_M Midspan coefficient

c_P Power coefficient

C_R Residual resistance coefficient

C_T Total resistance coefficient

c_T Sail thrust coefficient

C_W Wave-making resistance coefficient

C_{air} Air resistance coefficient

$C_{R,FnKrit}$ Froude critical residual resistance coefficient, Hollenbach

$C_{R,std}$ Standard residual resistance coefficient, Hollenbach

CD_l Longitudinal resistance coefficient, Blendermann

$CD_{l,AF}$ Longitudinal resistance coefficient with respect to the frontal projected area of the vessel, Blendermann

CX_{AF} Longitudinal force coefficient

CY Side force coefficient

D Drag force

D Flettner rotor diameter

d_e Diameter of end plate

D_P Diameter propeller

F_f Frictional resistance force

F_n Froude number

$F_{n,Krit}$ Critical Froude number, Hollenbach

$F_{n,max}$ Maximum Froude number, Hollenbach

g Gravitational acceleration

H Flettner rotor height

H Hull roughness

k Form factor

k_c Roughness height of an equivalent sand grain

k_s^+ Roughness Reynolds number

k_{rough}^+ Upper band of the transitional rough regime

k_{smooth}^+ Lower band of the transitional rough regime

L' Lift per unit span

L Lenght of ship hull

L Lift force

L_{Fn} Froude lenght, Hollenbach

L_{oa} Length overall

L_{os} Length over surface, Hollenbach

L_{pp} Length between perpendiculars

L_{wl} Length of waterline

N_{boss} Amount of bossings

N_{boss} Amount of tunnel thrusters

N_{brac} Amount of brackets

N_{rud} Amount of rudders

p Local pressure

p_{atm} Atmospheric pressure

q Dynamic pressure of apparent wind, Blendermann

R Radius

R_R Rotor radius

R_{air} Air resistance force

$R_{T,max}$ Maximum total resistance, Hollenbach

$R_{T,mean}$ Mean total resistance, Hollenbach

S Side force

S Wetted surface of the hull

s_H Lateral-plane centroid with respect to the waterline, Blendermann

s_L Lateral-plane centroid with respect to the main section, Blendermann

S_w Wetted surface of the hull

T	Thrust force
T	Vessel draft
T_A	Aft draft, Hollenbach
T_F	Front draft, Hollenbach
T_{sail}	Thrust force from sail
TWS_{10}	True wind speed at 10 m above the surface
$u(y)$	Velocity gradient
U	Inflow speed/Free-stream velocity
u	Apparent wind speed
U^*	Frictional velocity
U_∞	Free stream velocity
U_θ	Circumferential velocity
v	Local velocity
V_s	Vessel speed
v_t	Tangential velocity
V_{rel}	Relative wind velocity
X	Longitudinal force, Blendermann
x_F	Yawning-moment lever arm, Blendermann
Y	Side force, Blendermann
z	Height above the surface
z	Surface elevation
z_0	Height above the surface at which TWS$_{10}$ was measured
z_F	Rolling-moment lever arm, Blendermann

Table of Contents

List of Figures

List of Tables

Chapter 1

Introduction

As the global shipping industry attempts to align with the Paris Agreement's goals and limit its environmental impact, the Norwegian government have set the goal of limiting the emissions of greenhouse gases by 50% by 2030 for domestic shipping and fishing. The Green Shipping Programme (GSP), a public-private partnership with the purpose of helping the Norwegian government's maritime strategies and plans (Green Shipping Programme, 2023), have estimated that to reach the goal the Norwegian fleet must consist of approximately 700 low-emission and 400 zero-emission ships by 2030 - "A huge challenge" (Green Shipping Programme, 2023).

As of July 2023, 49 of a total of 132 car ferry connections in Norway are electrical, constituting approximately 37%. In alignment with the ambitious and stringent directives of the Norwegian government, mandating a 50% reduction in greenhouse gas emissions from domestic shipping and fishing by 2030, the use of batteries in ferry connections is on a consistent rise. Figure 1.1 is based on statistical data from Tilnull (2023), and show this notable, and still increasing, trend in electric ferry connections from around 0.75% in 2013 to approximately 37% in 2023.
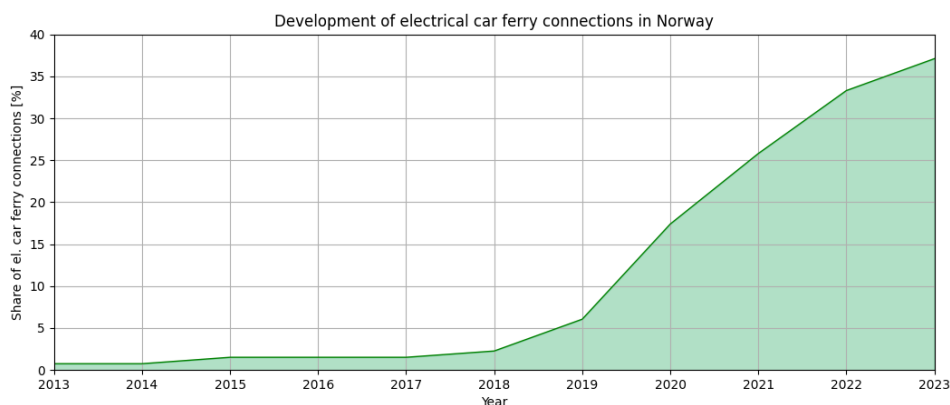
Figure 1.1: Development of electric car ferry connections based on data from Tilnull (2023). Source: https://www.tilnull.no/ferger

The maritime application of batteries poses significant challenges due to the large-scale nature of these energy storage systems. Unlike traditional electric car batteries, a maritime battery may be several hundred times larger, underscoring the increased complexity and strict requirements for factors such as safety, maintenance and reliability. Table 1.1 from a paper published by MAN Energy Solutions (2019) compares battery capacity, character and approximated project costs as of 2019. The largest electric vessels as of 2019 had a battery capacity of 4100 kWh. For comparison, MF Bastø Electric is today's largest operating electric ferry and has a battery capacity of 4300 kWh (Fosen, 2019). The battery cost per kWh depends on the type of battery system but is

typically equal to approximately 11%[1] of the total project cost MAN Energy Solutions (2019).

The expected lifetime of marine batteries is set to 10 years as the current standard in the marine industry (MAN Energy Solutions, 2019). For a vessel with a lifetime of 20-25 years, a midlife exchange of the battery package is expected. By including the battery exchange, the cost of the battery relative to the total project cost becomes even more significant than the initial 11%[2]. Understanding the load cycle of batteries, including charging and discharging patterns, is crucial for achieving the intended battery lifespan. Overloading can lead to frequent replacements and additional costs (DNV, 2016). Hybrid systems are a common approach for offloading the battery to maximize its lifetime.

With a shipowner's goal of maximizing the profit whilst aligning with the requirements of emissions, the operation, and choice of type, of hybrid solution becomes more challenging. You want to operate the battery in a manner that fulfils its designed lifetime, but you also want to emit as little as possible. With seasonal changes and short charging times at the docks, a common scenario is that either the battery will be discharged further than intended resulting in faster battery degradation or, to spare the battery and cost of potentially more frequent battery exchange, the engine will be used and the emissions become more significant than planned. The motivation of this thesis is therefore to explore whether it is possible to prolong the lifetime of a battery, reducing the risk of the additional cost of an unplanned battery exchange and reducing the need, use, and potential emissions of the engine in a hybrid system solution by the use of wind-assisted propulsion.

Table 1.1: Table from MAN Energy Solutions' paper on batteries on board ocean-going vessels (MAN Energy Solutions, 2019) highlighting the battery capacities of different vessels and products.

	Year	Battery capacity	Character	Project costs (approx.)
Mobile phone	2019	15 Wh	High-energy, short life	50 USD
Nissan Leaf	2018	40 kWh	High-energy, medium life	20 000 USD
Battery peak shaving, Grieg Star 50 000 dwt	2015	67 kWh	High-power, long life	200 000 USD (1.5m NOK)
Tesla Model S100d	2013	100 kWh	High-energy, medium life	100 000 USD
MAN Lion's City E (MAN Truck & Bus)	2019	480-640 kWh	High-energy, long life	-
Ampere - first modern electric car ferry	2015	1000 kWh	Medium-power, long life	-
Aurora and *Tycho Brahe* - world's largest electric vessels[3]	2018	4100 kWh	Medium-power, long life	35 m. USD (300 m. SEK)

Why wind?

Various fuels and energy sources such as LNG, methanol, and hydrogen are being explored and to some extent used as alternative fuels in shipping. However, they all include a production phase which commonly is fuelled by nonrenewable sources. Hence, the benefit of using alternative fuels like hydrogen is counteracted by the emissions generated during the production process.

Wind-assisting technology presents a distinct advantage in that only the sails require production, minimizing the resource-intensive aspects associated with other propulsion methods. Wind, as an inherent natural energy source with a longstanding historical and scientific foundation, further enhances the appeal and feasibility of this technology.

The Flettner rotor is chosen as the source of auxiliary propulsion in this thesis. The Flettner rotor

---

[1] by assuming a price of 1000 USD/kWh (current price per kWh (MAN Energy Solutions, 2019)), a battery capacity of 4100 kWh would have a battery cost equal to approximately 11.71% of the total project cost of 35mUSD, which is the approximate price of the largest electric vessels of 2019 (ref. Table 1.1).

[2] ditto

[3] Per 2019

is a rotating cylinder providing thrust and lift using the Magnus effect. One of the reasons behind the choice of using Flettner rotor compared to other sail technologies i.e., soft or rigid wing sails, ventilated foil sails or soft sail systems, is because they are known to provide high values of thrust compared to their projected sail area. Another reason is their "easy" operability/manoeuvrability.

1.1 Problem statement and Objective

The objectives of this thesis is to investigate the following

1. What are the potential energy savings on a battery electric car ferry by using Flettner rotors as auxiliary propulsion?

2. Can the potential energy savings help reduce the depth of discharge (DoD), and therefore increase the battery's lifetime?

Approach to answer the problem statement

The problem objectives of the thesis will be investigated by performing a case study on a battery-driven pendulum ferry in Trondheimsfjorden. The sail forces from the Flettner rotor are modelled in Python using wind data collected from two adjacent buoys to the ferry connection. The resistance and needed propeller power are derived from a speed-power prediction from the design phase of the ferries obtained from the ship operator of the ferries. While waiting for data from the ship operator, an empirical resistance model is also derived using methods such as Hollenbach for the residual resistance, and Blendermann for the air resistance. The results of the power generation from the Flettner rotors are used to estimate the DoD, and the potential savings in the battery's cycle life.

1.2 Structure of thesis

The thesis is structured by introducing relevant hydrodynamic and aerodynamic theory related to the understanding and modelling of the resistance of the vessel and the forces and operation of the Flettner rotor.

Chapter 2 comprises of relevant ship hydrodynamic theory, the implementation of an empirical resistance model and the comparison between the empirical model and CFD analysis. Chapter 3 comprises of relevant aerodynamic theory related to Flettner rotors, including the implementation of how to model these forces. The source and analysis of the wind data is explained in Chapter 5. The case study is introduced in Chapter 6, while the results are found in Chapter 7. Chapter 8 comprises the conclusion and a short note on Further Work.

1.3 Previous work

The pursuit of sustainable and efficient maritime operations has led to a renewed interest in wind-assisted propulsion technologies. Among these, the Flettner rotor has emerged as a promising solution for reducing fuel consumption and emissions in the shipping industry. This section reviews the contributions of recent studies to the understanding and application of wind-assisted propulsion systems, particularly focusing on rotor sails and their relevance to the objectives of this thesis.

1.3.1 Modelling of wind-assisted ships

Tillig and Ringsberg (2020) presents an approach to analytically capture the interaction between the aero- and hydrodynamic interaction effects between the sails, the superstructure and the hull of wind-assisted cargo ships in *Design, operation and analysis of wind-assisted cargo ships*. They developed a performance prediction model called "ShipCLEAN" which uses a combination of empirical and analytical formulations in combination with propeller and hull standard series to predict the performance of wind-assisted ships. Based on the ship type and its main dimensions i.e., length overall (L_{oa}), breadth, draft and displacement, the model uses empirical formulations to estimate dimensions not directly provided, i.e., (L_{pp}), depth, and superstructure dimensions. For example for ferries, the superstructure is assumed to have a superstructure length equal to their L_{pp}, and the superstructure height is based on estimations of the numbers of decks. The results of the study highlights that to fully exploit the potential energy savings of Flettner rotors on ships, it is important to account for the the aero- and hydrodynamic interaction effects and using a 4 degree-of-freedom ship performance model. They also pointed out the importance of controlling the rotational speed of each rotor individually to maximize the energy savings.

For resistance calculations, ShipCLEAN employs empirical methods to divide the hull resistance into various components including calm water resistance, added resistance due to waves, shallow water, fouling, ice, and drift. The implementation and methods used for estimating the resistance is found in their previous paper *A generic energy systems model for efficient ship design and operation*, Tillig et al. (2017). This paper presents a model for analysis of a ship's energy flow in the entire energy system for both its subsystems as well as in a holistic way to capture the interactions between the components to optimize energy efficiency. This paper was followed by Tillig and Ringsberg (2019), *A 4 DOF simulation model developed for fuel consumption prediction of ships at sea*, where they solve the moment and force balances for the ship in four degrees-of-freedom to include the external moments and forces caused by the environment at sea. This includes and captures involuntary speed losses and engine limits in the ShipCLEAN model.

The model from Tillig et al. (2017) specify the main resistance calculations used by ShipCLEAN and the basis for the aero- and hydrodynamic interaction effects presented in Tillig and Ringsberg (2020). For the resistance calculations, Tillig et al. (2017) predicts the static and dynamic power consumption of a ship which is used as input to ShipCLEAN (Tillig and Ringsberg, 2020). The static power prediction model is used as initial speed power prediction in calm water. For the wetted surface and resistance prediction they follow the ITTC procedure based on a reference water temperature and density, i.e.,

$$R_t = \frac{\rho_w}{2} V_s^2 S_w c_T, \tag{1.1}$$

where ρ_w is the water density, V_s^2 is the vessel speed, S_w is the wetted surface of the hull and c_T is the total resistance coefficient expressed as

$$c_T = (1+k)c_F + c_R, \tag{1.2}$$

where c_F is the two-dimensional frictional resistance coefficient. This incorporates the resistance due to the viscosity of the water and the roughness of the hull. k is the form factor that accounts for the three-dimensional viscous resistance effects, and c_R is the residual resistance coefficient estimated using Holtrop-Mennen. The wetted surface was predicted based on method proposed by Kristensen et al. (2012).

In the dynamic power prediction model, the frictional resistance coefficient were computed repeatedly along a simulated journey to account for the changes in density and viscosity, due to changing water temperature, and the hull roughness. The wind resistance was modelled using a method proposed by Blendermann (1994) that proposes coefficients for the wind resistance coefficient dependent on the ship type and apparent wind angle. To account for the added resistance due to wind and waves, they used an empirical transfer function proposed by ITTC (2014). It is also noted that this method is only meant for wave height up to 2 m, and they suggest more sophisticated methods for increasing the accuracy. The rudder resistance was computed using drag coefficients from Schneekluth and Bertram (1998). The resistance due to drift was estimated using

the lift and drag ratio derived by Kramer et al. (2016). The residual resistance coefficient and the form factor remained unchanged in the dynamic power prediction model.

For the aerodynamic effects and Flettner rotor forces, Tillig and Ringsberg (2020) used both analytical and empirical approaches. The interaction effects between the rotors and the superstructure were captured by analytically solving the Navier-Stokes equation for incompressible, potential flow. The thrust- and side forces generated by the Flettner rotors were calculated from lift-, drag- and power coefficients based on CFD results from Li et al. (2012) corrected to fit full-scale measurements.

Tillig and Ringsberg (2020) also proposes a method for controlling the rotational speed of each rotor individually based on the spin ratio, which represents the speed of the rotor, i.e., the rotor's tangential speed at the surface, relative to the incoming local wind speed, the net rotor power. The optimal rotational speed of the rotor is hence defined as the rotational speed that returns the maximum net rotor power, where the net rotor power is defined as the rotor's generated thrust power minus the rotor's power consumption.

The methodology proposed by Tillig et al. (2017), Tillig and Ringsberg (2019) and Tillig and Ringsberg (2020) provides a framework for analyzing the impact of rotor sails on ship performance in addition to methods for modelling wind-assisted ships.

1.3.2 Wind-assisted propulsion performance studies

The research paper *A Comeback of Wind Power in Shipping: An Economic and Operational Review on the Wind-Assisted Ship Propulsion Technology* by Chou et al. (2021) performs a secondary data review analysis to identify the key factors for operational efficiency of wind-assisted ship propulsion (WASP) technology and the potential fuel savings. The key factors affecting the operational efficiency of WASP technologies were categorized into environmental, on-board, and commercial factors. The environmental factors highlight the importance of wind speed and direction, with higher wind speeds enhancing the WASP's energy output and fuel savings. It also underscores the consideration that higher wind speeds often are accompanied with higher wave heights, which can negatively impact the ship performance. The authors imply that models for more accurate fuel and energy savings should include side forces and yaw moments to account for the environmental effects. The study also points out that various WASP technologies perform better in different seasons. The conclusion of this statement is based on a route simulation for a vessel along the Argentina-UK trade lane equipped with 1) a Flettner rotor and 2) a wingsail. The result from the simulation indicate that the Flettner rotor performed better in the winter season while the wingsail performed better in the summer season. The reason for the Flettner rotor performing better in the winter season was explained to be due to the higher wind speeds in the Northern Hemisphere during the winter.

Lu and Ringsberg (2020) compared different three different WASP technologies on an Aframax Oil Tanker on a route between Gabon and Canada in *Ship energy performance study of three wind-assisted ship propulsion technologies including a parametric study of the Flettner rotor technology*. The different WASP technologies investigated were wingsail, DynaRig and Flettner rotor. They developed a 4 degrees-of-freedom ship performance prediction model to evaluate the potential energy savings. The research also included a parametric study of the Flettner rotor for a second ship for evaluating the impact of its dimensions and operating conditions. The parametric study of the Flettner rotor included a Handysize Bulk Carrier, also operating on a route between Gabon and Canada. The simulation model used in this paper is based on the work from Tillig et al. (2017) and Tillig and Ringsberg (2019). The case was performed for the three WASP tehcnologies along the same route with the same estimated time of arrival of 313h, to ensure similar and comparable simulation conditions. The results from the simulation model was compared to commercial voyage records i.e., noon reports of route and operational conditions. The simulations were performed using recorded environmental data for the wind speed and direction along the route for an Aframax Oil Tanker and the Handysize Bulk Carrier. The total fuel consumption of the vessels along the route with the different WASP technologies were compared to with that without sails. The result highlights that the Flettner rotor produced the most fuel savings compared to the other sail

technologies. It is imprtant to notice that the maximum rotational speed of the Flettner rotor in this study was 600 rotations per minute (RPM). Based on the parametric study of the Flettner rotor for the Handysize Bulk Carrier, it was highlighted that the total fuel savings were more sensitive to the speed of the ship than the speed of the rotor. The extra required fuel consumption for increasing the speed 0.5 knot would be covered by the further savings from the Flettner rotor.

Chapter 2

Ship Hydrodynamics and empirical resistance model

The objective of the thesis is to evaluate whether the use of Flettner rotors as auxiliary propulsion can help reduce the energy consumption of the ferry and hence potentially help prolong the battery lifetime and reduce overall costs and emissions. The first step is therefore to investigate the energy consumption of the ferry without Flettner rotors. The energy consumption can be estimated by the propulsive power needed to operate the ferry, which again is dependent on the vessel's resistance through the water and air.

The ferries evaluated in this thesis operate along the ferry connection Flakk-Rørvik in Trondhiems-fjorden. To be able to investigate the effect of the Flettner rotors as accurately as possible in a real case, the ship operator of the ferries agreed to share some data to be used for the prediction of the resistance. A CFD analysis performed by an independent consultant in the design phase was provided. The CFD analysis included a speed-power prediction and some graphic results of the wave pattern and elevation around the hull. The analysis did not include the resistance directly, but by assuming a propulsion efficiency based on the propeller type and system of the ferries, it derived from the speed-power prediction. The resistance derived from the CFD analysis is therefore not the exact resistance of the ferries, but an approximation dependent on the choice of propulsive efficiency. The empirical resistance model explained in this section was developed during the wait for the data from the ship operator as a precautionary measure in case the required data could not be obtained.

A vessel sailing through the water experiences complex 3D flow patterns and effects around the hull. These effects are difficult to model, and depending on factors such as budget, time constraints or available facilities, model testing or CFD calculations (sometimes both) are usually performed to obtain as accurate predictions as possible. Based on data from previously performed model tests and practical experience, empirical models are derived. As these models typically are based on "old fashioned" hull forms, they do not include empirical relations for all types of ships and hull shapes. The accuracy of the results from the prediction based on these models must be taken with care.

This chapter introduces the theory of the resistance components and the empirical models used to predict the total resistance of the ferries. A comparison between the resistance predicted from the empirical model and the resistance derived from the speed-power prediction of the CFD report is also included to investigate the accuracy of these empirical models on a ferry.

2.1 Vessel Resistance

When a ship is sailing in the ocean, it will experience a resistive force due to the ocean, wind and waves. The resistance of a ship is the force the ship has to exert on the water to be able to move

forward. It is the total net force acting in the opposite direction of motion. The resistance of a sailing ship can generally be divided into three main components

1. Viscous resistance
    (a) Frictional resistance
    (b) Hull roughness
    (c) Pressure resistance

2. Wave resistance, i.e., wave making and breaking

3. Air resistance

Figure 2.1 from Guldhammer and Harvald (1974) illustrates the typical contributions of the different resistance components to the total resistance. From the figure it is seen that for lower Froude numbers, i.e., 0.15 - 0.20, the viscous resistance is the most dominating component, while for Froude numbers of values i.e., 0.25 - 0.30, the other components also have a more significant contribution to the total resistance.
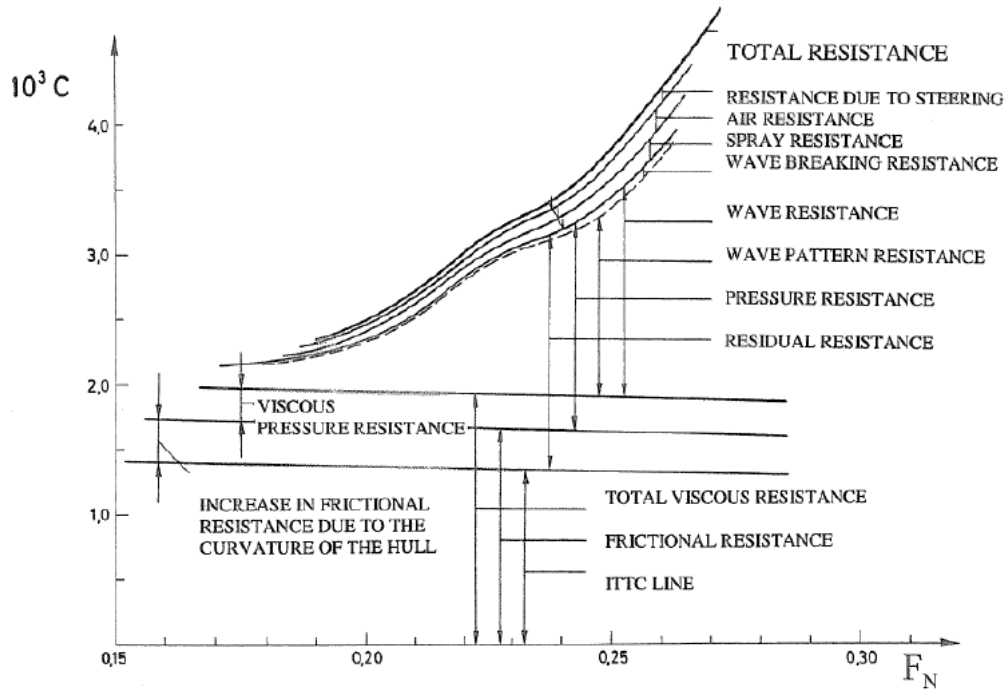
Figure 2.1: The different resistance components' contribution to the total resistance of a normally displaced ship (Guldhammer and Harvald, 1974).

To investigate the effect of the rotor sails on the ferry, the required propeller power is needed. The propeller needs to produce power large enough to overcome the resistance of the vessel. Hence a prediction or estimation of the resistance is calculated. When estimating the total resistance of a vessel, the calm water resistance is considered. General theory of the resistance components used and needed to perform the case study of this thesis is introduced in the following sections.

2.1.1 Viscous resistance

Frictional resistance

When a blunt body is moving through a viscid fluid, it will experience a pressure force from the fluid. This pressure force can be decomposed into components acting normally and tangentially to the body and direction of local fluid motion. The component acting tangentially to the body is the shear stress or the tangential pressure force per unit area. The viscosity of the fluid creates shear stress in the boundary layer, which is a phenomenon commonly referred to as friction. Figure 2.2 illustrates the shear stress, τ, on a very thin flat plate. No-slip condition on the plate creates the velocity gradient $u(y)$. Outside the boundary layer, the velocity gradient, $u(y)$, equals the free-stream velocity, U. The shear stress is proportional to the velocity gradient and the dynamic viscosity of the fluid, μ. The horizontal velocity gradient $u(y)$ illustrated in Figure 2.2 is representative of a laminar boundary layer. Equation Equation 2.1 expresses the frictional stress on the plate and is also applicable to turbulent boundary layer flow (Faltinsen, 2006). In the latter case, the velocity u means a time-averaged velocity on the time scale of turbulence.

$$\tau = \mu \frac{\partial u}{\partial y} \tag{2.1}$$
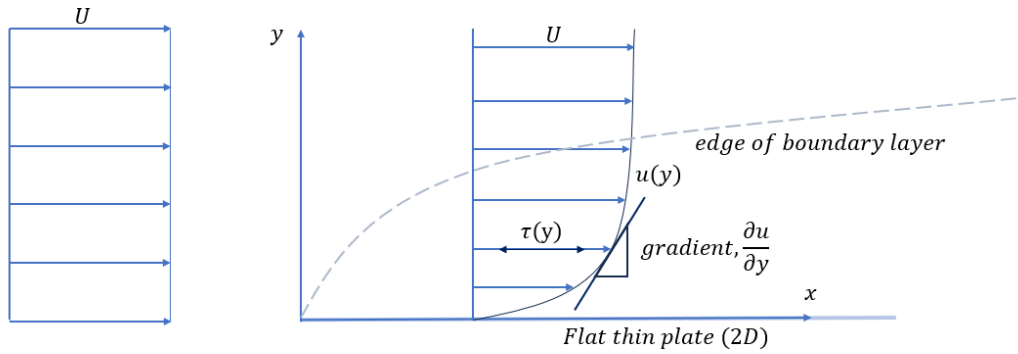
Figure 2.2: Shear stress acting tangentially to the flat plate and the fluid flow.

To separate the shear stress from the normal stress, the shear stress can be measured by considering a very thin flat plate moving longitudinally in the fluid. As the plate is infinitely thin, the only force that can act on the plate is the shear force or the friction force. The frictional force on a ship is therefore defined as the frictional force on a flat plate of the same speed, area and length as that of the ship (Minsaas et al., 2016). This is a common procedure when estimating or predicting the frictional force on a ship hull. To account for the 3D effects caused by the volume of the ship, the frictional resistance is corrected with a form coefficient. The implementation of this procedure is also explained in this chapter.

The frictional resistance coefficient, C_F, can be expressed using the frictional force, F_f, the wetted surface of the hull, S, and the hull-velocity, U,

$$C_F = \frac{F_f}{0.5 \, \rho \, U^2 \, S}. \tag{2.2}$$

Based on creating the best correlation between model- and full-scale trial results for vessels, a correlation line was proposed by ITTC in '57. Given in equation (2.3). This equation is proved to agree well with experimental results for flows along flat plates (Faltinsen, 2006).

$$C_F = \frac{0.075}{[\log R_e - 2]^2} \tag{2.3}$$

To take into consideration that the vessel has volume and is not a flat plate, the frictional resistance is corrected with the aforementioned coefficient, which is called the form factor, k. There exist many empirical equations to approximate this coefficient. Equation (2.4) is MARINTEK's standard equation for form-factor (Steen, 2011) and is used in this thesis.

$$k = 0.6\phi + 145\phi^{3.5}, \quad \phi = \frac{C_B}{L_{wl}}\sqrt{(T_{AP} + T_{FP})B} \tag{2.4}$$

In equation (2.4) C_B is the block coefficient, L_{wl} is the length of the ship in the waterline, B is the ship breadth and T_{AP} and T_{FP} is the draught at the aft and front perpendicular respectively.

ITTC'57's friction line from equation (2.3) corrected with the form factor can now be expressed as

$$C_F(1 + k) = \frac{0.075}{[\log(R_e) - 2]^2}(1 + k). \tag{2.5}$$

Hull roughness

The frictional coefficient from ITTC's 1957 model-full scale correlation line, equation (2.3), assumes a smooth hull. The roughness of the hull due to factors such as paint, welding and fouling, causes additional frictional resistance. As seen in Figure 2.27, the frictional resistance for vessel's of lower Froude numbers can contribute as much as 70-90% of the total resistance. The frictional resistance increases due to hull roughness, hence this must be taken into account.

The influence of the roughness on the viscous resistance is usually characterized by using the height of an equivalent sand-grain. Figure 2.3 illustrates typical types of roughness including an example of the height of an equivalent sand-grain, k_s. k is this context the roughness height and is used for other types of roughness i.e., geometrically regular roughness for example due to bolts and screws on the hull.
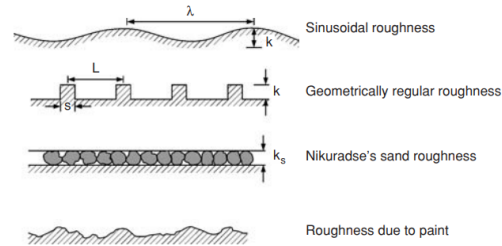
Figure 2.3: Illustration of different types of hull roughness from Faltinsen (2006).

A paper from Kadivar et al. (2021) reviews the fundamentals and theories of turbulent flow over rough surfaces and highlights its complexity and need for further research. The paper has been used to briefly explain the hull roughness' contribution to the frictional resistance force in addition to the behaviour of the empirical equations used to express this.

The boundary layer over a smooth surface differs from the boundary layer over a rough surface. Figure 2.4 (Kadivar et al., 2021) illustrates the boundary layer over a smooth surface compared to a rough surface. As indicated by Figure 2.4(a), the boundary layer over a smooth surface can typically be divided into three regions; 1) Viscous sublayer, also called the inner layer, 2) Buffer layer, also called the overlap layer, 3) Turbulent region or the Outer layer. In the Viscous sublayer, viscous shear dominates. On a scale of the inner layer, the outer layer is "infinitely" far away (Faltinsen, 2006). This highlights how small the viscous sublayer is compared to the turbulent outer layer. At some point from the leading edge, flow instability occurs and transition to the turbulent outer layer is initiated. Figure 2.4(b) illustrates the same flow only over a rough surface. The roughness elements lead to flow instability close to the plate. Depending on the roughness, this can lead to disruption of the viscous sublayer. Figure 2.5 illustrates more detail this effect.
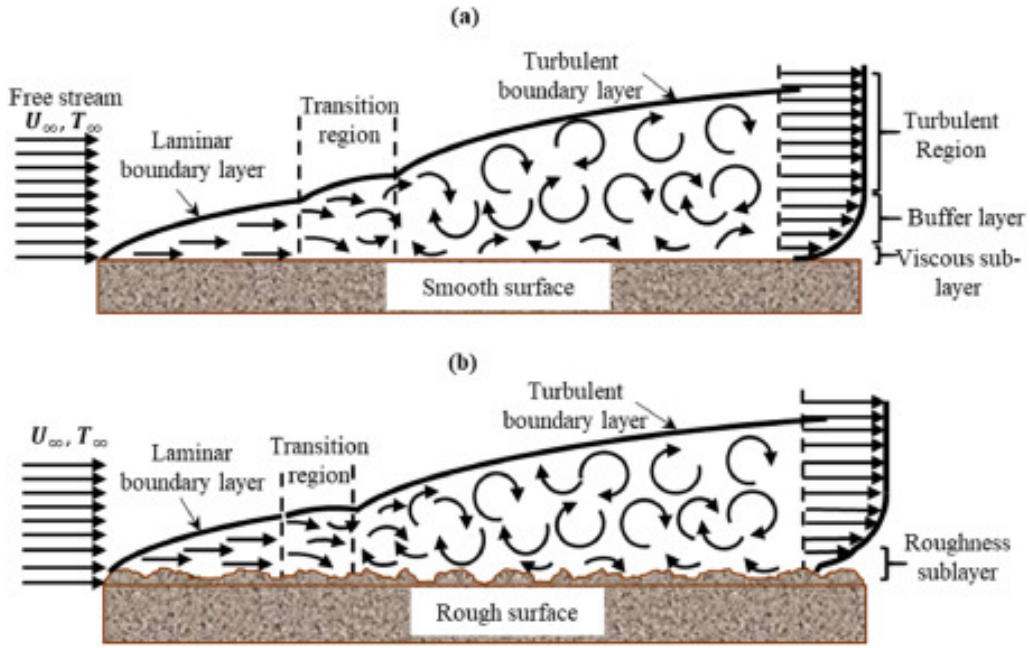
Figure 2.4: Boundary layer along a smooth and rough surface (Kadivar et al., 2021).

In Figure 2.5(c) one can see how the roughness obtrudes into the fully turbulent region and disrupts the viscous sublayer compared to Figure 2.5(a) where the roughness is fully embedded into the viscous sublayer. k_s^+ is the roughness Reynolds number and is defined with the frictional velocity U^* as the characteristic velocity and k_s as the characteristic length. k_s is the roughness height of an equivalent sand grain as seen in Figure 2.3 (Faltinsen, 2006).

$$k_s^+ = \frac{k_s U^*}{\nu} \tag{2.6}$$

k_{smooth}^+ and k_{rough}^+ are the lower and upper bands of the transitional rough regime, respectively. The transitionally rough regime is illustrated in Figure 2.5(b).
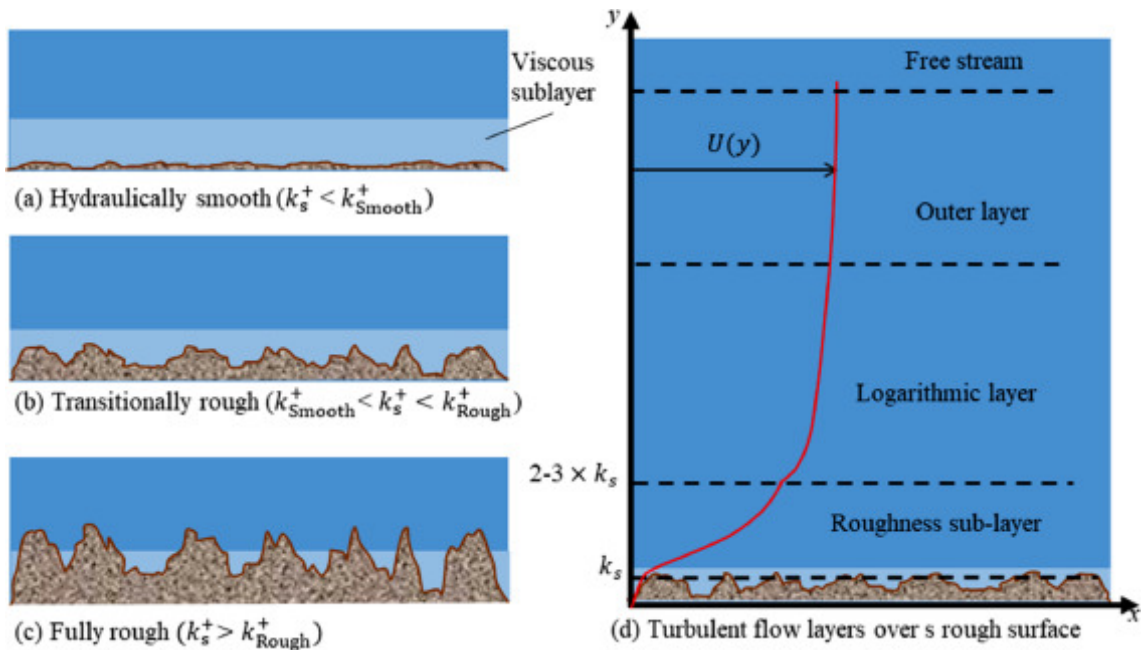
Figure 2.5: More detailed illustration on how a fully rough flow destroys the viscous sublayer from (Kadivar et al., 2021).

When taking the hull roughness into account, the frictional resistance coefficient becomes the sum of the frictional resistance coefficient for smooth surfaces, C_F (eq. (2.3)), plus the additional frictional resistance coefficient due to hull roughness, ΔC_F.

$$C_F = C_F + \Delta C_F \tag{2.7}$$

Based on measurements of resistance in towing tanks, many empirical equations have been proposed for estimating the coefficient due to hull roughness. The Norwegian Marine Technology Research Institute, MARINTEK (now called SINTEF, but referred to as MARINTEK in the thesis), uses equation (2.8). This equation is only relevant for full-scale ships and to some extent accounts for the details in the roughness, such as seen in Figure 2.3 (Faltinsen, 2006). In this equation, $C_F = C_{F,ITTC}$ from equation (2.3).

$$\Delta C_F = \left[110 (H \cdot V_s)^{0.21} - 403 \right] C_F^2 \tag{2.8}$$

From the Proceedings of 25th ITTC - Volume 2 (Steen et al., 2008), equation (2.9) proposed by Townsin (1990) was suggested to be used for an approximation of ΔC_F. The equation proposed by Townsin includes Reynolds number dependency and was derived from integral 3D boundary layer methods. Different from the equation (2.8) used by MARINTEK, equation (2.9) proposed by Townsin accounts for the correlation between model test and full scale in addition to the effect of roughness.

$$\Delta C_F = 0.044 \left[\left(\frac{H \cdot 10^{-6}}{L_{wl}} \right)^{1/3} - 10 R_e^{-1/3} \right] + 0.000125 \tag{2.9}$$

In both equation (2.8) and (2.9), H is the average hull roughness given in μm (10^{-6} m) and corresponds to k in Figure 2.3. H typically has a value between 50 - 200 μm. Both equations are dependent on the Reynolds number.

The hull roughness, H, for newly built or docked ships usually has a value of 150 μm, and ΔC_F usually has a value between 0.0002 and 0.0008 (Faltinsen, 2006).

Figure 2.6 shows how the total frictional resistance coefficient, $C_F + \Delta C_F$, becomes independent of R_e when R_e becomes large enough. As illustrates in Figure 2.5, in a fully rough flow the roughness elements cause large turbulent mixing which disrupts and destroys the viscous sublayer. The roughness Reynold number (eq. (2.6)) is larger than the upper band for the transitionally rough regime, $k_s^+ > k_{Rough}^+$, and the frictional drag becomes independent of the Reynolds number on the plate. As seen in Figure 2.6, $\Delta C_{F,MARINTEK}$ experiences this effect slightly earlier than $\Delta C_{F,ITTC}$.
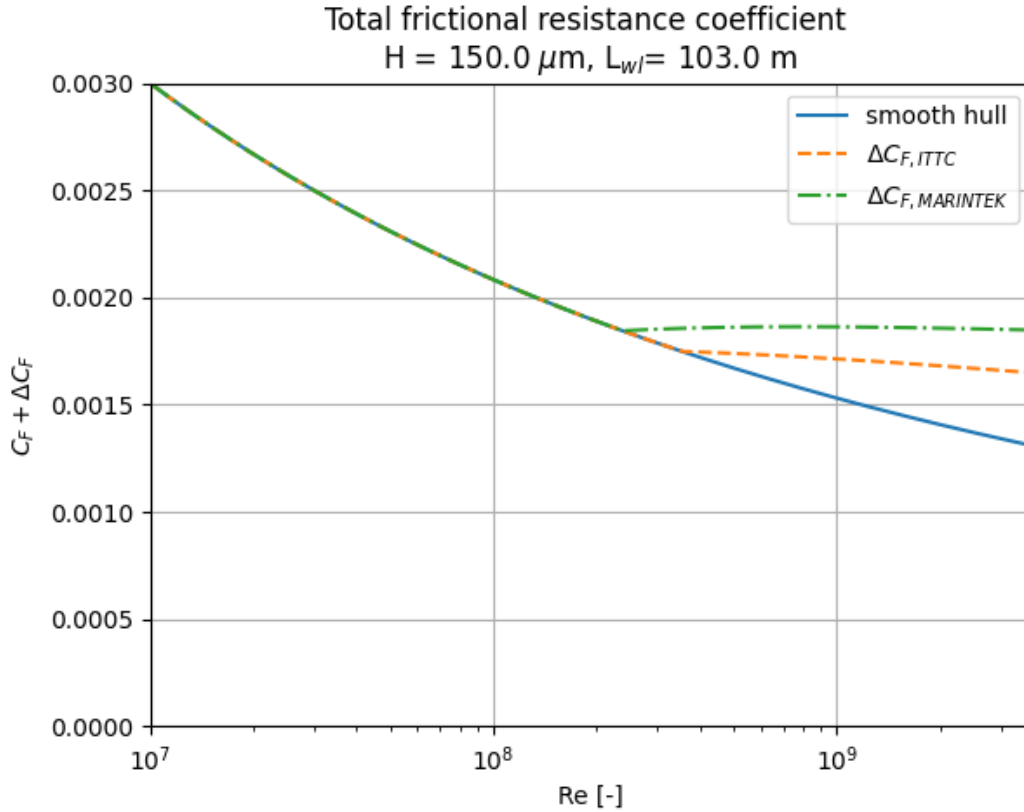
Figure 2.6: Total frictional coefficient, $\Delta C_F + C_F$, with equations (2.9) and (2.8) with roughness, $H = 150\mu$m, and vessel with $L_{wl} = 103$ m.

Figure 2.7 shows the equation used by MARINTEK (eq. (2.8)) and the equation recommended by ITTC (eq. (2.9)) for increasing hull roughness. For $L_{wl} = 103$ m and a ship speed of 12 kn, both equations give negative ΔC_F for an average hull roughness of 100 μm, and the equation used by MARINTEK gives a ΔC_F approximately half of the value for $\Delta C_{F,ITTC}$ for $H = 300\mu$m. For $H = 150\mu$m, which is the typical value used for the average hull roughness for newly built or docked ships, $\Delta C_{F,ITTC}$ gives a value almost 70% larger than $\Delta C_{F,MARINTEK}$. At the maximum of $H = 300\mu$m, $\Delta C_{F,MARINTEK}$ gives a value less than 0.0002, which is a typical minimum value of ΔC_F for newly built or docked ships. The ferry that is to be investigated in the case study was newly built in 2018 and has L_{wl} and design ship speed equal to the values used in Figure 2.7. As the ship is 5 years old (per 2023) and the author has no knowledge of the last docking, the equation for ΔC_F recommended by ITTC will be used to account for the hull roughness to avoid underestimation of ΔC_F.
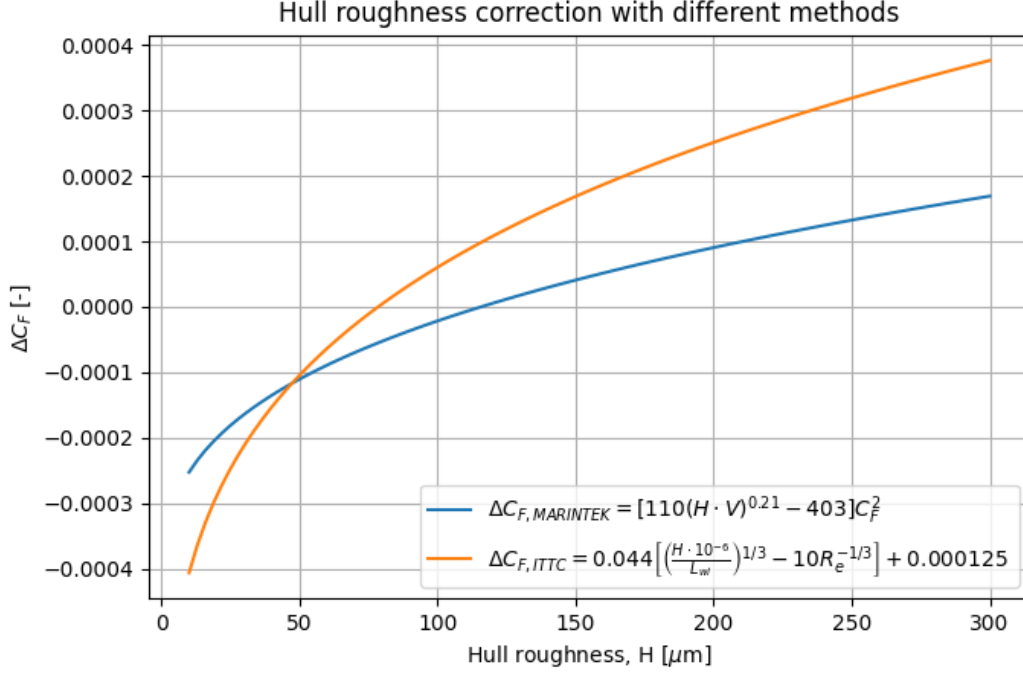
Figure 2.7: Comparison of the different empirical approximations to the added resistance for increasing hull roughness. $L_{wl} = 103$ m and $V_s = 12$ kn ≈ 6.17 m/s.

The total frictional resistance coefficient becomes as defined in equation (2.7). To include the effects caused by the volume of the ship, the total frictional coefficient corrected by the form factor

$$C_F = (C_F + \Delta C_F)(1 + k). \qquad (2.10)$$

Here, k is the form factor accounting for the fullness of the hull and is defined in equation (2.4).

Wetted surface, S

The wetted surface area is the area of the hull that is in contact with the surrounding water and is an important factor in the calculation of the resistance. There are many different methods for estimating the wetted surface area using the main dimensions. Transocean (Transocean Coatings, 2022) suggests an estimation of the wetted surface using only the length between perpendiculars L_{pp}, breadth and draught

$$S = (2T) + B + L_{pp}C_H \quad [\text{m}^2]. \qquad (2.11)$$

In equation (2.11) C_H is the hull-shape factor and has the values $C_H = 0.9$ for large tankers, $C_H = 0.85$ for bulk carriers and $C_H = 0.7 - 0.75$ for smaller dry/general cargo vessels. The factor is empirically found and is based on typical hull shapes for different vessels.

Another method commonly used for estimation of the wetted surface is equation (2.12) from Taylor (1893). The wetted surface is calculated using the vessel's volume displacement ∇, L_{wl} and a wetted surface constant k

$$S = k\sqrt{\nabla L_{wl}}, \quad [\text{m}^2], \qquad (2.12)$$

where the constant k is found from reading from the contour lines in Figure 2.8. The volume displacement, ∇, can be found using the definition of the block coefficient

14

$$C_B = \frac{\nabla}{L_{pp}\,B\,T} \quad [\text{-}].\tag{2.13}$$
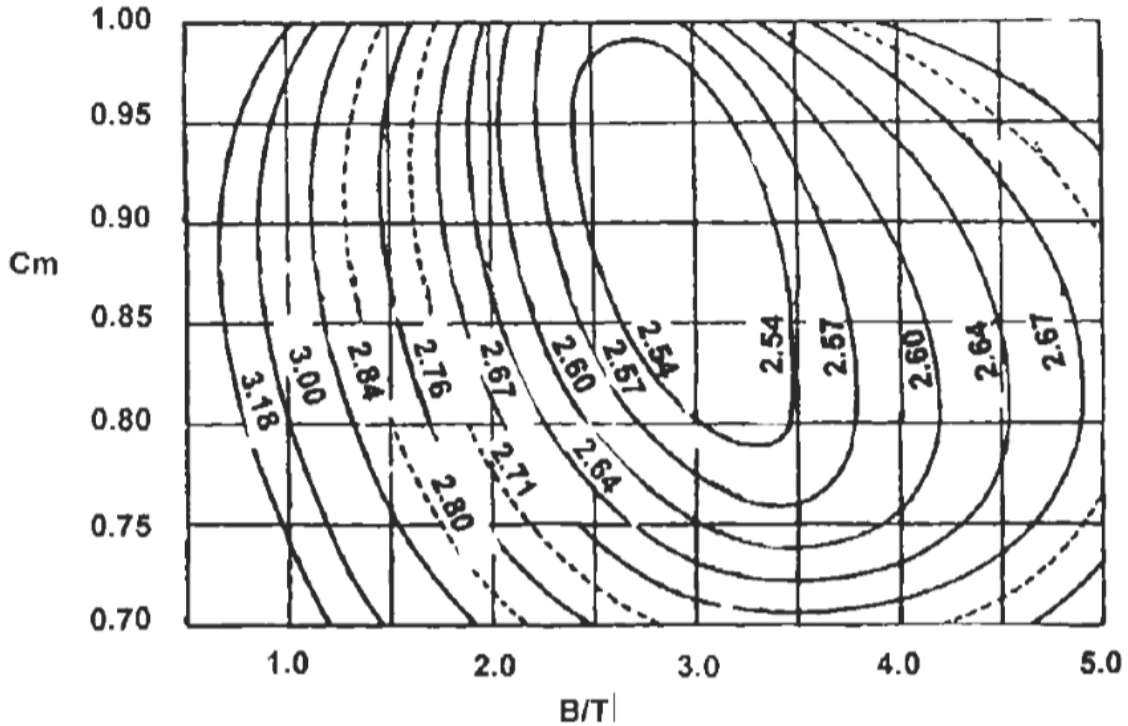
Figure 2.8: Diagram for determination of the constant, k, from equation (2.12) (Taylor, 1893). B/T is the breadth/draft ratio and C_M is the mid-span coefficient.

The difference of the wetted surface using the method from Transocean Coatings (2022) (eq. (2.11)) and the method proposed by Taylor (1893) (eq. (2.12)) and Figure 2.8 with $k = 2.82$, gave a difference of less than 3%. The difference of the frictional resistance force, R_F (eq. (2.5)) using the different methods for the wetted surface was less than 2%. Where the method from Transocean Coatings (2022) gave a slightly higher result than Taylor (1893). The choice between the methods will not significantly impact the resistance calculation, however, the method from Transocean Coatings (2022) (eq. (2.11)) is used in fear of underestimating the frictional resistance force.

Pressure resistance

The component of the pressure force that acts normally on the body is a result of both wave-making and viscous flow effects i.e., flow separation and generation of vortices and circulation. To consider the effect of the viscous flow effects without the influence of free surface effects i.e., wave-making and breaking, the ship hull can be regarded in a case with negligible free-surface motion where the wave resistance does not matter. Considering Foude numbers less than approximately 0.15, this can be done by considering a double-body approximation. This approximation treats the ship's submerged part as if it were mirrored across the water's surface, creating an imaginary "double" of the submerged part above the water. This simplification allows for easier mathematical analysis of the flow, especially for understanding the pressure distribution and the resulting forces on the hull. The concept of the double body is illustrated in Figure 2.9 from Faltinsen (2006).
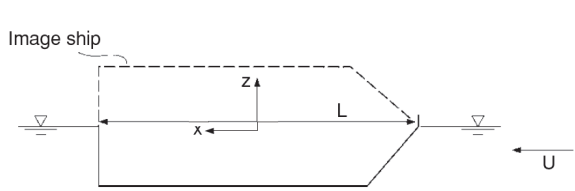
Figure 2.9: Illustration of the double-body approximation from Faltinsen (2006). Inflow speed U on a ship hull of length L.
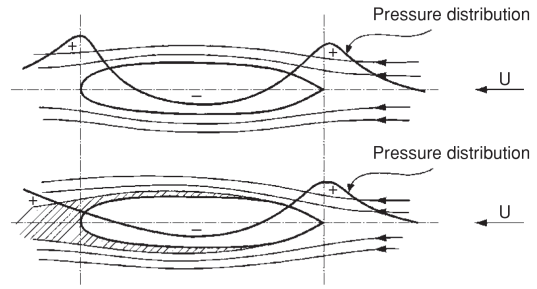
Figure 2.10: (Faltinsen, 2006)

By assuming inviscid fluid, the flow around the double-body at the waterline will have a pressure distribution around the hull as illustrated in the upper figure of Figure 2.10. As the streamlines illustrate, the wider the spacing the lower the flow velocity. The velocity is seen to be lowest at the bow and at the stern in the upper figure. According to D'Alembert's paradox from potential flow theory, no hydrodynamic force will act on a body in an infinite fluid without circulation. The upper figure of Figure 2.10 illustrates this case where the pressure distribution around the hull will cancel each other resulting in a net zero pressure force. As the ambient pressure is neglected, the resulting force due to the pressure distribution is zero. In the lower figure of Figure 2.10 the boundary layer is included, illustrated by the shaded area. The boundary layer is a viscous area and generally increases in thickness towards the ship's end. This means that the boundary layer is thinnest at the fore part and thickest at the aft part of the hull. This effect of the boundary layer affects the pressure distribution such that the pressure on the fore part does not cancel the pressure on the aft part of the hull. In the bow part, the effect of the boundary layer is said to be negligible (Faltinsen, 2006).

As the velocity of the flow is reduced, i.e., after passing the fullest part of a body or for a widening passage, the pressure will increase. As the fluid flows into an increasing pressure gradient, also known as an adverse pressure gradient, separation might occur. As the flow separates it takes the form of vortices and eddies. When the flow is separated from the body, the pressure difference between the attached and non-attached flow results in an increased pressure drag. The wider the wake created by the separation, the higher the pressure drag. As illustrated in figure 2.11, a well-designed and streamlined ship hull is therefore important to reduce this effect. The sharper the edges and the less streamlined geometry, the faster the separation and the larger the wake. The aft of the ship hull and submerged transom sterns or appendages typically experience this effect.
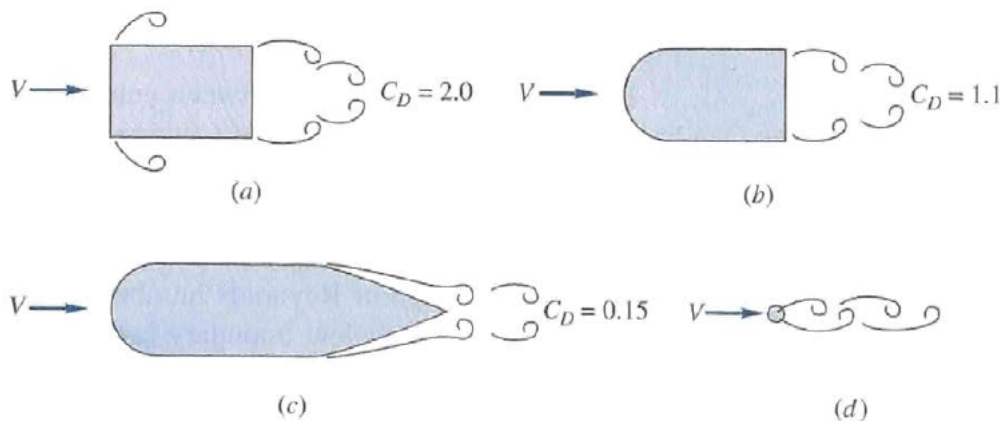
Figure 2.11: The effect of streamlined bodies on flow separation, wake size and the drag pressure coefficient, C_D. Courtesy to Minsaas et al. (2016).

The double-body approximation simplifies the problem by ignoring the water's surface, effectively eliminating the wave-making resistance, i.e.,

$$C_T = (1+k)C_F + \underbrace{C_W}_{=0} \quad \xrightarrow{\text{double body}} \quad C_T = (1+k)C_F, \tag{2.14}$$

the three-dimensional effects of the viscous pressure resistance is thus accounted for by the form factor, k.

2.1.2 Wave resistance

The wave resistance is resistance related to wave making, wave breaking and generation of wave patterns.

As seen in Figure 2.1, the wave resistance consists of the resistance due to the generation of wave patterns around the hull and the wave breaking resistance. As indicated in Fig. 2.1, the wave pattern resistance is the most significant contributor to the total wave resistance.

Generally, there are two types of waves on a ship's hull

1. waves due to local disturbances following the hull,

2. free waves.

The waves due to local disturbances that follow the hull are called the inner wave system. They are also known as Bernoulli waves because they are related to the pressure-velocity distribution around the ship.

Bernoulli states that the energy is conserved along a streamline, and is given in equation (2.15). For the left-hand side to stay constant, an increase in the local velocity, v, results in a decrease in the local pressure, p. This relation is visualized in Figure 2.12. In equation (2.15), the fluid density is given by ρ, the surface elevation by z and g is the gravitational acceleration.

$$\frac{1}{2}\rho v^2 + \rho g z + p = constant \tag{2.15}$$
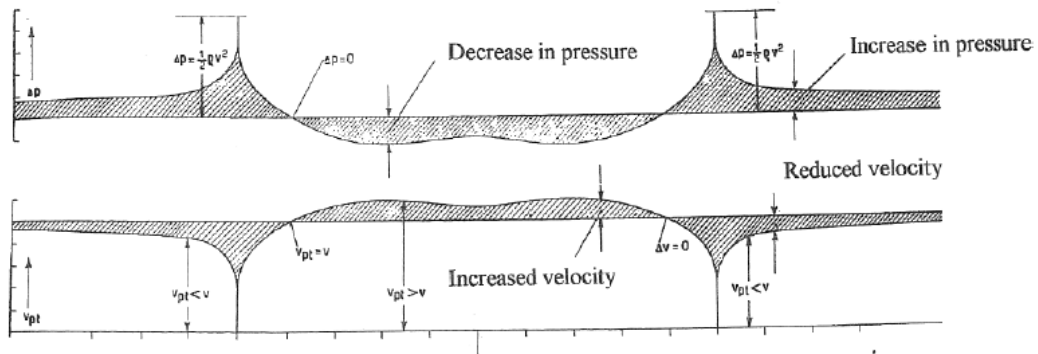
Figure 2.12: Relation between the pressure and velocity around a ship hull according to Bernoulli's equation, (2.15). Figure courtesy to Minsaas et al. (2016).

As seen in Figure 2.12, the velocity is reduced as the flow approaches the bow. To give room for the bow, the fluid is pushed to the sides and around the hull resulting in a decrease in the local fluid

velocity. According to Bernoulli along a streamline, a decrease in velocity results in an increase in the pressure. However, on the free surface, there is a boundary condition stating that the pressure has to equal the atmospheric pressure, p_{atm}.

$$\frac{1}{2}\rho v^2 + \rho g z + p_{atm} = constant, \qquad \text{on the free surface} \tag{2.16}$$

The increase in pressure is compensated by an increase in the free surface, z. The same phenomenon happens near the middle of the ship where the local velocity is at a maximum. For a streamline not on the free surface, this would result in a decrease in pressure. However for a streamline on the free surface, this results in a reduction of the free surface. The change in the surface elevation follows the ship and creates waves, especially near the bow and the stern.
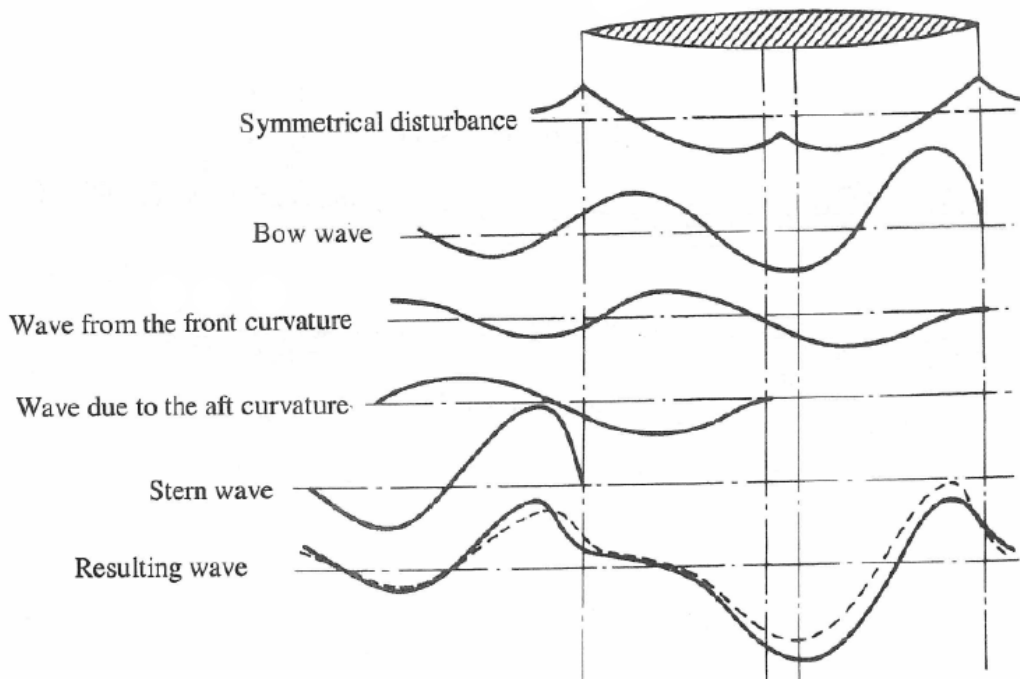
Figure 2.13: Wave generation around a ship hull. The bow and stern have significant free surface elevation and wave generation. Figure with courtesy to Minsaas et al. (2016).

The free wave pattern consists of waves with different angles, α, relative to the direction of travel. Based on the angle α, two wave systems can be defined

1. Transverse waves: $0° < \alpha < 35°$

2. Diverging waves: $35° < \alpha < 90°$

which together contribute to the wave pattern called the Kelvin Wave Pattern named by the British mathematician, mathematical physicist and engineer Lord Kelvin.
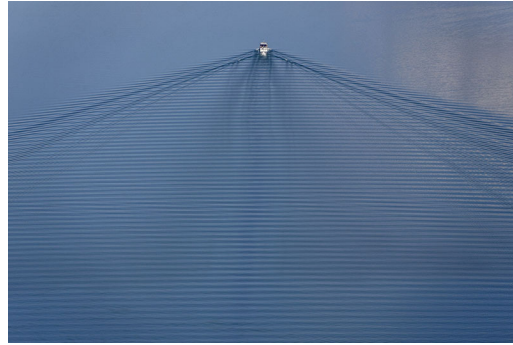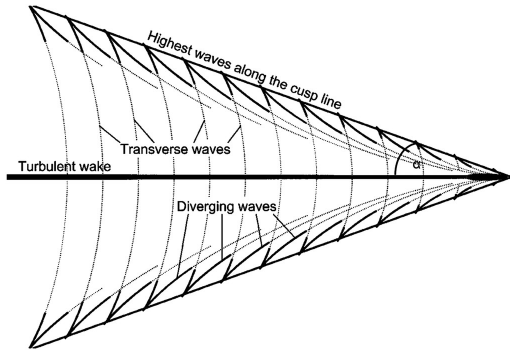
Figure 2.14: Divergent and transverse wave pattern from a moving pressure point. Figure courtesy to Rätsep et al. (2020).

Figure 2.15: Transverse and diverging waves generated by a vessel at sea. Photo courtesy to Leidorf.

Figure 2.14 (Rätsep et al., 2020) illustrate the difference between transverse and diverging waves. The figure also illustrates the angle at which the common wave front formed by the diverging and transverse waves are generated. This angle of approximately $\alpha = 19.5°$ is called the Kelvin angle.

The Bernoulli waves, or the inner wave system, do not directly cause wave resistance. It is by interfering or through its influence on the generation of the free wave pattern, that wave resistance is caused. Hence, wave resistance is only caused by the free wave pattern. As seen in Figure 2.16, the transverse wave system is the main contributor to the wave resistance.
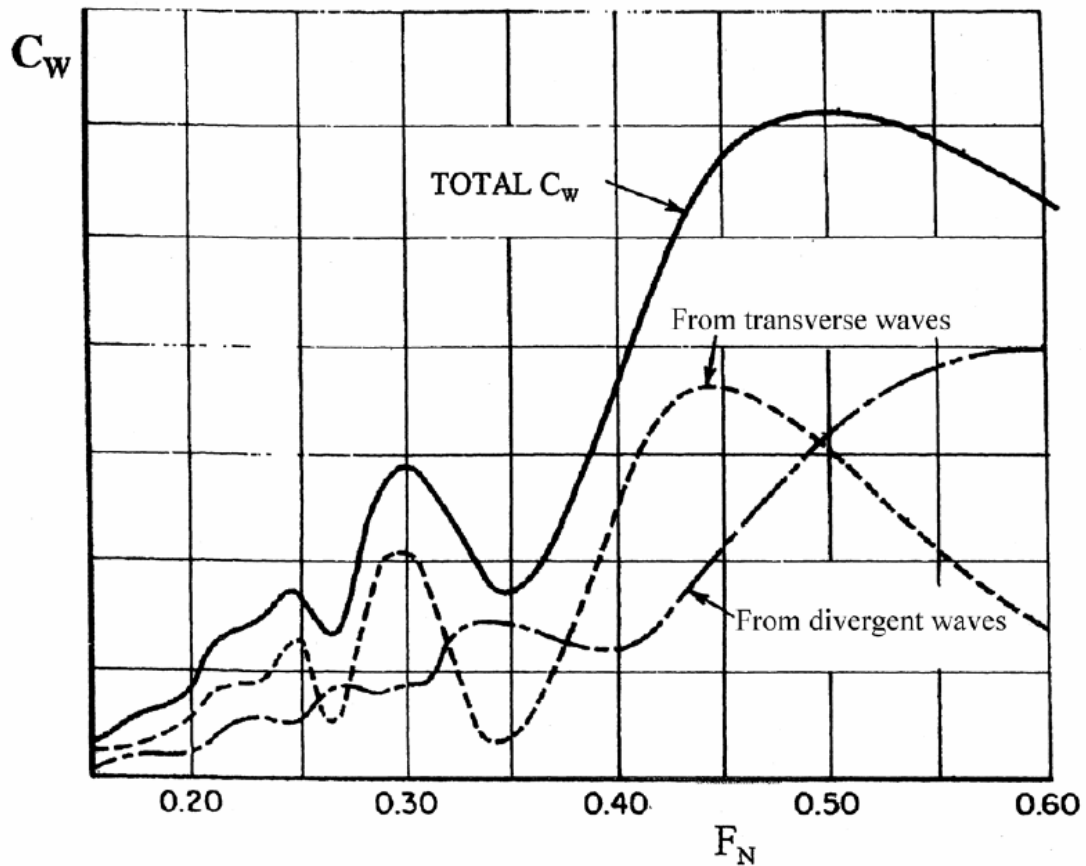
Figure 2.16: Contribution from transverse and diverging waves to the total wave resistance, C_W. Figure courtesy to Minsaas et al. (2016).

The wave resistance components and the total wave resistance in Figure 2.16 were calculated using numerical methods i.e., CFD. As seen in Figure 2.1, the residual resistance mainly consists of wave resistance. The wave resistance can hence be estimated by calculating the residual resistance.

Residual resistance, Hollenbach

The residual resistance includes the remaining resistance effects that are not dependent on environmental conditions. This typically includes wave pattern resistance.

As mentioned in the chapter about vessel resistance, the total calm water resistance of a sailing ship can generally be divided into 1) viscous resistance, including frictional resistance, hull roughness and viscous pressure resistance, 2) wave resistance and 3) air resistance. In the previous sections, the frictional resistance and correction for hull roughness and curvature of the hull have been approximated with different empirical models. The viscous pressure resistance is to some extent accounted for by the form factor, and the wave resistance is estimated using Hollenabach.

In this thesis, Hollenbach's method is used to estimate the residual resistance as it is regarded as rather straightforward to implement in computer programs without compromising its accuracy.

Hollenbach's method is an empirical approach for estimating merchant vessels' resistance during the preliminary design phase. It was proposed in his paper "Estimating resistance and propulsion for single-screw and twin-screw ships" (Hollenbach, 1998), and is based on a thorough regression analysis from the results of 433 model tank tests performed in the Vienna Ship Model Basin in the period from 1980 to 1995. Based on his work he was able to develop coefficients for estimation of mean resistance, as well as minimum and maximum resistance values. The minimum and maximum resistance values are useful for evaluating ship hull designs as they propose resistance values for optimal and suboptimal ship hull designs based on the same geometrical dimensions.

As mentioned earlier, the total resistance coefficient C_T consists of the frictional resistance coefficient, C_F, and the residual resistance coefficient C_R. Hollenbach's method is used to estimate the residual resistance coefficient.

In addition to using L_{wl} and L_{pp}, Hollenbach introduces the parameter Length Over Surface, L_{os}. The length of surface, L_{os} is defined as the length between the most fore and aft point of the ship below the waterline. The definition of L_{os} compared to L_{pp} and L_{wl} is illustrated in Figure 2.17 (Hollenbach, 1998).
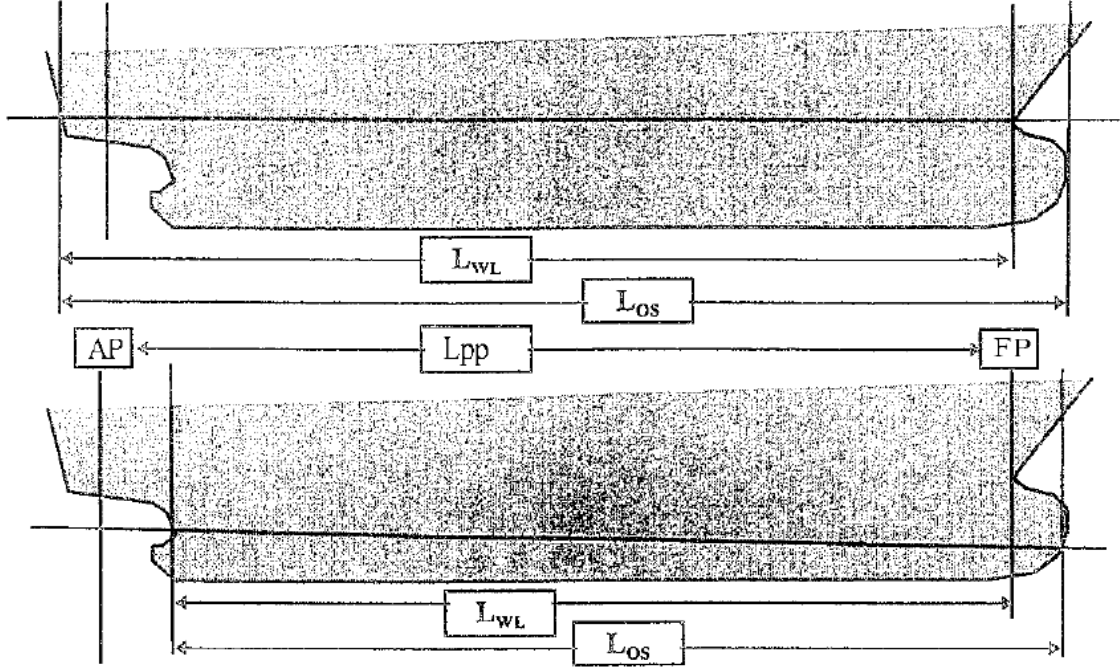
Figure 2.17: Definition of length between perpendicular, L_{pp}, length of waterline, L_{wl}, and length over surface, L_{os}, used in Hollenbach's method. Figure with courtesy to Hollenbach (1998).

Following Hollenbach's method, the Froude number is defined in a particular manner dependent on the parameter L_{fn}, which value is defined in Table 2.1. The Froude number is a dimensionless number describing the relation between the inertial and gravitational forces. It is an important parameter describing the wave-making resistance. In that context, the Froude number represents the energy required to create the waves that push the water out of the way of the hull. The Froude number for Hollenbach's method is defined in (2.17).

$$F_n = \frac{V_s}{\sqrt{gL_{fn}}} \tag{2.17}$$

Table 2.1: Definiton of L_{fn} based on the ratio of L_{os} and L_{pp} (Steen, 2011).

Ratio between L_{os} and L_{pp}	L_{fn}
$L_{os}/L_{pp} < 1.0$	L_{os}
$1.0 < L_{os}/L_{pp} < 1.1$	$L_{pp} + (2/3) \cdot (L_{os} - L_{pp})$
$1.1 < L_{os}/L_{pp}$	$1.0667 \cdot L_{pp}$

Hollenbach defines the the residual resistance coefficient, C_R as in (2.18), and is similar in model and full-scale.

$$C_R = \frac{R_R}{\frac{1}{2}\rho V_s^2\, T\, B} \tag{2.18}$$

The residual component consists of several components including a standard value, $C_{R,std}$ and a Froude number critical value, $C_{R,FnKrit}$. Based on coefficients obtained from the regression analysis performed by Hollenbach (1998), the residual resistance coefficient can be expressed as in (2.19) where $C_{R,std}$ and $C_{R,FnKrit}$ are given in Equations (2.20) and (2.21) respectively.

21

$$C_R = C_{R,std} \cdot C_{R,FnKrit} \cdot k_L \cdot \left(\frac{T}{B}\right)^{a1} \cdot \left(\frac{B}{L_{pp}}\right)^{a2} \cdot \left(\frac{L_{os}}{L_{wl}}\right)^{a3} \cdot \left(\frac{L_{wl}}{L_{pp}}\right)^{a4} \cdot \left[1 + \frac{T_A - T_F}{L_{pp}}\right]^{a5}$$
$$\cdot \left(\frac{D_P}{T_A}\right)^{a6} \cdot (1 + N_{rud})^{a7} \cdot (1 + N_{brac})^{a8} \cdot (1 + N_{boss})^{a9} \cdot (1 + N_{thr})^{a10}$$

<div align="right">(2.19)</div>

$$C_{R,std} = b_{11} + b_{12} \cdot F_n + b_{13} \cdot F_n^2 + C_B \left(b_{21} + b_{22} \cdot F_n + b_{23} \cdot F_n^2\right) + C_B^2 \left(b_{31} + b_{32} \cdot F_n + b_{33} \cdot F_n^2\right)$$

<div align="right">(2.20)</div>

$$C_{R,FnKrit} = max \left[1.0, \left(\frac{F_n}{F_{n,Krit}}\right)^{C_1}\right]$$

<div align="right">(2.21)</div>

$$F_{n,Krit} = d_1 + d_2 \cdot C_B + d_3 \cdot C_B^2$$

<div align="right">(2.22)</div>

$$k_L = e_1 \cdot L_{pp}^{e_2}$$

<div align="right">(2.23)</div>

(2.22) defines the critical Froude number, $F_{n,Krit}$, which results in the added residual resistance $C_{R,FnKrit}$ from (2.21). Hollenbach's method assumes that when the vessel operates at a speed that exceeds the critical Froude number of $F_n = 1.0$, the wave resistance will have a significant increase in growth. From Hollenbach's definition of the residual resistance coefficient in (2.19), the Froude critical residual resistance coefficient $C_{R,FnKrit}$ ((2.21)) and the standard residual coefficient $C_{R,std}$ ((2.20)) are multiplied. This means that the added residual resistance from the critical Froude number regime will not be added when $F_n \leq 1.0 \leq F_{n,Krit}$.

In equation (2.19), T_A and T_F is the draught at the aft and fore perpendicular, respectively. D_P is the propeller diameter, while N_{rud}, N_{brac}, N_{boss} and N_{thr} is the number of rudders, brackets, bossings and tunnel thrusters, respectively. The coefficients a_1, a_2... etc. are found in Appendix C.1.

Hollenbach's method is valid for Froude numbers in the regime

$$F_{n,min} = min(f_1, f_1 + f_2(f_3 - C_B))$$

$$F_{n,max} = g_1 + g_2 C_B + g_3 C_B^2$$

The maximum and minimum resistance are limits with 5% deviation from the mean resistance. Minimum resistance is the resistance to expect for an optimal hull design, while maximum resistance is the resistance to expect from suboptimal or poor hull designs. The maximum resistance is given by (2.24).

$$R_{T,max} = h_1 R_{T,mean}$$

<div align="right">(2.24)</div>

2.1.3   Air resistance

A ship sailing at sea does not only displace the water surrounding the hull, but it also displaces the air surrounding the superstructure and the part of the ship not in the water. The air resistance is affected by the shape and area of the ship above the waterline, the ship's speed and the wind speed. For normal speed operation and no wind, the resistance due to air generally contributes to

3-6% of the total resistance. However, container vessels in headwind or high-speed crafts might experience air resistance up to 10% of the total resistance.

$$R_{air} = C_{air} \frac{1}{2} \rho_{air} V_{rel}^2 A \qquad (2.25)$$

Equation (2.25) expresses the air resistance of the ship above the waterline. In eq.(2.25) C_{air} is the air resistance coefficient for the superstructure which usually is based on measurements from earlier wind tunnel tests for similar ships. V_{rel} is the relative velocity between the wind speed and the ship speed. When determining the air resistance, V_{rel} equals the speed of the ship. A is the transverse or longitudinal projected area of the superstructure. Equation (2.25) states that the air resistance is proportional to the projected area of the superstructure and to the square of the ship's speed.

The relative wind speed relative to the direction of travel can be expressed as in equation (2.26), where TWA is the true wind direction relative to the ship's heading. In equation (2.26), the direction of travel is assumed to be 0° at all times. Given that TWA = 0° is head wind, a ship heading of 0° means sailing into head wind. V_s is the ship speed and TWS is the true wind speed.

$$V_{rel} = \text{TWS} \cos\left(\text{TWA}\right) + V_s \qquad (2.26)$$

Using equation (2.26), the change in resistance due to the wind can be expressed as in equation (2.27).

$$\Delta R_{air} = C_{air} \frac{1}{2} \rho_{air} \left(V_{rel}|V_{rel}| - V_s^2\right) A \qquad (2.27)$$
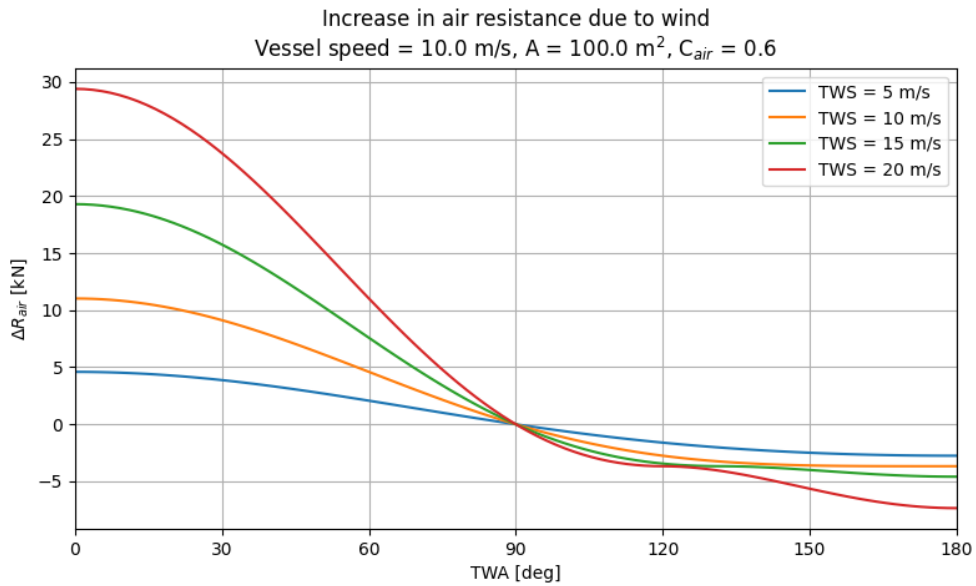
Figure 2.18: The change in air resistance for a ship with a transverse projected area, $A = 100$ m^2 and a vessel speed of 10 m/s for different TWS and TWA.

As seen in Figure 2.18, the increase in air resistance almost doubles for each 5 m/s increase of the TWS for head wind. The reduction of air resistance in tail wind, or TWA = 180°, is much less than the increase of air resistance in head wind.

Blendermann

Air resistance on ships is usually estimated by the results of previous wind tunnel tests of similar ships. Blendermann (1994) performed a parametrical study on wind loading on ships based on wind tunnel tests for various ship types at the Institute of Naval Architecture, University of Hamburg. All the test data were from low-turbulent uniform flow. The parameters governing the aerodynamic loading of the ships were identified using linear regression.

The air resistance in this case study is estimated using the methodology proposed by W. Blendermann (Blendermann, 1994). His paper (Blendermann, 1994) proposed a parametrical loading function based on the solution of the Helmholtz-Kirchoff plate (mathematical flow over a flat plate with open wake). The proposed loading function is semi-empirical as it combines the measured data from the wind tunnel tests with the mathematical solution of the Helmholtz-Kirchoff plate.

The coordinate system of the method is seen in Figure 2.19 and is from his paper Blendermann (1994).
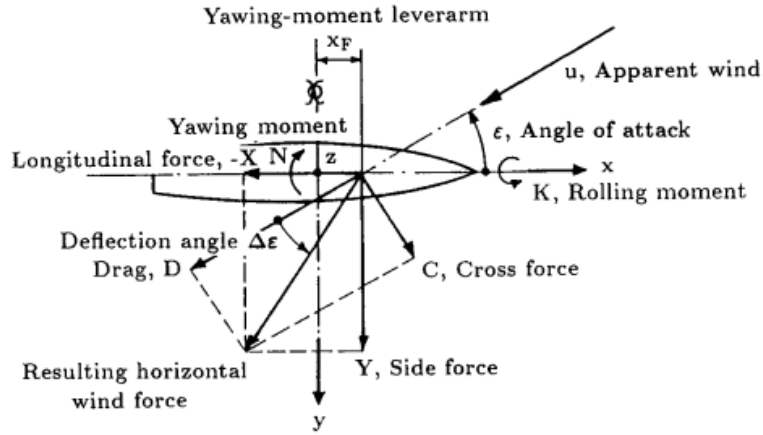
Figure 2.19: Coordinate system for the method proposed by W. Blendermann. Figure courtesy to Blendermann (1994).

The longitudinal-force and side-force coefficients are expressed in equation (2.28).

$$CX_{A_{\mathrm{F}}} = \frac{X}{q \times A_{\mathrm{F}}}, \quad CY = \frac{Y}{q \times A_{\mathrm{L}}} \tag{2.28}$$

In equation (2.28), A_F is the frontal area, and A_L the longitudinal area, of the vessel in $[\mathrm{m}^2]$. X and Y are the longitudinal- and side-force experienced by the vessel. q is the dynamic pressure of the apparent wind and is defined in equation (2.29). ρ_{air} is the air density in $[\mathrm{kg/m}^3]$ and u is the apparent wind speed in $[\mathrm{m/s}]$.

$$q = \frac{\rho_{air}}{2} u^2 \tag{2.29}$$

Wind tunnel tests were performed on different types of vessels with dimensions given in table 2.2. The result of the test is seen in figure 2.20.

Table 2.2: Main dimensions of vessels used in wind-tunnel testing. A_L and A_F are the lateral and frontal areas of the vessels, respectively. s_L and s_H are the lateral-plane centroids with respect to the main section and above the waterline, respectively.

	L_{pp} [m]	L_{oa} [m]	B [m]	A_L [m²]	A_F [m²]	s_L [m]	s_H [m]
Container ship	194.50	210.75	30.50	3751.10	802.00	-3.87	10.08
Ferry	139.60	143.90	17.35	2125.80	325.30	1.36	8.15
Offshore supply vessel	58.40	62.00	13.00	336.80	137.50	7.95	4.08
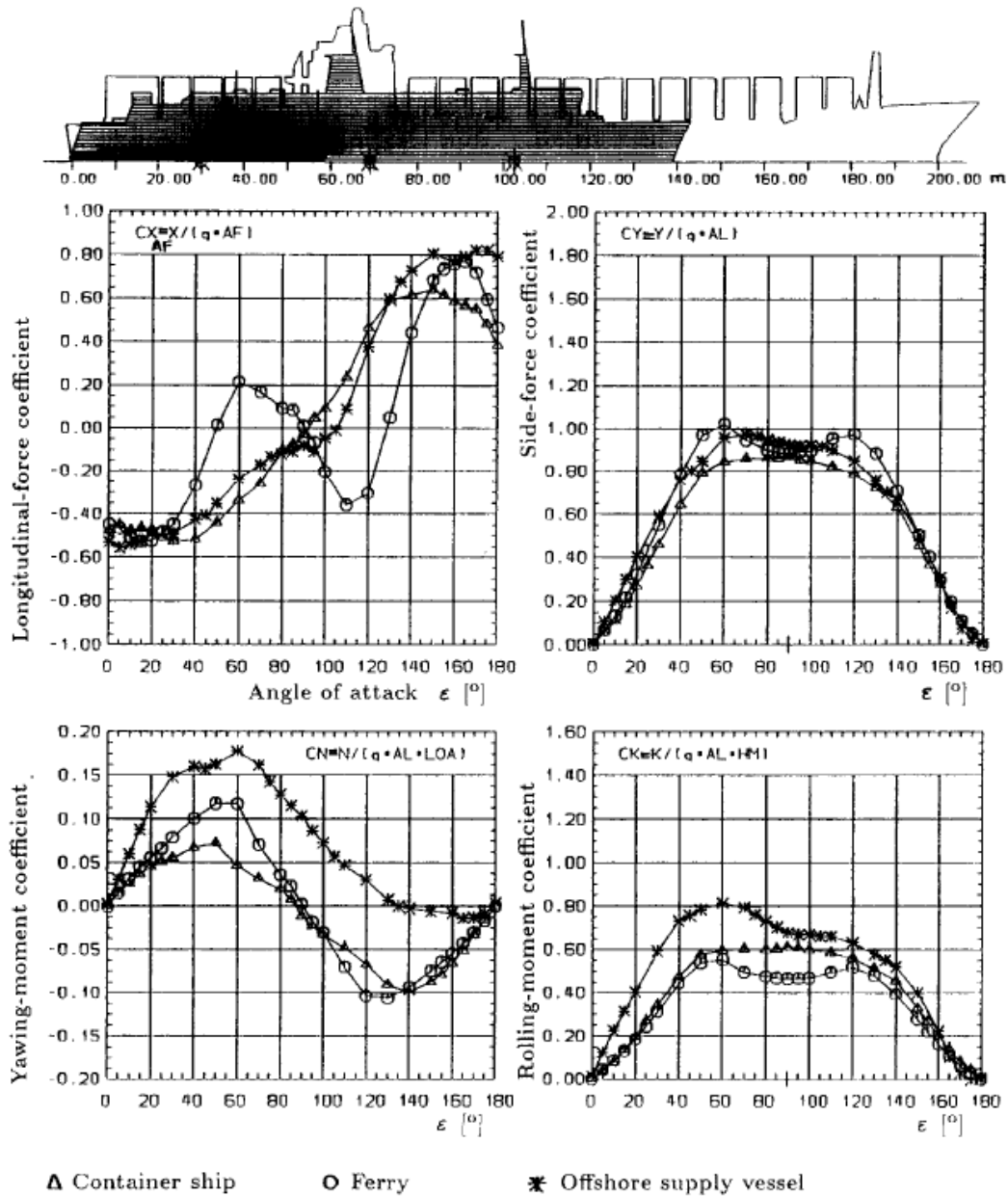
Figure 2.20: Results from wind tunnel testing (Blendermann, 1994).

Using the parametrical loading functions from the solution of the Helmholtz-Kirchoff plate in combination with wind-tunnel tests, the longitudinal-force coefficient can be expressed as in equation (2.30). Reference data for the coefficients CD_t, CD_l, δ and κ is seen in figure 2.21.

The shape of the longitudinal-force coefficient, CX_{A_F}, from the results of the wind tunnel for

25

the ferry differs from container ship and offshore supply vessel. The author commented in the conclusion that the longitudinal force changes sign within the quadrant of wind attack. The ferry begins to experience a longitudinal force/propulsive force from the wind when the wind is still slightly ahead of the beam, and slightly abaft of the beam, and becomes more significant as it approaches the beam wind.

$$CX_{A_{\mathrm{F}}} = -CD_l \frac{A_{\mathrm{L}}}{A_{\mathrm{F}}} \frac{\cos\varepsilon}{1 - \frac{\delta}{2}\left(1 - \frac{CD_l}{CD_{\mathrm{t}}}\right)\sin^2 2\varepsilon} \tag{2.30}$$

Coefficients of lateral and longitudinal resistance, cross-force and rolling-moment coefficients; reference data

Type of vessel	CD_{t}	$CD_{1A_{\mathrm{F}}}$ $\varepsilon = 0$	$CD_{1A_{\mathrm{F}}}$ $\varepsilon = \pi$	δ	κ
Car carrier	0.95	0.55	0.60	0.80	1.2
Cargo vessel, loaded/container on deck, bridge abaft ⊗	0.85	0.65/0.55	0.55/0.50	0.40	1.7/1.4
Container ship, loaded	0.90	0.55	0.55	0.40	1.4
Destroyer	0.85	0.60	0.65	0.65	1.1
Diving support vessel	0.90	0.60	0.80	0.55	1.7
Drilling vessel	1.00	0.70 ÷ 1.00	0.75 ÷ 1.10	0.10	1.7
Ferry	0.90	0.45	0.50	0.80	1.1
Fishing vessel	0.95	0.70	0.70	0.40	1.1
Liquified-natural-gas tanker	0.70	0.60	0.65	0.50	1.1
Offshore supply vessel	0.90	0.55	0.80	0.55	1.2
Passenger liner	0.90	0.40	0.40	0.80	1.2
Research vessel	0.85	0.55	0.65	0.60	1.4
Speed boat	0.90	0.55	0.60	0.60	1.1
Tanker, loaded/in ballast, bridge aft	0.70	0.90/0.75	0.55/0.55	0.40	3.1/2.2
Tender	0.85	0.55	0.55	0.65	1.1
Mean of data set	0.86	0.62	0.59		
Standard deviation	0.09	0.13	0.12		

Figure 2.21: Coefficients for different types of vessels to be used in the parametrical loading functions in equation (2.30) from Blendermann (1994).

The air resistance of the ferries Munken and Lagatun, which sail the ferry connection Flakk-Rørvik, is estimated using the parametrical loading functions and the coefficients proposed by Blendermann (1994).

Due to the lack of exact dimensions of the ferries, the projected lateral and frontal area above the waterline is estimated by regarding the hull as a rectangle, and the superstructure as a triangle. Figure 2.22 illustrates the division of the ferry Lagatun's area into a rectangle and triangle. Lagatun and Munken have the same main dimensions.
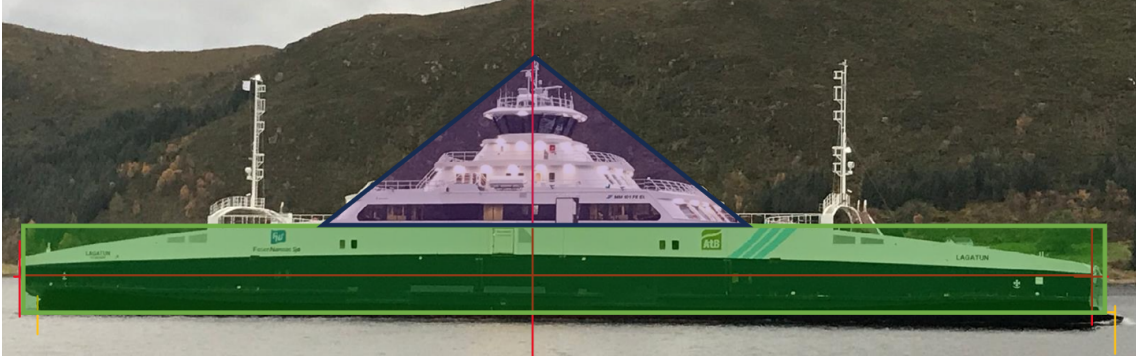
Figure 2.22: Ferry area above waterline

The height and length of the triangle and the rectangle were estimated using Microsoft PowerPoint. The L_{OA} of the ferries is known from Marine Traffic, and by measuring the L_{OA} in Microsoft PowerPoint, a ratio between full-scale and figure was found. Using this ratio, the dimensions of the rectangle and triangle were estimated. The dimensions are listed in Table 2.3.

Table 2.3: Estimations of the dimensions for the projected lateral and frontal area of the ferries. The ferry Lagatun is used in the figure and is from Marine Traffic.

	L [m]	H [m]	B [m]
Rectangle	107.53	9.25	17.2
Triangle	42.73	17.09	17.2

The implementation of the parametrical loading function for the longitudinal-force coefficient, CX_{A_F} was done in Python, and the results were compared to the paper for validation.

The plots and graphs from the paper were digitized using an online "plot digitizer". In Figure 2.23 the results from Blendermann's calculation (Blendermann, 1994) were digitized with three different plot-digitizers, and are labelled *Blendermann R.V computation1, 2, 3 from (fig.11)*. The calculation from the implementation of the parametrical loading function in Python is the red line and is labelled *Blendermann R.V with parametrical loading function*. The result from the implementation in Python (red line) and the results from the calculation in the paper (orange, yellow and green line) should match perfectly.

They have the same shape, however, after $CX_{A_F} = 0$, the results begin to differ with the maximum difference of $CX_{A_F} \approx 0.1$.
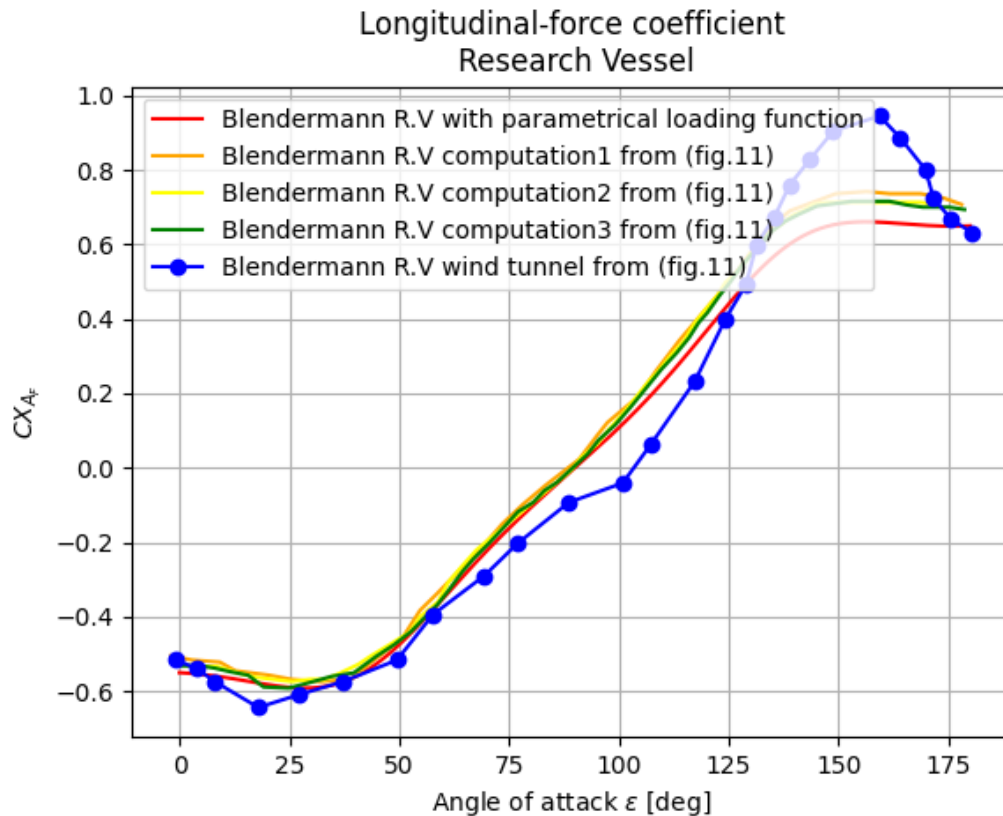
Figure 2.23: Comparison of the results from the calculation of CX_{A_F} from the Python implementation and the paper of Blendermann (1994) for a research vessel.

The longitudinal-force coefficient for the ferry Lagatun is seen in Figure 2.24. The force coefficient of Lagatun is calculated with parameters of different types of vessels from the table in figure 2.21 and compared with the ferry used by Blendermann (Blendermann, 1994). Blendermann's computation of CX_{A_F} for the ferry from his paper (the red line) corresponds almost perfectly with the calculation of CX_{A_F} for Lagatun with 'ferry' parameters (green line). However, both *Blendermann Ferry computation* and *Lagatun with 'ferry' parameters* have a deviation from the wind tunnel test of the ferry from his paper (Blendermann, 1994). As an attempt to try and match the wind tunnel test, the longitudinal-force coefficient for Lagatun was calculated with different vessel parameters, i.e., Ferry, Passenger liner, Speed boat and Fishing vessel, to see which have the better correlation with the wind-tunnel test.
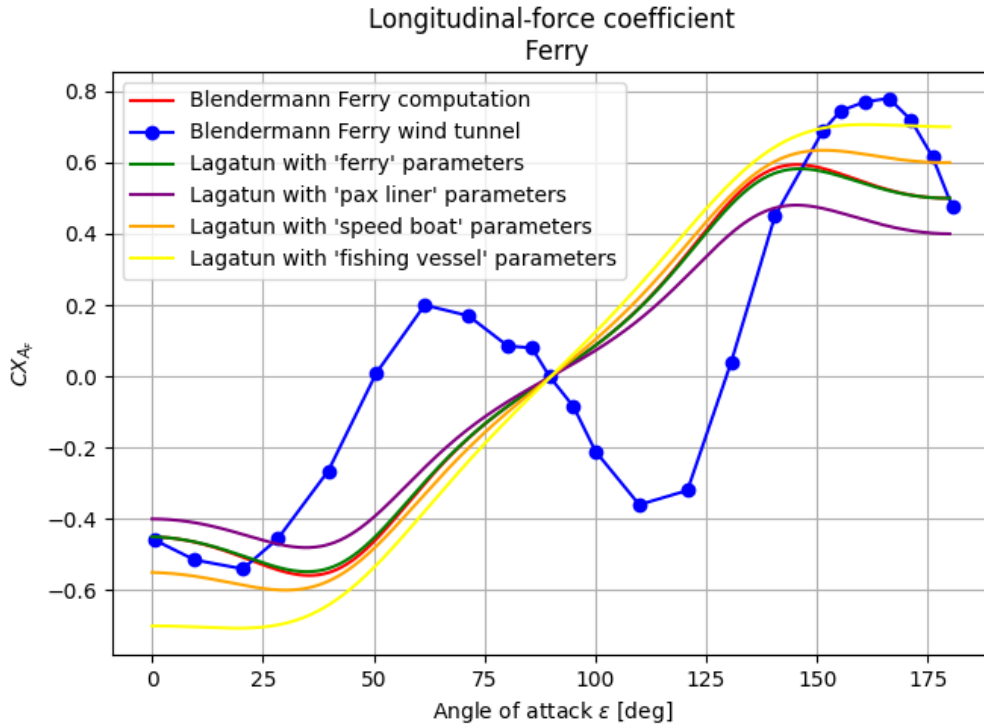
Figure 2.24: Comparison of the results from the calculation of CX_{A_F} from the Python implementation and the paper of Blendermann (1994) for the ferry Lagatun with different vessel-parameters
.

The Kendall's Taus correlation coefficient measures the relationship between two datasets which are not assumed to be linear or to follow any specific pattern, and is used to evaluate which of the different vessel parameters best correlates with the wind-tunnel test.

```
1  correlation coeff Ferry          : 0.5105625952496572
2  correlation coeff Passenger liner: 0.5105484162498538
3  correlation coeff Fishing vessel : 0.562361897247186
```

This indicates that the parameters for the fishing vessel better suit the estimation for the longitudinal-force coefficient for the Lagatun ferry. However, as the difference is less than 0.05 between using parameters for a Fishing vessel and a Ferry, the parameters were used.

2.2 Resistance model

The empirical resistance model is validated against data obtained from the shipping company of the ferries. During the wait for the data from the shipping company, the empirical resistance model was developed as a precautionary measure in case the required data could not be obtained.

The shipping company provided a CFD analysis, including a speed-power prediction based on the CFD calculations. The resistance has never been directly given. The resistance referred to as "CFD" in the plots in this section is the total resistance derived from the speed-power prediction by assuming a propulsive efficiency, η_D. A propulsive efficiency of $\eta_D = 0.7$ was assumed considering the ferries' Azipull and controllable-pitch propulsion system, known for its slightly higher efficiency.

To uphold the privacy and confidentiality of the ferries of the shipping company, the data has been anonymized by not showing any values of either the calculated resistance from the empirical model or the resistance derived from the CFD analysis. The plots in this section are presented to illustrate any conformity between the empirical models and the data from the CFD report.

29

2.2.1 Empirical model vs CFD analysis

The calm water resistance of the ferry was estimated using empirical models. The frictional resistance, hull roughness and form factor followed a standard procedure proposed by ITTC (2014). Air resistance was approximated using coefficients proposed by Blendermann (1994), and the residual resistance was determined using the Hollenbach method.

As discussed in the model explanation (2.1.2), Hollenbach is based on conventional ships such as tankers, container ships or bulk carriers, with block coefficients in the range of approximately 0.5 to 0.83. The ferry in this case has a block coefficient of 0.36, significantly outside this range.

Hollenbach's method for the mean residual resistance, assuming single-screw and design draft, has a certain validity range for entities i.e. the length, block coefficient, etc. The validity range of Hollenbach's method compared to the values of the ferry used in the case are seen in Table 2.4, where the values that are out of the validity range are highlighted in bold font. The ferry's values fall outside the validity range for $L/\nabla^{1/3}$, C_B, and B/T. The length-to-displacement ratio exceeds the range, whilst the block coefficient undershoots. This indicates that the ferry is more slender than the ships used to develop the Hollenbach method.

Table 2.4: Validity range of Hollenbach's method (mean resistance, single-screw, design draft) compared to the ferry used for the case.

	L [m]	$L/\nabla^{\frac{1}{3}}$	C_B	L/B	B/T	L_{os}/L_{wl}	L_{wl}/L	D_P/T
Hollenbach	[42.0, 205.0]	[4.49, 6.01]	[0.60, 0.83]	[4.71, 7.11]	[1.99, 4.00]	[1.00, 1.05]	[1.00, 1.06]	[0.43, 0.84]
Ferry	101.0	**8.183**	**0.36**	6.62	**4.469**	1.05	1.03	0.674

Although Hollenbach is not meant for ferries or other relatively slender vessels with lower values of C_B, the mean residual resistance was further calculated with Hollenbach and the ferry's C_B of 0.36 with the knowledge that the result most likely would be inaccurate. The decision to apply Hollenbach's method, despite its original design for different vessel types, was based on an initial assumption that frictional resistance would dominate the ferry's total resistance. In vessels like tankers or bulk carriers, frictional resistance can constitute up to 70-90% of the total resistance, particularly at lower speeds (MAN Energy Solutions, 2018). Given the ferry's average speed of 11.8 to 12 knots indicating neither a particularly slow nor fast-moving ferry, a first guess was that a significant portion of the resistance would consist of frictional resistance. Hence, the wave resistance resistance would not be of relative significance. This is later in the section proven to be an incorrect assumption.

Figure 2.25 compares the total resistance from the empirical model with the resistance derived from the speed-power prediction of the CFD analysis. The empirical model estimates a total resistance 34.28% lower than the resistance derived from the speed-power prediction from the CFD analysis. As Hollenbach is not meant to be used for vessels of such low block coefficients, the total resistance with the empirical model was also calculated by setting the block coefficient to the lower value of the C_B validity range for mean residual resistance, single-screw, design draft condition, namely $C_B = 0.6$. This resulted in a mean deviation from the resistance derived from the CFD analysis of approximately 42.24%. By setting C_B to the maximum value of the validity range of Hollenbach for the aforementioned condition, the mean deviation from the resistance derived from the CFD analysis became approximately 37.50%. From this it can be observed that by using the maximum value of Hollenbach's validity range for C_B the total resistance deviated less from the resistance derived from the CFD analysis than when using the minimum value of C_B's validity range.
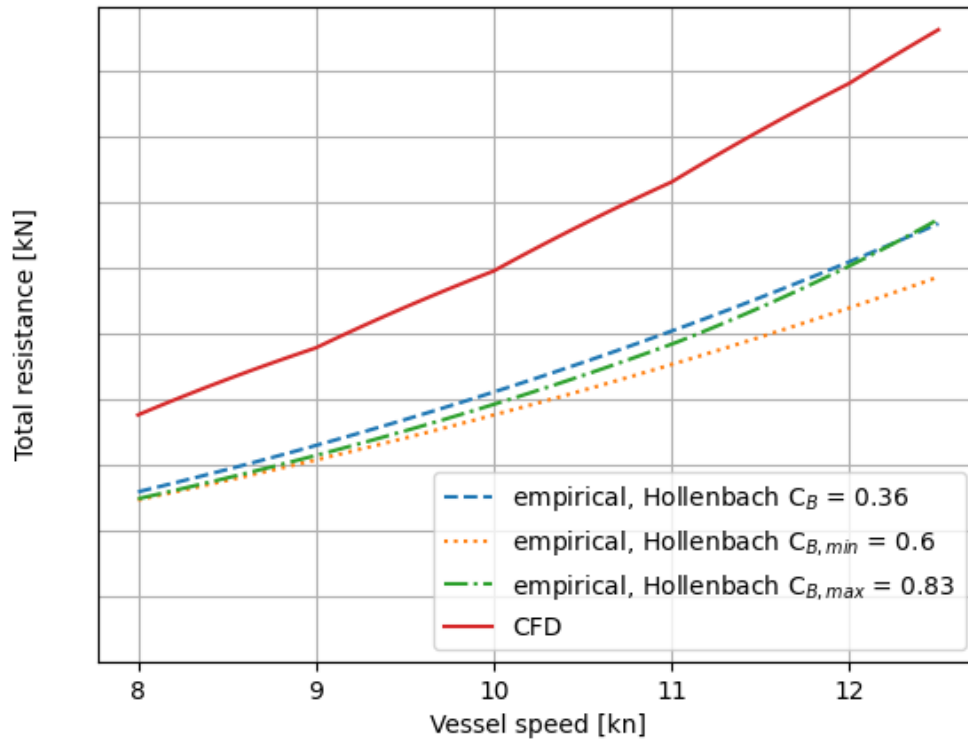
Figure 2.25: Comparison of the resistance calculations from the empirical model with the speed-power prediction from the CFD analysis from the shipping company for the min and max value for C_B's validity range in addition to the ferry's value of $C_B = 0.36$. The test condition for the speed-power prediction was Beaufort scale 2 in headwind, which equals a TWS of approximately 2.45 m/s and TWA = 0.0. The y-axis goes down to zero.

An explanation for why a C_B value significantly out of the validity range could result in a mean deviation from the total resistance from the CFD analysis less than both the minimum and maximum value for C_B for Hollenbachs validity range can be seen by analyzing the behaviour of the Hollenbach model for various values of C_B. There would be reason to believe that the minimum value of C_B's validity range would provide a result more close to the result when using of $C_B = 0.36$ than the maximum value of C_B's validity range. Figure 2.26 shows the shape of the mean residual resistance for the original validity range of C_B and how it changes when expanding the range to include the C_B of the ferry. It appears from Figure 2.26 that Hollenbach's method is developed such that the minimum value of the validity range (of C_B) results in a minimum mean residual resistance value. When evaluating the shape for a wider C_B range, including $C_B = 0.36$ for the ferry, the residual resistance is seen to have a convex shape. This means that very high and very low values of C_B result in high residual resistance with a minimum value for $C_B = 0.6$.

Using $C_B = 0.36$ and $C_B = 0.83$ in the Hollenbach model for mean residual resistance results in a smaller mean deviation from the total resistance based on the CFD analysis compared to $C_B = 0.6$. Knowing that $C_B = 0.83$ indicates a substantial contribution from residual resistance, there is reason to believe that the contribution of the residual resistance to the total resistance of the ferry is more significant than first anticipated. The result from comparing the results of the empirical resistance model and the total resistance derived from the speed-power prediction of the CFD analysis reveals a significant deviation. This supports the fact that Hollenbach should not be used for ship types not falling into the dimensional validity range specified by the method.
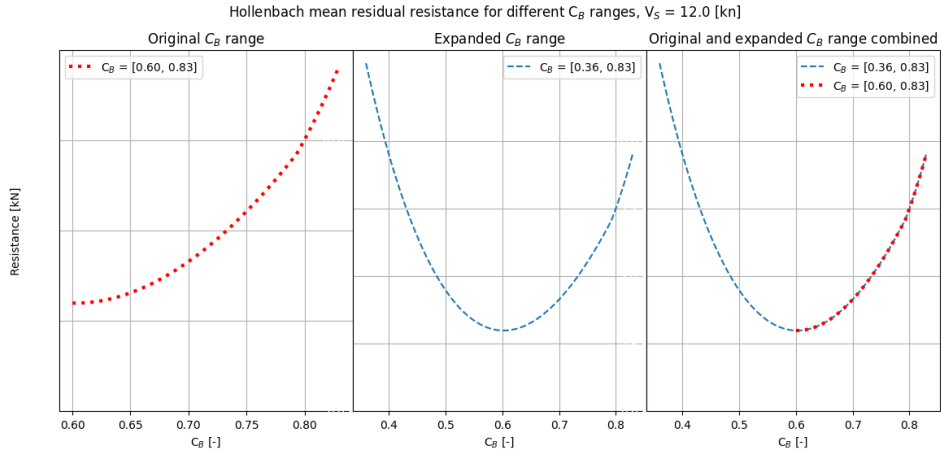
Figure 2.26: Hollenbach's mean residual resistance for various ranges of C_B. Original C_B range refers to the validity range of C_B for single-screw, design draft condition. The expanded C_B range is "stretched" to include C_B of the ferry. Vessel speed, $V_s = 12$ [kn]. The y-axis goes down to zero.

The different resistance component's contribution to the total resistance for $C_B = 0.36$ is shown in Figure 2.27. In this figure, the mean deviation of the total resistance from the empirical model and the total resistance derived from the CFD analysis is approximately 36%. For a vessel speed of 8.0 kn, the contribution from the frictional resistance, residual resistance and air resistance is 70.6%, 14.9% and 14.4% respectively. At $V_s = 8$ kn, the Froude number for the ferry is 0.129. From theory one can expect that the frictional resistance is the dominating part of the total resistance for such Fn values. The calculations from the empirical resistance model result in the frictional resistance contributing with ≈70% of the total resistance, while the wave making and air resistance contribute with 14.97% and 14.41% each, respectively.

```
1 contributions relative to empirical 8 kn:
2 relative contribution of frictional resistance : 70.60864376149009  %
3 relative contribution of air resistance        : 14.412693420984581 %
4 relative contribution of wave making resistance: 14.978662817525338 %
```

By increasing the vessel speed to 12.5 kn, the relative contribution of the frictional resistance increased from 14.97% to 22.14%, while the relative contribution of the frictional resistance decreased from 70.60% to 67.82%.

```
1 contributions relative to empirical 12.5 kn:
2 relative contribution of frictional resistance : 67.82615775210526  %
3 relative contribution of air resistance        : 10.030170247926671 %
4 relative contribution of wave making resistance: 22.143671999968074 %
```

From Figure 2.27 it is seen that the deviation between empirical resistance model and resistance predicted based on the CFD resistance increases for increasing vessel speed and Froude number.
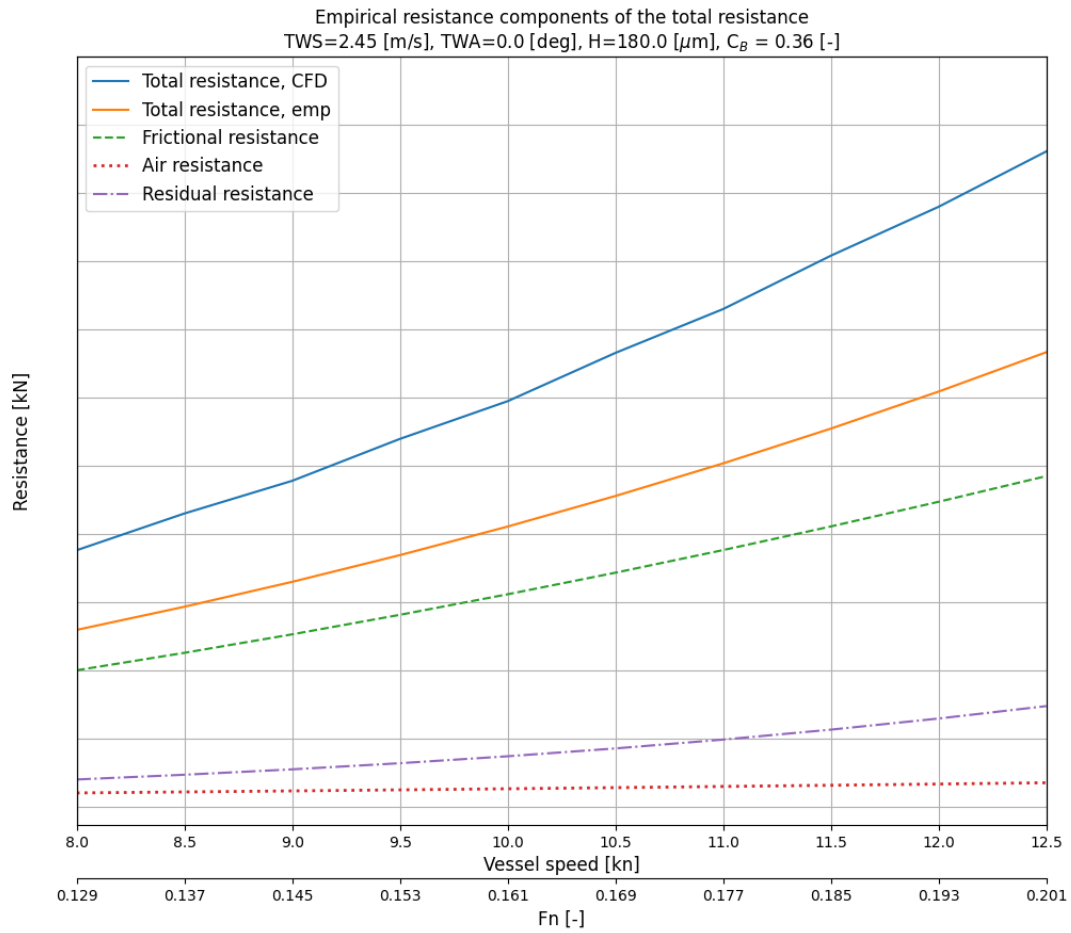
Figure 2.27: Resistance components' contribution to the empirical total resistance for vessel speed varying from 8 to 12 kn. Conditions under calculation were Beaufort scale 2 in headwind giving a TWS = 2.45 m/s, TWA = 0.0 deg. The hull roughness, H = 180 μm and C_B of the ferry equal to 0.36, and the propulsive efficiency η_D assumed equal to 0.7. The y-axis goes down to zero.

Figure 2.28 shows the empirical resistance components' contribution to the total resistance where the residual resistance is calculated for C_B = 0.36, 0.6 and 0.83 to illustrate their impact on the mean deviation of the total resistance from the CFD analysis. For the ferry's C_B of 0.36, the mean deviation of the total empirical resistance to the resistance based on the CFD analysis is approximately 34.28%. As the total empirical resistance deviates less from the resistance from the CFD analysis for the upper limit of C_B than the lower limit, it reason to believe that the residual resistance in fact has a significant contribution to the total resistance. The convex shape of Hollenbach's residual resistance when evaluated as a function of C_B, including values outside Hollenbach's validity range, where C_B = 0.6 serving as a base point (illustrated in Figure 2.26) highlight how this method is not meant for vessels with dimensions outside its validity range.
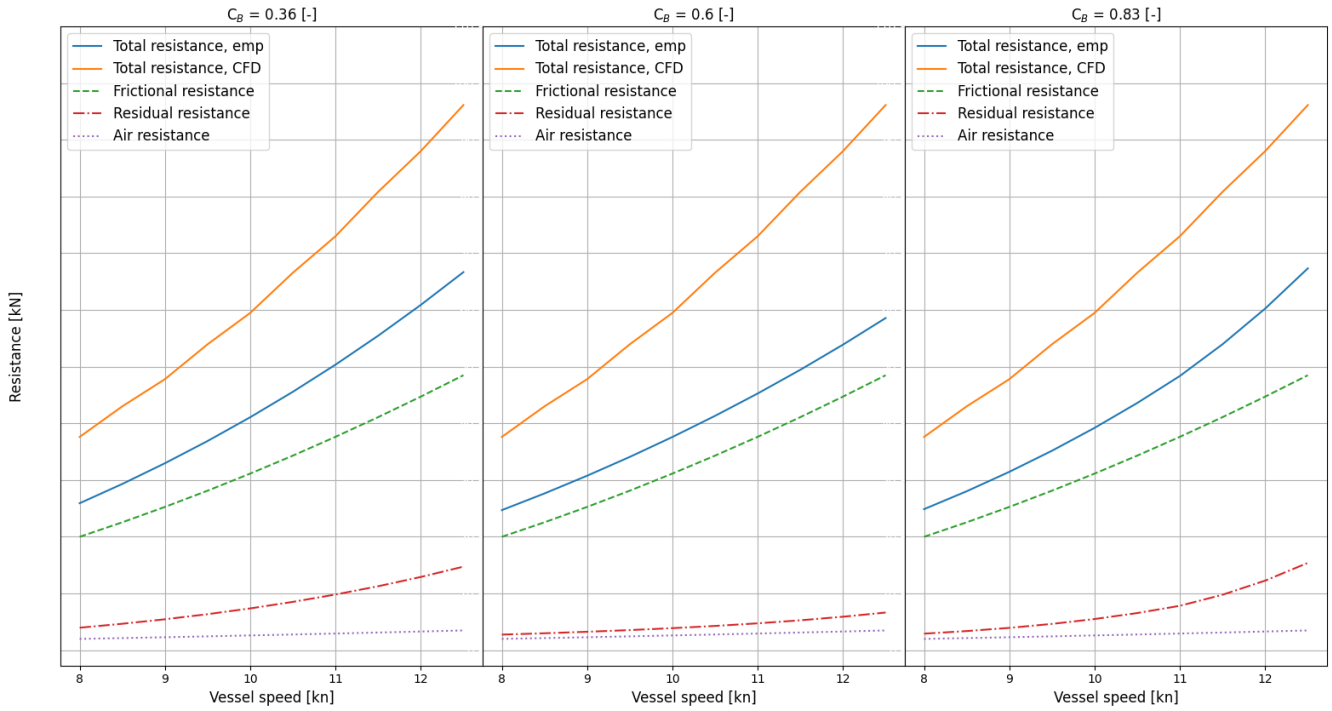
Figure 2.28: Empirical resistance components using the ferry's design C_B and the upper and lower value for the validity range of C_B for Hollenbach from the empirical model. The y-axis goes down to zero.

Chapter 3

Aerodynamics and FR model

3.1 Aerodynamics of Flettner Rotors

A Flettner rotor is a rotating vertical cylinder with endplates that generates lift by using the Magnus effect. When the air flows past the cylinder, the rotational motion of the cylinder generates a velocity difference between each side. This velocity difference generates a pressure difference, which again results in a lift and a drag force perpendicular and parallel to the flow, respectively. Figure 3.2 illustrates this pressure difference and the lift force generated by the Magnus effect of a Flettner rotor.

The name comes from the German engineer Anton Flettner who was the first to introduce a ship using rotating cylinders to generate lift for propulsive effect. In cooperation with several German and Swiss physicists and engineers, Anton Flettner refitted a schooner (a type of sailing vessel) seen in Figure 3.1 with two rotating cylinders.

Figure 3.1: Buckau, the first rotor ship. The Flettner rotors were refitted to a schooner. Figure from the United States Library of Congress's Prints and Photographs.
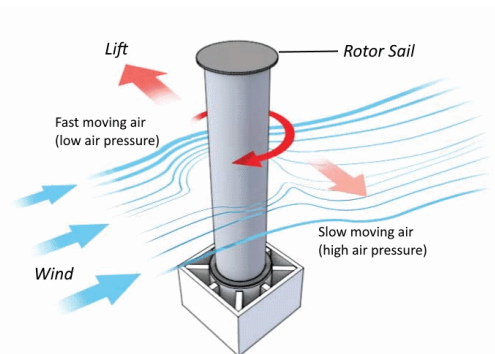
Figure 3.2: Magnus effect on a rotor sail generating a lift force acting perpendicular to the inflow. Figure courtesy to Korei (2017).

The flow phenomena around a 3D rotating cylinder include complex boundary layer theory and fluid dynamics. When using Flettner rotors as auxiliary propulsion on ships, one or more of the rotors are mounted on top of the deck. The rotational motion of the rotor is powered by an electric generator, and its rotational speed can be controlled to fit the sailing conditions.

As the ship is in motion and with wind from the open sea or fjord, the Flettner rotor will primarily operate in conditions with turbulent flow. In contrast to laminar flow where the flow is well organized into layers, turbulent flow mixes the layers via eddies and swirls. Its characteristics

are generally defined as irregular velocity and pressure that vary with high frequency (Faltinsen, 2006). The Reynolds number is commonly used to differ laminar and turbulent flow and the flow is typically defined as turbulent for a Reynolds number greater or equal to 1E+05. A Flettner rotor with a 5 m diameter operating at a wind speed of as little as 0.5 m/s will still have a Reynolds number of 1E+05,

$$Re = \frac{D\,U}{\nu} = \frac{5\,\mathrm{m} \cdot 0.5\,\mathrm{m/s}}{1.8E - 05} \approx 1.39E + 05,$$

where U is the free stream velocity, in this case, the wind speed, D the rotor diameter and ν the kinematic viscosity of air.

Literature on high Reynolds number flows around cylinders is easier to find on stationary cylinders. There appears to be a slight research gap on high Reynolds number flow around rotating cylinders. Research in this area is important to understand the generation of lift and drag and the rotor's behaviour for different spin ratios, Reynolds numbers and aspect ratios (Height/Diameter) to better control the rotors and optimize their performance under operation.

The performance of a Flettner rotor in terms of its ability to generate lift, can usually be described by the three key parameters

1. Spin ratio, SR

2. Aspect ratio, AR

3. End plate, d_e/D.

To get a better understanding and interpretation of the results from the Flettner rotor model, some of the findings about the behaviour of the lift and drag coefficient for varying spin ratios, aspect ratios and end plates from open literature about high Reynolds number flow around rotating cylinders will be discussed in the following.

The spin ratio (SR), also called the velocity ratio, is defined as the ratio between the tangential velocity generated by the rotation of the Flettner rotor and the local inflow velocity, giving the definition

$$SR = \frac{v_t}{u},$$

where v_t is the tangential velocity and u is the local inflow velocity.

Karabelas et al. (2012) performed a numerical study solving for the Reynolds-Averaged Navier–Stokes (RANS) via the finite-volume method and modified k-ϵ turbulence model. A similar numerical study was performed by Yao et al. (2016/10) with the fluid dynamic software FLUENT 6.3. Both studies showed similar results for the behaviour of the drag and lift coefficient for varying spin ratios and Reynolds numbers. Figure 3.3 from Yao et al. (2016/10) shows how the stagnation and separation points change for varying Reynolds numbers and spin ratios (α). The spin ratio in this paper is denoted α. As the spin ratio increases, the stagnation point is shifted downwards from the centerline. An explanation for this phenomenon is the addition of the

As the cylinder rotates clockwise, the tangential velocity from the motion of rotation and the tangential velocity from the free stream velocity will act in opposite directions on the surface of the lower side of the cylinder. This means that the upper side of the cylinder has co-flow, and the lower side of the cylinder has an adverse flow. When the magnitude of the tangential velocity components in the adverse flow becomes equal, they will cancel each other resulting in a total velocity equal to zero, which is seen on the surface as a stagnation point. This occurs at two points on the lower side of the cylinder surface. Figure 3.3 shows that the higher the spin ratio, the more dislocated the stagnation point on the lower surface. The higher the value of the spin ratio, the higher the magnitude of the tangential free stream velocity has to be to be able to equal the

tangential velocity from the spin ratio. The velocity of the free stream velocity increases towards a maximum as it reaches the bottom point of the cylinder surface.

Another thing to notice is how the increase in spin ratio inclines the wake area behind the cylinder downwards. As the lower side of the cylinder experiences an adverse flow, due to the cylinder's direction of rotation, the separation point on this side will occur for larger angles. The separation of the flow on the upper surface shifts more towards the centerline for increasing spin ratios. Meaning, that an increase of the spin ratio results in a decrease in the separation point on the upper side of the cylinder.

This can be summarized by: the front stagnation point and the rear separation point move towards each other for increasing spin ratios. As mentioned, when the spin ratio increases, the tangential velocity of rotational speed will increase, resulting in a continuously increasing velocity on the upper surface and decreasing velocity on the lower surface of the cylinder (given a clockwise rotation). As the velocity on the upper surface increases, the pressure on this side will decrease. For the lower side, the velocity decreases and the pressure increases. The result of this means that an increasing spin ratio results in an increasing upward lift force.
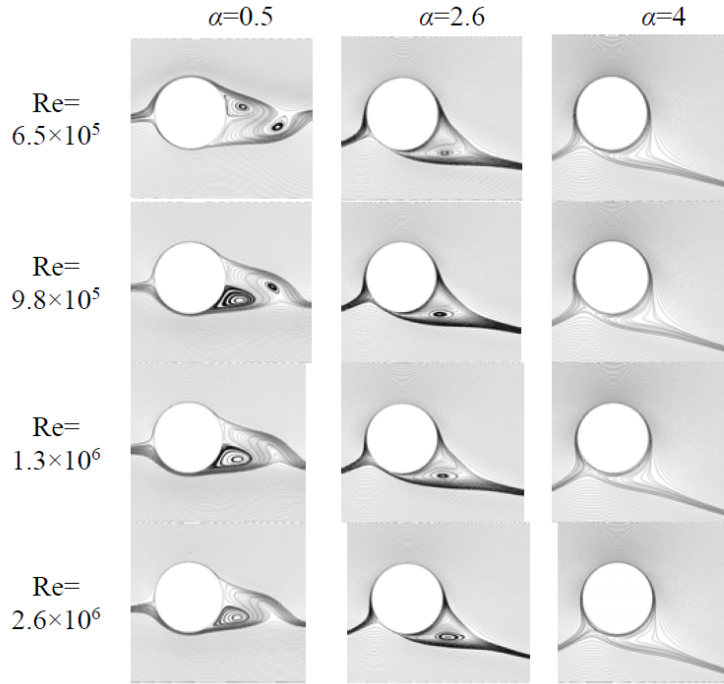
Figure 3.3: Flow fields for a stationary and rotating cylinder for varying spin ratio (here α) and Reynolds number, R_e. The flow is from left to right and the cylinder rotates clockwise. Figure courtesy to Yao et al. (2016/10).

Kutta-Joukowski's theorem gives a relation between the circulation of a flow and the lift coefficient for a 2D body. The circulation is a measure of the velocity component that is tangential to the path. Mathematically, this is defined as the line integral of a vector field around a close path. Given a vector field $\mathbf{V}$ and the surface S, this can be expressed as

$$\Gamma = \oint_{\partial S} \mathbf{V} \cdot \mathrm{d}\mathbf{l} = \iint_S \nabla \times \mathbf{V} \cdot \mathrm{d}\mathbf{S} = \iint_S \omega \cdot \mathrm{d}\mathbf{S}, \tag{3.1}$$

where ∇ is the operator representing the gradient, $\mathrm{d}\mathbf{l}$ is an infinitesimal line element of the boundary, $\mathrm{d}\mathbf{S} = \mathbf{n}\,\mathrm{d}S$ is the normal for an infinitesimal surface element of the boundary δS of the open surface S. The circulation can also be expressed with the flux of vorticity through the surface, $\omega = \nabla \times \mathbf{V}$. The vorticity is a measure of the local rotation of the fluid. Different from vorticity

which is a vector field that describes the local rotation rate of fluid particles, circulation is a scalar quantity that describes the overall fluid rotation around a closed loop or path.

Kutta-Joukowski's theorem then gives the lift per unit span, L', as

$$L' = \rho U \Gamma, \tag{3.2}$$

where ρ is the fluid density, U is the free stream velocity and Γ is the circulation defined in equation (3.1). The circulation for a cylinder whose surface area equals $2\pi R$, where R is the radius, then becomes

$$\Gamma = \int \int_S \omega \cdot d\mathbf{S} = \omega \cdot 2\pi R. \tag{3.3}$$

Inserting the result of equation (3.3) into Kutta-Joukowski's theorem (eq. (3.2)), the lift over the surface of a cylinder can be expressed as

$$L = \rho U \Gamma = \rho U \omega 2\pi R. \tag{3.4}$$

The lift coefficient then becomes

$$C_L = \frac{L}{(1/2)\,\rho\,U^2}, \tag{3.5}$$

where L is the lift defined in equation (3.4). The spin ratio, SR is the ratio between the tangential velocity/the circumferential velocity of the cylinder and the free stream velocity/inflow velocity

$$\text{SR} \quad \text{or} \quad \alpha = \frac{U_\theta}{U_\infty} = \frac{\Gamma}{U_\infty} = \frac{2\pi R \omega}{U_\infty}. \tag{3.6}$$

Using Kutta-Joukowski's theorem to express the lift in combination with the definition of the spin ratio from equation (3.6), one can see that the lift coefficient is proportional to the spin ratio

$$C_L \propto \text{SR}. \tag{3.7}$$

The aspect ratio is defined as the ratio between the rotor's height and diameter

$$AR = \frac{H}{D}.$$

The Flettner rotor is equipped with an end plate, also called Thom disc, at the top of the cylinder. The size of the end plate is often given as a ratio relative to the cylinder diameter

$$\frac{d_e}{D},$$

where D is the cylinder diameter and d_e is the diameter of the end plate.

3.2 Flettner Rotor

3.2.1 Apparent wind

The wind conditions experienced by a moving vessel are influenced by both the true wind speed and angle, and the vessel's own speed and direction. True wind speed (TWS) refers to the wind's speed in a stationary environment, while true wind angle (TWA) denotes the angle between the true wind direction and the vessel's heading.

Conversely, the apparent wind speed (AWS) and angle (AWA) describe the wind's perceived speed and direction from the perspective of the moving vessel. These factors are affected by the vessel's movement through the water relative to the true wind direction.

During upwind sailing, the apparent wind speed exceeds the true wind speed, and the apparent wind angle shifts forward in the direction of the vessel's motion. Conversely, when sailing downwind, the apparent wind speed is lower than the true wind speed, and the apparent wind angle shifts aft or backward.

A thorough comprehension of true and apparent wind dynamics is essential for optimizing sailing performance, maneuverability, and safety. Proper adjustments to the vessel's sails, heading, and course, accounting for changes in apparent wind conditions, can significantly enhance sailing efficiency, increase speed, and mitigate the risk of loss of control.

The relation between the true and apparent wind is illustrated in Figure 3.4.
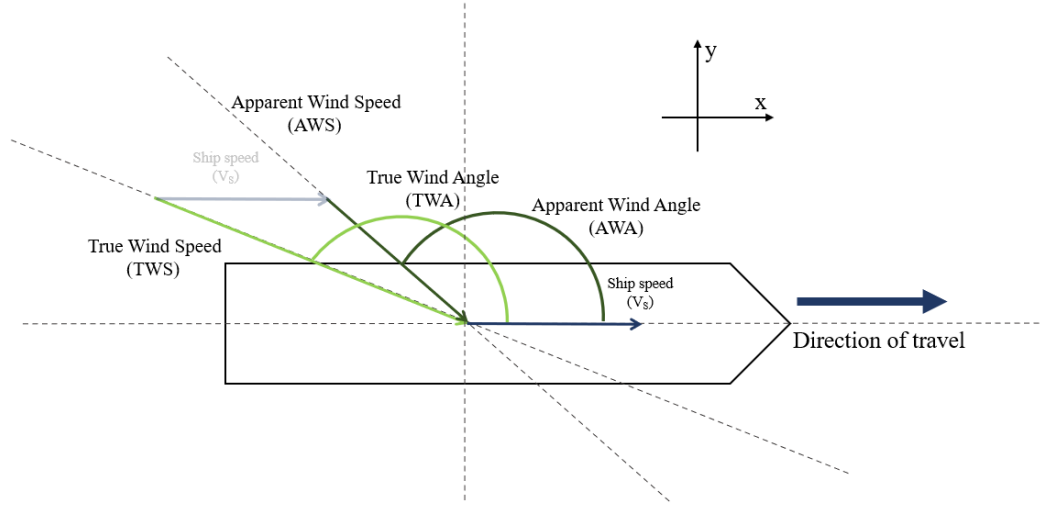
Figure 3.4: Illustration of apparent wind speed, AWS, and apparent wind angle, AWA

The AWS and AWA are defined using vector addition and geometry.

The true wind speed can be decomposed into an x- and y-component.

$$\text{TWS}_x = \text{TWS} \cdot \cos\left(\text{TWA}\right) \tag{3.8}$$

$$\text{TWS}_y = \text{TWS} \cdot \sin\left(\text{TWA}\right) \tag{3.9}$$

The apparent wind speed can further be expressed by the use of the x- and y-component of the true wind speed and the ship speed, V_s. Using vector calculus, the apparent wind speed and angle can be expressed as in equations (3.12) and (3.13).

$$\text{AWS}_x = \text{TWS} \cdot \cos\left(\text{TWA}\right) + V_s \tag{3.10}$$

$$\text{AWS}_y = \text{TWS} \cdot \sin\left(\text{TWA}\right) \tag{3.11}$$

$$\text{AWS}^2 = \text{AWS}_x{}^2 + \text{AWS}_y{}^2$$

$$\text{AWS}^2 = \text{TWS}^2 \cdot \cos^2\left(\text{TWA}\right) + 2 \cdot \text{TWS} \cdot \cos\left(\text{TWA}\right) \cdot V_s + V_s{}^2 + \text{TWS}^2 \cdot \sin^2\left(\text{TWA}\right)$$

$$\text{AWS} = \sqrt{\text{TWS}^2 + V_s{}^2 + 2 \cdot \text{TWS} \cdot \cos\left(\text{TWA}\right) \cdot V_s} \tag{3.12}$$

$$\text{AWA} = \arctan\left(\frac{\text{AWS}_y}{\text{AWS}_x}\right) = \arctan\left(\frac{\text{TWS} \cdot \sin\left(\text{TWA}\right)}{\text{TWS} \cdot \cos\left(\text{TWA}\right) + V_s}\right) \tag{3.13}$$

The AWA is calculated using arctan, which returns a value between $[-\pi, \pi]$. To ensure positive values for the AWA, all negative values are transformed to their corresponding positive value by adding 2π.

Figure 3.5 shows how the apparent wind speed decreases towards a minimum for an apparent wind angle of 180°. At an AWA of 180°, the vessel is moving in the opposite direction than the wind.
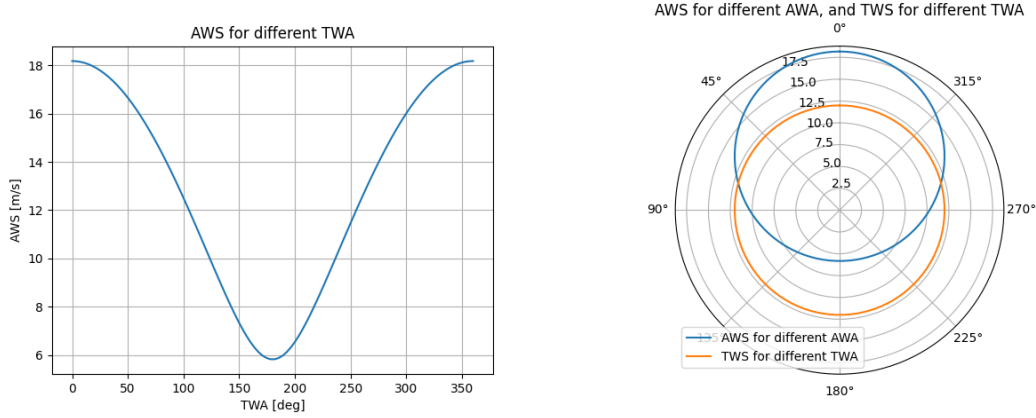
Figure 3.5: Apparent wind speed and apparent wind angle for true wind angle from 0° to 360°. TWS = 12 [m/s] and V_s = 12 [kn].

3.2.2 Wind gradient

The speed and heading of the vessel are not the only factors affecting the wind speed and direction experienced by the sails.

The wind speed increases with height above the earth's surface. The wind speed gradient accounts for the increase in wind speed as the distance from the surface of the earth increases. The surface of the earth creates a boundary layer, called the atmospheric boundary layer, such that the wind speed decreases with proximity to, and roughness of, the surface. The wind speed's variation within the atmospheric boundary layer is for engineering purposes often approximated using a power law (Kaltschmitt et al., 2007) i.e.,

$$\text{TWS}(z) = \text{TWS}_{10} \left(\frac{z}{z_0} \right)^\alpha, \tag{3.14}$$

where α is the power law exponent, also known as the Hellmann coefficient. TWS_{10} is the wind speed at 10 m above the surface, and z_0 is the distance at which TWS_{10} was measured, in this case, 10 m. The height above the surface where the wind speed is wanted is then found by setting the value for z.

3.2.3 Sail forces and governing equations

Figure 3.6 illustrates the definition of the coordinate system. The AWS and AWA create a drag force acting parallel or in line with the apparent wind. The drag force, D, is defined as positive when acting in the negative x-direction. Perpendicular to the drag force, there exists a lift force represented by L. The lift and drag force can be used to express the thrust and side force produced by the sails.
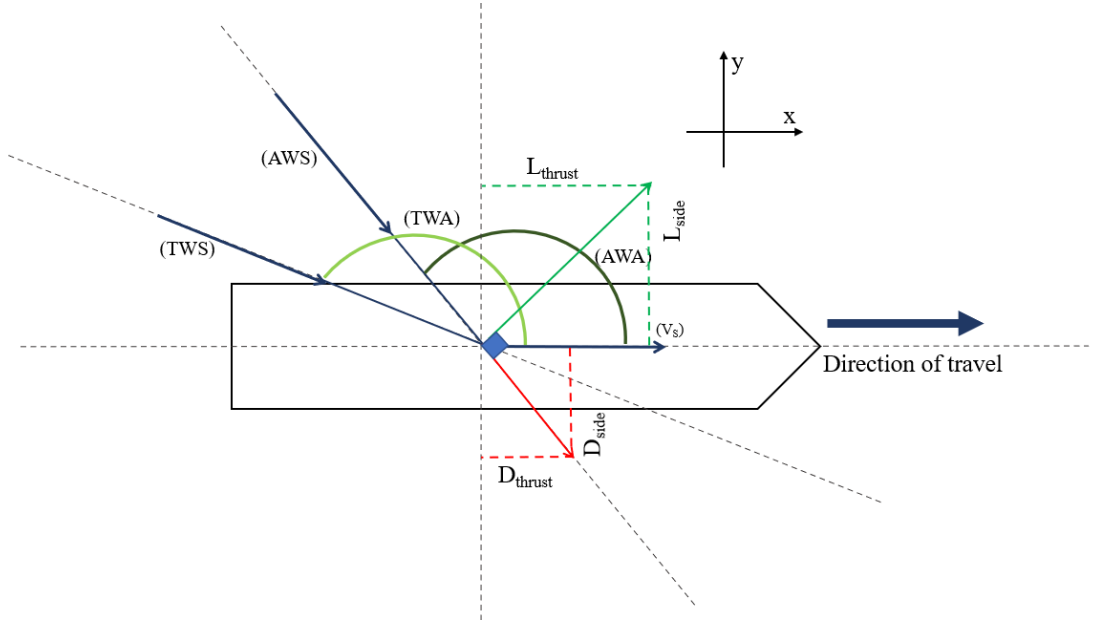
Figure 3.6: Definition of the coordinate system and positive direction of travel.

$$T = L_{thrust} - D_{thrust} \quad \Rightarrow \quad T = L \sin\left(\text{AWA}\right) - D \cos\left(\text{AWA}\right) \tag{3.15}$$

$$S = D_{side} + L_{side} \quad \Rightarrow \quad S = D \sin\left(\text{AWA}\right) + L \cos\left(\text{AWA}\right) \tag{3.16}$$

The thrust and side force are found from the lift, L, and drag, D. The lift and drag are found from equations (3.17) and (3.18), and the lift and drag coefficients, c_L and c_D given in equations (3.19) and (3.20). Based on results from CFD analysis performed by Li et al. (2012), Tillig and Ringsberg (2020) fitted polynomials based on these results corrected to better fit full-scale measurements. The full-scale measurements were performed on a cruise ferry equipped with single 4×24m Flettner rotor. Force transducers were used to measure the thrust and side force, while the power consumption was measured as the power needed to rotate the rotor.

$$L = \frac{1}{2} c_L \rho_{\text{air}} A_{\text{sail}} \, \text{AWS}^2 \tag{3.17}$$

$$D = \frac{1}{2} c_D \rho_{\text{air}} A_{\text{sail}} \, \text{AWS}^2 \tag{3.18}$$

$$c_L = -0.0046\,\text{SR}^5 + 0.1145\,\text{SR}^4 - 0.9817\,\text{SR}^3 + 3.1309\,\text{SR}^2 - 0.1039\,\text{SR} \tag{3.19}$$
$$c_D = -0.0017\,\text{SR}^5 + 0.0464\,\text{SR}^4 - 0.4424\,\text{SR}^3 + 1.7243\,\text{SR}^2 - 1.641\,\text{SR} + 0.6375 \tag{3.20}$$

The power and thrust coefficient is given as

$$c_P = 0.0001\,\text{SR}^5 - 0.0004\,\text{SR}^4 + 0.0143\,\text{SR}^3 - 0.0168\,\text{SR}^2 + 0.0234\,\text{SR}, \tag{3.21}$$

$$c_T = \frac{T_{\text{sail}}}{1/2\,\rho_{\text{air}}\,A_{sail}\,\text{AWS}^2}, \tag{3.22}$$

where T_{sail} is the thrust force generated from the sails. SR is the spin ratio, which refers to the ratio of the tangential speed of the rotor and the speed of the local incoming wind. The spin ratio is given in equation (3.23), where AWS is the apparent wind speed, R_R is the rotor radius and ω

is the rotational speed of the rotor in [rad/sec]. The rotational speed of a Flettner Rotor is often given in rotations per minute [rpm], which equals $2\pi/60.0$ [rad/sec].

$$SR = \frac{\omega R_R}{AWS} \tag{3.23}$$

The spin ratio of a Flettner Rotor with constant TWS, and ship speed, V_S, for varying apparent wind angles are seen in figure 3.7a. The spin ratio reaches its maximum at an AWA of 180°. As seen in figure 3.5, is when the AWS has its minimum. Figure 3.7b shows how the spin ratio has a maximum when the apparent wind speed is lowest, which corresponds with the observations of the relation between the apparent wind speed and angle and spin ratio in figures 3.5 and 3.7b.

(a) Spin ratio for varying AWA   **(b)** Spin ratio for varying AWS
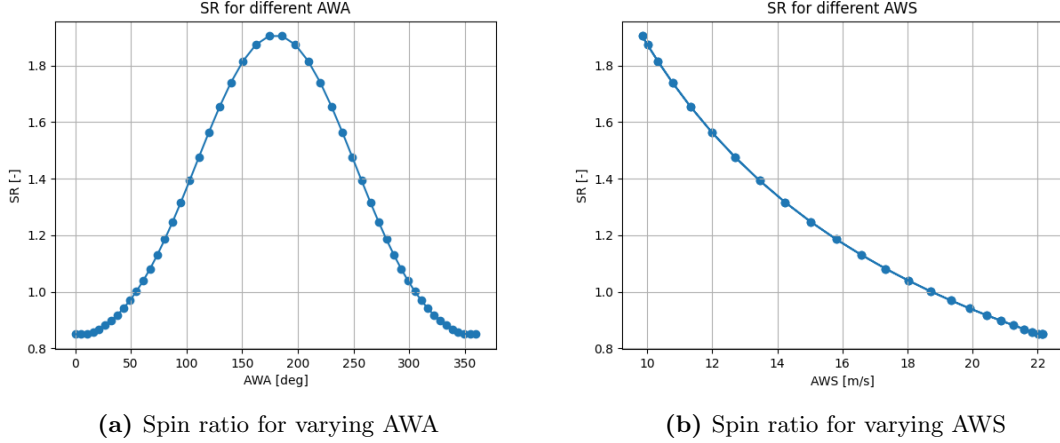
Figure 3.7: Spin ratio for varying AWA and AWS with constant TWS and ship speed V_s.

3.2.4 RPM optimization

The optimization of the rotational speed of the Flettner rotors is based on the procedure presented in the paper of Tillig and Ringsberg (2020). Interaction between the superstructure and rotor sails is not taken into account during this optimization.

To minimize the required propeller thrust and maximize the potential thrust generation from the Flettner rotors, the rotational speed of the rotors is adjusted and optimized for the given weather and sailing conditions. The rotational speed of each rotor is optimized in two steps where the initial rotational speed for each wind and sailing condition is the one that maximises the net power of the rotor itself, i.e.,

$$\arg\max\left\{P_{\text{netRotor}}(\text{SR}) = (c_T(SR) - c_P(SR))\frac{1}{2}\rho_{\text{air}}A_{\text{sail}}\text{AWS}^3\right\}, \tag{3.24}$$

where c_P and c_T are the power and thrust coefficient respectively. They are both functions of the spin ratio, SR, and are polynomials given in equations (3.22) and (3.21).

The initial optimal rotational speed is hence the rotational speed for each given apparent wind speed and angle that maximizes equation (3.24). The thrust of the sails is then calculated using this initial rotational speed. If the thrust with the initial rotational speed exceeds the vessel resistance, i.e.

$$T_{\text{sail}} > R_T, \tag{3.25}$$

the rotational speed is iteratively reduced until the condition no longer is true. This is the second step of the optimization procedure and is only performed if condition (3.25) is true.

3.3 Validation of Flettner Rotor model

The Flettner rotor model was validated by comparison between results presented in Tillig and Ringsberg (2020) for the same operating conditions.

To ensure a valid implementation, a comparison between the model from Tillig and Ringsberg (2020) was compared to the implementation in this thesis through personal contact with one of the authors. The comparison in seen in Figure 3.8 where the model for the Flettner rotor forces from Tillig and Ringsberg (2020) is labelled *F. Thies*, and the model implemented in this thesis is labelled *Wangen*.

From the comparison between the models in Figure 3.8 it is seen that the models perfectly align for spin ratios up to approximately 3. Through communication with one of the authors, it was mentioned that due to continous improvements in the model pressented in their paper *Design, operation and analysis of wind-assisted cargo ships* (Tillig and Ringsberg, 2020), the Flettner rotor model had been slighly modified. This explains the discrepancy in the values for the thrust coefficient for spin ratios greater than approximately 3.
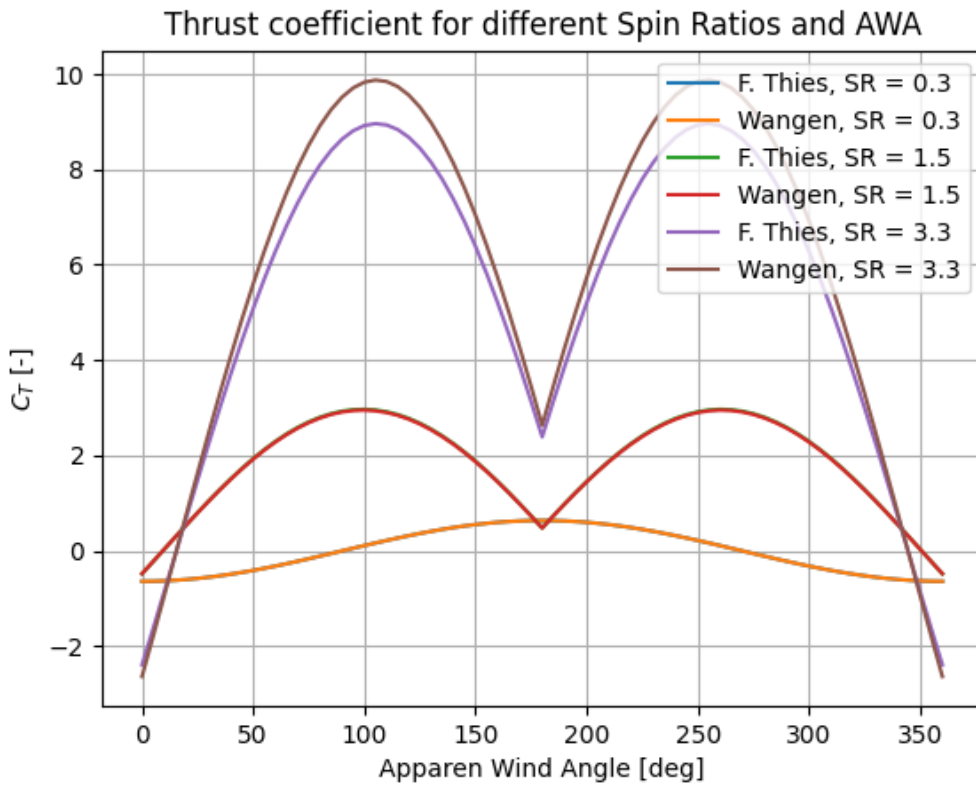
Figure 3.8: Validation of thrust coefficient, C_T for varying AWA and SR. *F. Thies* denotes the model from Tillig and Ringsberg (2020) and *Wangen* denotes the model developed and implemented in this thesis.

Chapter 4

Batteries and battery model

4.1 Battery theory and modelling of lifetime

This section gives a brief introduction to the relevant theory needed for understanding the general behaviour modelling of a marine battery.

In a lithium-ion battery, ions move between the positive and negative electrodes during the charging and discharging processes as visualised in Figure 4.1. With repeated cycles of charging and discharging, the battery's ability to accumulate ions at the negative electrode (where some of the chemical reactions occur) will gradually decline. This degradation is referred to as a reduction in the battery's capacity, meaning it can hold less charge over time. This natural process is inherent to the chemistry of lithium-ion batteries (DNV, 2016).
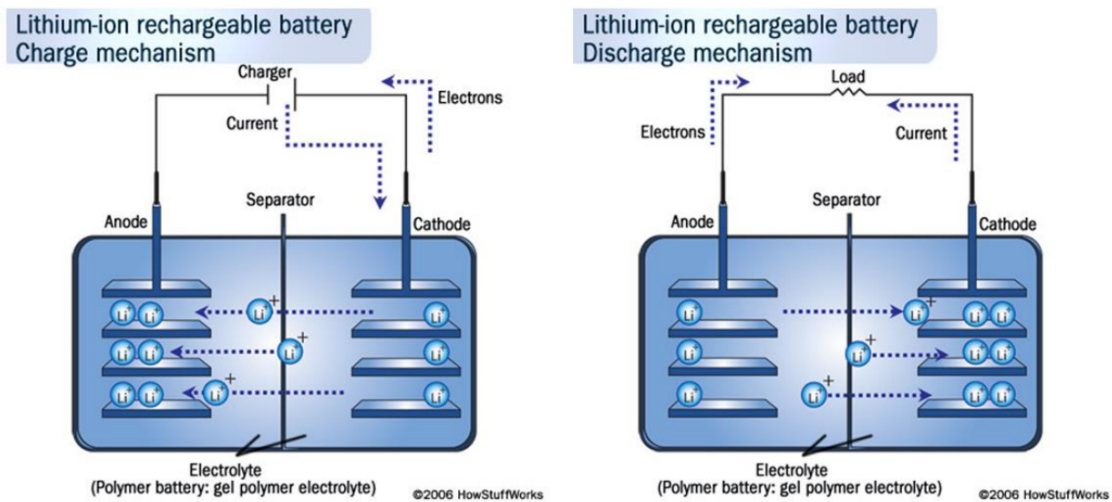
Figure 4.1: The basic components of a lithium-ion battery from DNV (2016).

A battery's cycle life is referred to the number of complete charge-discharge cycles it can perform before the nominal capacity diminishes to less than 80% of its initial rated capacity (VerLab) (Ellingsen et al.). This threshold, where the battery's capacity falls below 80%, is considered the end of its useful life (Fox, 2014). The Depth of Discharge (DoD) is a metric that reflects the proportion of a battery's total capacity that has been utilized in each charging and discharging cycle compared to its usable capacity. For example, a DoD of 80% means that only 80% of the battery's total capacity is utilized during each cycle. This leaves a buffer of 20% unused capacity to extend the battery's longevity. DoD is seen to have a prominent effect on the lifespan of the

battery. Monitoring and managing the DoD is essential in battery management systems to optimize performance and prolong the battery's operational life (DNV, 2016).

4.1.1 Battery Degradation and Lifetime Reduction

Several factors contribute to battery degradation. Temperature, and the DoD are the two most significant contributors. The optimal temperature for a lithium-ion battery ranges from 15-30°C. The temperature changes according to the seasons. The DoD on the other hand is to some extent subject to control. As mentioned above, the DoD is the percentage of the rated capacity of a battery that has been discharged or utilized during a specific partial cycle. It represents the amount of energy taken from the battery relative to its total capacity during a given discharge event. High currents, substantial DoD fluctuations, and continuous charging and discharging from empty to full results in accelerated degradation DNV (2016).

While certain key factors influencing battery lifespan are known, the development of accurate models remains challenging. Nevertheless, DoD has demonstrated a notable correlation with battery longevity (Kalogirou, 2017). The relationship between DoD and the cycle life of a typical lithium-ion battery is illustrated in Figure 4.2. Knowing the battery capacity and the DoD, it is possible to give an estimate on the effect of the cycle life of the battery.

It is worth to notice the values along the y-axis in Figure 4.2. For a change in DoD from 0-10%, the cycle life has decreased from 1 000 000 to below 400 000. The relationship appears to be logarithmic (Guo et al., 2015) (Striebel et al., 2004), however another source claim the relationship is reciprocal but drawn on a logarithmic paper (VerLab). For recreational purposes in this case, a logarithmic relation provides a sufficient depiction of the data's behavior.
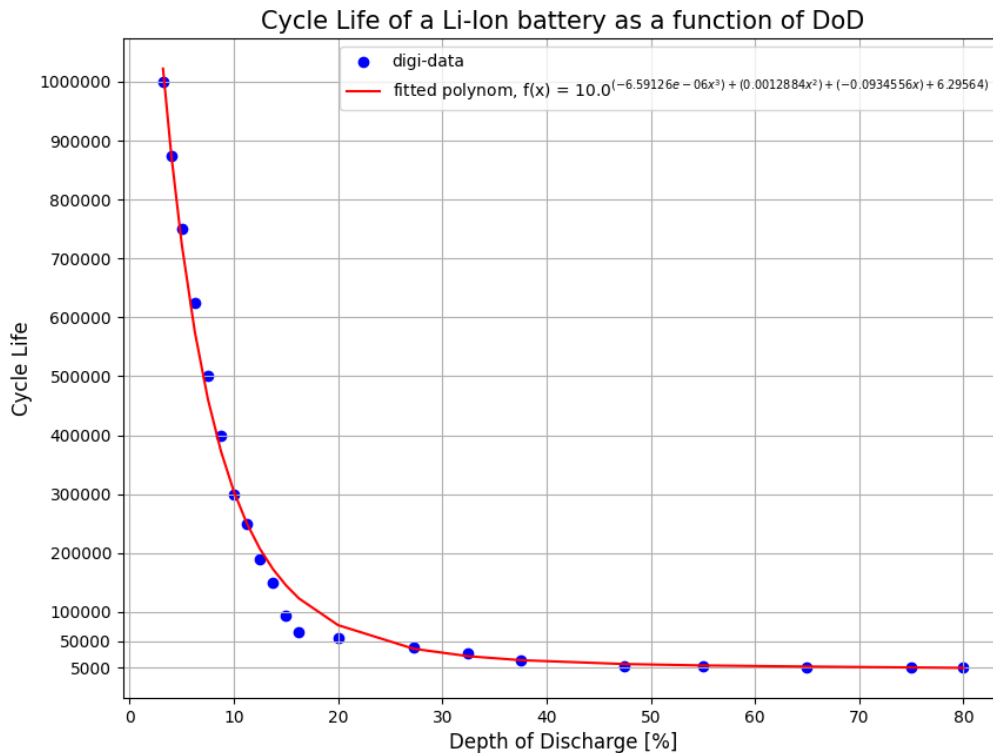
Figure 4.2: Relation between the DoD and battery cycle life based on Kalogirou (2017)

The DoD of the ferry is calculated by the amount of power consumed per crossing divided by the

total battery capacity, i.e.,

$$\text{DoD} = \left(\frac{\text{Power Consumed Per Crossing}}{\text{Total Battery Capacity}} \right) 100\%. \qquad (4.1)$$

Using the curve from Figure 4.2 and equation (4.1), it is possible to derive a very simplified model for this otherwise complex system. The inclusion of this very simplified model is only to get an indication of the effect the sail forces can have on the battery by easing the load on the propeller and the energy consumption of the ferry as a whole.

The polynomial for the curve in Figure 4.2 is expressed in (6.1.2), and was found by creating a third order function that was forced to go through four chosen data points on the curve from Kalogirou (2017). The data points were read from a similar figure from Kalogirou (2017) showing the relationship between cycle life and DoD, and are referred to as "digi-data" in Figure 4.2. The code for fitting the polynomial is found in Appendix B.1.

$$f(x) = 10.0^{\left(-6.59126e-06x^3 \right) + \left(0.0012884x^2 \right) + \left(-0.0934556x \right) + 6.29564 \right)} \qquad (4.2)$$

Modelling Change in Battery Cycle Life

The battery change in the battery cycle life can be estimated by evaluating the change in DoD. Figure 4.2 is based Kalogirou (2017), and illustrate the typical relationship between the cycle life and DoD of a typical Li-Ion battery. By calculating the derivative of the function, it is possible to get an estimate of the change in cycle life due to a change in DoD. A 3rd order polynomial was fitted to the curve that expresses the relationship between the battery cycle life and DoD from Kalogirou (2017).

To estimate the effect changing the DoD has on the cycle life, the derivative of the fitted polynomial in equation (6.1.2) is used, i.e.,

$$\frac{d}{dx}f(x) = e^{x\left(-0.0000151769\,x^2 + 0.00296665\,x - 0.215189 \right)} \left(-89.9384\,x^2 + 11720.2\,x - 425071 \right). \qquad (4.3)$$

Chapter 5

Wind data

5.1 Wind Data and Sources

This thesis studies the use of rotor sails as auxiliary propulsion on an electric ferry connecting Flakk to Rørvik in Trondheimsfjorden. A proper analysis requires a good comprehension of the wind conditions in the fjord and along the ferry connection. This section elaborates on the sources of the wind data used in the case in addition to analysis and an investigation of the influence of the fjord's geometry on the wind speed and direction.

The wind data is collected from the publicly available measurements from OceanLab Observatory (SINTEF OceanLab) within the time frame of one year, 25th of November 2022 to 25th of November 2023. The data is sourced from the Munkholmen and the Ingdalen buoy in Trondheimsfjorden, which are located on either side of the ferry connection. Figure 5.1 shows the location of the sensors with the ferry connection Flakk-Rørvik in the middle. The distance from the sensors to Flakk is $\approx$ 8.9 km and $\approx$ 12.6 km for sensors Munkholmen and Ingdalen respectively.
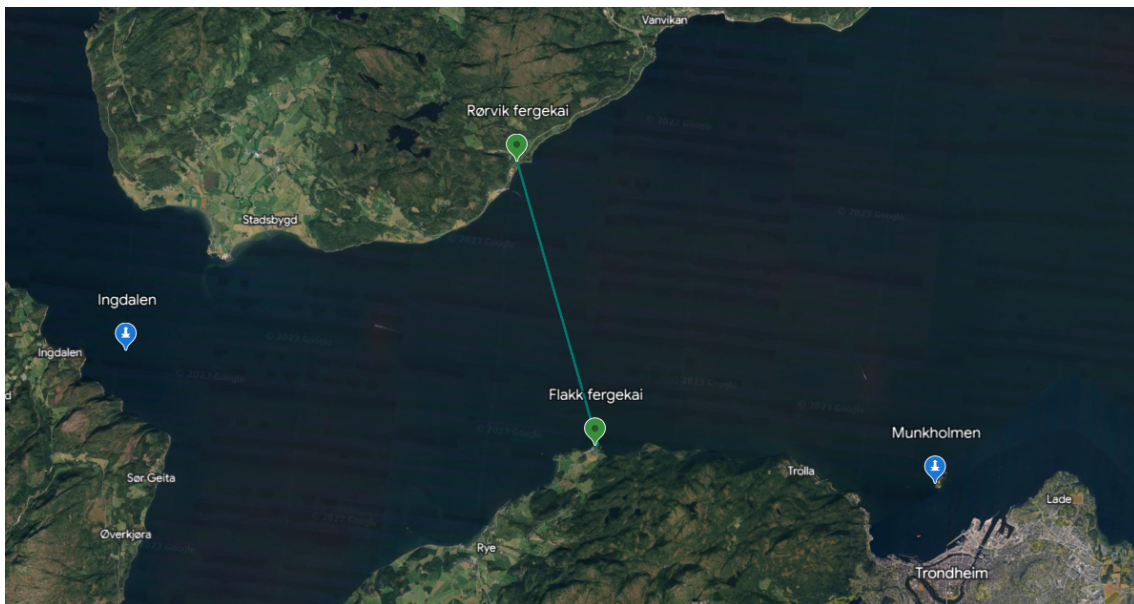
Figure 5.1: The Munkholmen and the Ingdalen sensor, located at each side of the ferry connection Flakk-Rørvik (green line).

Both buoys measure several entities, among others salinity, temperature and wind. The buoys are both provided by Hydrosphere (2023) and are seen in Figure 5.2. The buoy at Munkholmen was

deployed in October 2021, while the buoy at Ingdalen was deployed in May 2022.

(a) Buoy located at the Munkholmen site

(b) Buoy located at the Ingdalen site
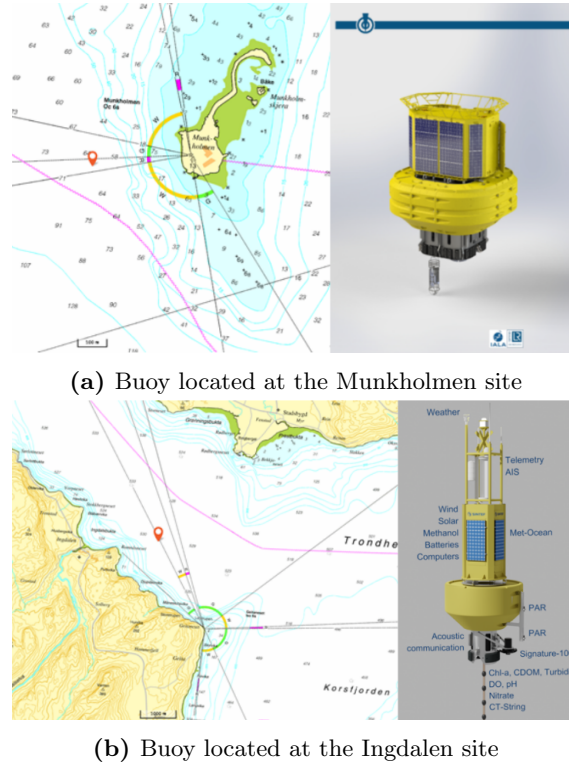
Figure 5.2: The buoys delivered by Hydrosphere (2023) located at the Munkholmen and Ingdalen site. Figures from OceanLab Observatory SINTEF OceanLab.

5.1.1 Wind Data Analysis

Wind data from the two buoys has been collected from the time range of November 2022 to November 2023 with a sampling frequency of 10 minutes. The buoy at Ingdalen has some downtime which has been filtered out. The downtime is during the winter months, starting from end of November 2022 until end of February 2023. This sensor is stationed more at open sea compared to the sensor at Munkholmen which is to some extent sheltered by Byåsen to its east and the Munkholmen island to its west. Through personal contact with OceanLab, it was discovered that the main reason for the downtime of this sensor was due to hardware updates. It is also worth mentioning, that by filtering out measurements from these months the results may underestimate the real potential of the Flettner Rotors as its during these months that the rotor's may produce most power (Lu and Ringsberg, 2020) (Chou et al., 2021). The power produced by a Flettner Rotor is a function of the wind speed to the power of three. This means that even smaller changes to the wind speed impact the power outcome.

In this section, the wind data is being analyzed when the measurement points at the timeframe where the Ingdalen sensor is down also is filtered out for the Munkholmen. This is to create an equal data basis. Additionally, a secondary analysis is conducted on all the data collected by the Munkholmen sensor to account for the influence of the winter months.

The distribution of wind speeds and directions is illustrated in Figure 5.3 for Ingdalen and Figure 5.4 for Munkholmen. The wind speed data appears to align better with a Weibull distribution than with a normal Gaussian probability distribution. The Weibull distribution displays a mean wind speed of approximately 4.3 m/s for the sensor located at Ingdalen and 4.9 m/s for the buoy at Munkholmen. By comparing the wind measurements of the two sensors, it is also seen that Munkholmen has a higher frequency of measurements of wind speeds between 4-6 m/s than Ingdalen which in return has a wider distribution with a longer tail. The wind direction was fitted using a Kernel Density Estimate (KDE) to visualise the underlying distribution of the results. KDE is a

non-parametric method that uses the observed data points to estimate the underlying probability density function. Mathematically, KDE can be expressed as

$$f(x) = \frac{1}{n \cdot h} \sum_{i=1}^{n} K\left(\frac{x - X_i}{h}\right),$$

(5.1)

where $K(x)$ is the kernel function, $X_1, X_2, ..., X_n$ are the data points, $f(x)$ is the KDE at a given point, x, and h is the bandwidth of the kernel function chosen as the weighting function (Drapala, 2023) (Waskom., 2023).

The post-processing of the results is done in Python where the KDE is found using the data visualization library "seaborn" (Waskom, 2021). Seaborn defaults to a Gaussian method for determining the smoothing bandwidth, hence also used here.

The mean wind direction from the measurements of the Ingdalen sensor is at 195.80°, while Munkholmen measured a mean wind direction of 186.04°. The wind measurements from the Ingdalen sensor display distributions that include more disturbances, which may indicate a more inconsistent measuring or bad data quality.
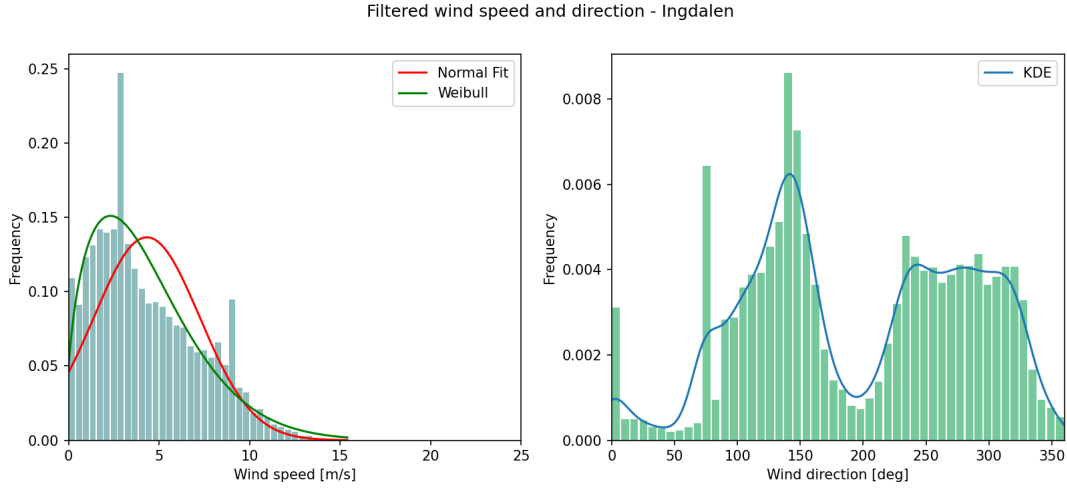
Figure 5.3: Distribution of filtered wind speeds and directions measured from the Ingdalen sensor from November 2022 to November 2023, where the downtime between November 25ht 2022 - February 21st 2023 is filtered out.
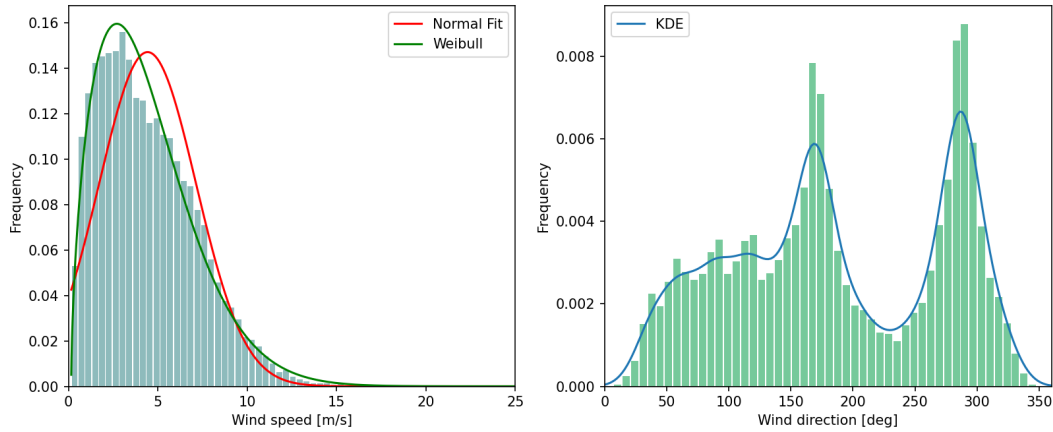
Figure 5.4: Distribution of filtered wind speeds and directions measured from the Munkholmen sensor from November 2022 to November 2023, where the timeframe for the downtime of the Ingdalen sensor between November 25ht 2022 - February 21st 2023 is filtered out.

Figure 5.5 show the wind measurements as windroses. From the figures it is seen that the Ingdalen sensor indicate more frequent wind coming from S-E, while the Munkholmen sensor indicate a more frequent wind coming from W/N-W, but also S. It is also worth noting that the colour scale on the figures Figure 5.5a and Figure 5.5b display different wind speed intervals. The darkest blue colour for the Ingdalen sensor is the wind speed interval 0.0-3.1 m/s, while for Munkholmen the darkest blue contains wind speed in the range 0.2-7.8 m/s. It appears that the directions of the wind for the different sensors can be explained by looking at the geometry of the fjord and its branches.
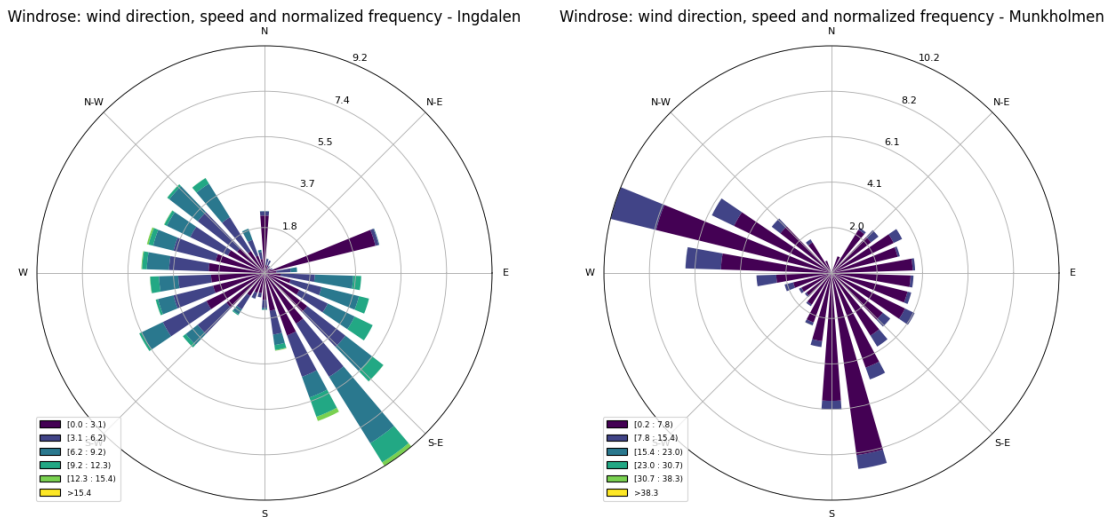
(a) Windrose, data from Ingdalen sensor

(b) Windrose, data from Munkholmen sensor.

Figure 5.5: Windroses of the data measured from the sensor at Ingdalen and Munkholmen.

Figure 5.6 illustrate how the branches of the fjord impact the direction the wind blows to. The windroses in Figure 5.6 is pi rotated to show where the wind blows to whereas the windroses in Figure 5.5 show the direction the wind blows from. It appears that the geometry of the fjord has a funneling effect on the wind and the wind direction follows the fjord's branches. It is seen that the sensor at Ingdalen has a significant frequency of the wind blowing N-E, into the branch between

Lensvik and Hasselvika, which is leading out to the coast of Norway. The majority of the rest of the wind appears to be directed towards Trondheimsfjorden. The Munkholmen sensor is placed more in a "bay", slightly sheltered by Byåsen to its east. However, it is also seen here that the wind has a tendency of blowing in the direction to the branches of the fjord.

It appears that Munkholmen contains higher frequency of measurements of slightly higher wind speeds than Ingdalen. One might think that the wind measured at the sensor at Munkholmen benefits from the funneling effect on the wind speed from the fjord-branches leading into Trondheimsfjorden.
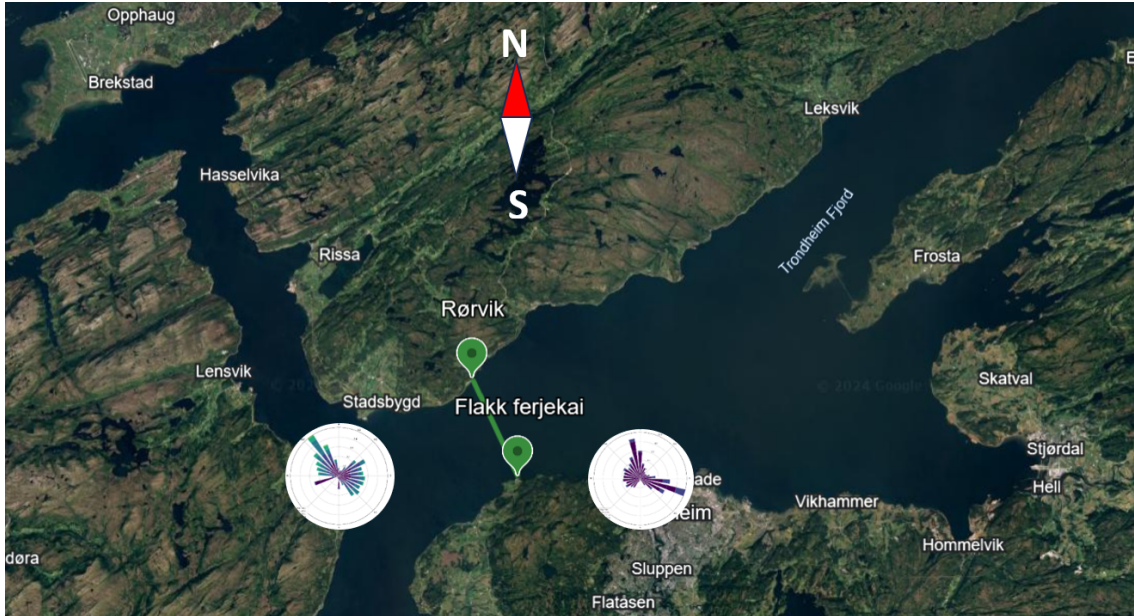
Figure 5.6: Windroses indicating the frequency of wind speed and direction the wind blows, based on measurements from the sensor at Ingdalen and Munkholmen in Trondheimsfjorden.

Seasonal variations have an impact on the weather and wind patterns. The generation of power by Flettner rotors depends on both wind speed and wind direction. The rotor power is a function of the wind speed to the power of three, hence higher wind speeds yields more power generated. Figure 5.7 illustrates the temporal dynamics of the wind speed measurements recorded by the sensor located at Munkholmen over a one-year period, spanning from November 2022 to November 2023. The dataset is partitioned into four distinct quarters, each representing a three-months interval. Each box represents the interquartile range (IQR) of wind speed values, where the central line denotes the median. The horizontal lines are the whiskers, which extend to 1.5 times the IQR and represent the data range, i.e., the minimum and maximum value within the given distance from the lower and upper quartiles. Any outliers beyond this range are individually marked. Breaking down the measurements into quarters allows for examination of the seasonal patterns and its impact on the wind speed throughout the given timeframe. From the figure it can be seen that the colder months, November - March, have a greater value for the median of about 5.3 m/s. The "warmer" months April - October have an approximately 30% lower median of approximately 3.8 m/s. Regarding only power generation and wind speeds, the measurements indicate that the "colder" months of November - March to be beneficial as they appear to serve higher wind speeds.
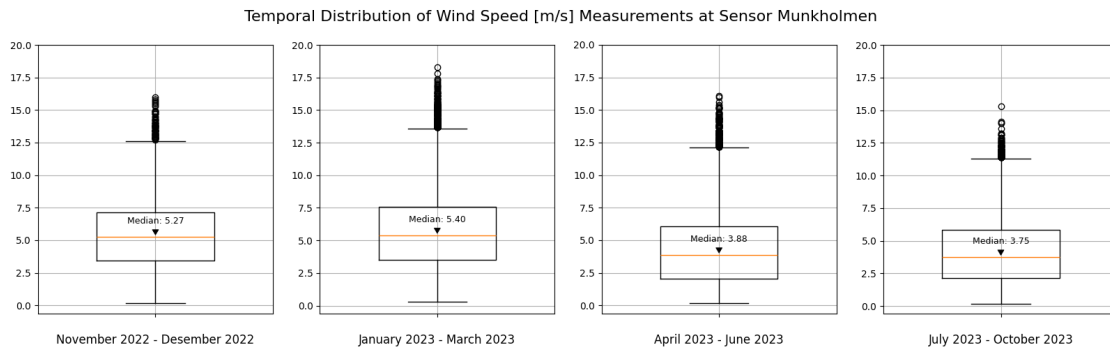
Figure 5.7: Box plot of the wind speed measured by the sensor at Munkholmen from November 2022 to November 2023 divided into quarters consisting of 3 months.

The sensor located at Ingdalen is missing data between 25th of November until 21st of February. The two most left boxes in Figure 5.8 for November 2022 - December 2022 and January 2023 - March 2023 thus contains only 3528 and 2545 measurements respectively. Comparing the amount of datapoints to the remaining quarters which contain between 12 036 and 17 566 measurements, the quarters November 2022 - December 2022 and January 2023 - March 2023 contain on average 80% less measurements. This means that the measurements from the sensor at Ingdalen during the months late November 2022 until late February must be interpreted with caution, as the reduced data density during this period may impact the overall representativeness and statistical robustness of the observed wind patterns. By comparing the measurements of wind speed from Munkholmen in Figure 5.7 with Figure 5.8 it is clearly seen that the measurements between January 2023 - March 2023 from the measurements at Ingdalen suggests observations opposite of those seen by the measurements from Munkholmen of the same period. This highlights the importance of cross-validation to reduce the potential of systemic biases by using more than one data source.
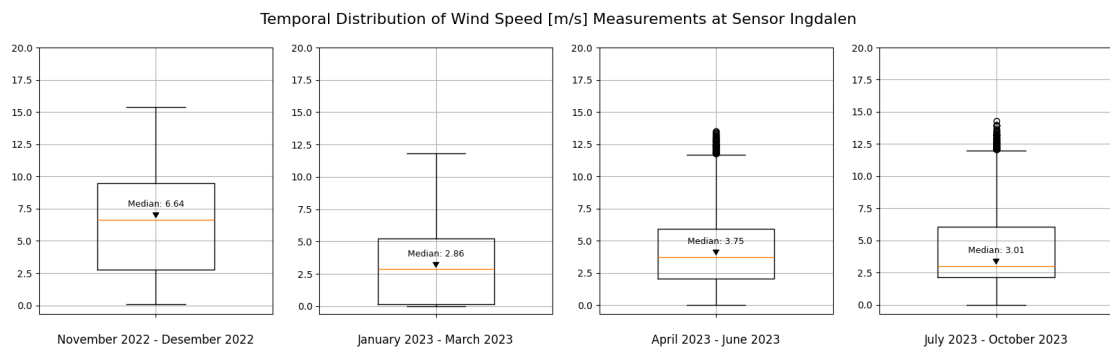
Figure 5.8: Box plot of the wind speed measured by the sensor at Ingdalen from November 2022 to November 2023 divided into quarters consisting of 3 months.

Quality and reliability of the wind data

The data collected by the sensors were 10 minutes averages resulting in 114 measurement point from each sensor every 24 hours. The 10 minute averaging smooths out any potential fluctuations or noise in the measurements. This time interval also captures some of the important details and features of the wind at the specific location without creating an unmanageable large dataset.

The sensor at Ingdalen has some downtime as seen in Figure 5.9. The reason for the downtime was explained to be due to hardware changes. These downtimes has been filtered out of both the datasets, to ensure consitencity and easier comparison of the results based on the different wind data sets. As seen in Figure 5.9, it is the winter months December, January and February where the sensor is down. The winter months typically has rougher weather and thus higher wind speeds. To evaluate the effect of the Flettner rotors also during these months, a second analysis

has been performed only on data from the Munkholmen sensor as it does not have any downtime and includes wind measurements of these of all months between November 2022 - November 2023.
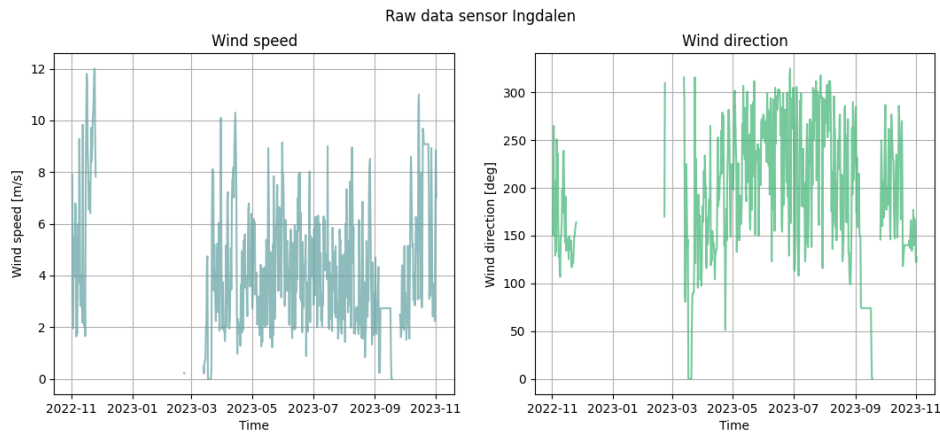
Figure 5.9: Raw data from sensor Ingdalen. Space indicates sensor downtime.

Regarding reliability of the wind data, it should have been compared to a another source. For an even more detailed analysis, the averaging intervals could have been reduced to include and capture even more of the details characteristics of the wind. Ideally would both the sensors have provided continuous data for the entire period November 2022 - November 2023.

True wind angle relative to vessel heading

The vessel's heading relative to the geographic coordinate system must be taken into account. The vessel is assumed to have two different headings depending on whether the route is sailing from Flakk to Rørvik or from Rørvik to Flakk. Using the longitude and latitude of both of the ferry wharves, the vessel headings are found as the azimuth angle between Flakk and Rørvik as the start and end points. The true wind speed is hence

$$\text{TWA} = \text{TWA} - \text{vessel heading}.$$

Chapter 6

Case study

To study the objectives of the thesis, a case study has been performed on a battery ferry sailing along the route Flakk-Rørvik in Trondheimsfjorden. In reality, there are two ferries operating along this route. Assuming that the ferries are identical, the case study will only be performed on one of them. The relevant technical information about the ferry is summarized in Table 6.1.

Table 6.1: The ship specifics of the ferry. Height refers to the height up to deck where the Flettner rotors are placed, A_F and A_L refers to the frontal and lateral area of the ferry's superstructure.

$\mathbf{L}_{pp}$ [m]	Breadth [m]	Height [m]	Hull Roughness [μm]	$\mathbf{A}_F$ [m^2]	$\mathbf{A}_L$ [m^2]
107.53	15.24	13.0	180	140.97	994.6525

The ferry route has a length of 7.4 km, and takes about 25 minutes with approximately 5 minutes at each berth for disembarking and embarking of new passengers and cars. The ferry connection consists of two ferries which crosses on average ≈39 times every day during the week. Each ferry crosses 46 times at the most and 34 times at the least.

The resistance used in the case is estimated from the CFD analysis performed on the hull, where air resistance on the superstructure is added using Blendermann's method (Ch.2, section 2.1.3) and hull roughness according to equations (2.10).

The case is performed for two wind datasets. One containing wind data from February 21st 2023 - 25th of November 2023 collected from both sensor Ingdalen and Munkholmen. The other dataset contains measurements only from Munkholmen, but includes the entire measurement periods to see the effects on the power generation due to the higher wind speeds during the winter months.

The case is performed for three different rotor sizes based on the Flettner rotors provided by Norsepower (2022) to evaluate which is most beneficial for balancing the generation of power, size and impact on the cycle life of the battery. The rotor specifics are listed in Table 6.2.

Table 6.2: Various rotor sizes for the Flettner rotors used in the case. Values from Norsepower (2022).

	Height [m]	Diameter [m]	Max rotational speed [RPM]	Electric motor nominal power [kW]
Rotor 1	18.0	4.0	225.0	60
Rotor 2	24.0	4.0	225.0	80
Rotor 3	30.0	5.0	180.0	115

6.1 Objective and assumptions

6.1.1 Objective

To evaluate the efficiency and effect of using Flettner rotors on the ferry, two Key Performance Indicators (KPIs) are defined

1. Saved Propeller Power, i.e., the amount of power saved in the ferry's propulsion system from the assistance provided by the Flettner rotors. This is measured by looking at the reduction in power consumption in kW compared to the scenario without Flettner rotors.

2. Change in Depth of Discharge of the Battery, i.e., quantifying the impact of the Flettner rotors on the overall battery energy consumption and usage.

6.1.2 Assumptions

Flettner rotor model:

- valid for AR = 6

- valid for max SR = 5

- valid for $d/d_e = 2$

- interaction between sail and superstructure is disregarded

- added resistance from drift and rudder angles is disregarded
  $\rightarrow$ in some cases the added resistance is greater than the benefit from additional thrust, hence sail should be reefed. These cases are not evaluated.
  $\rightarrow$ sail forces may need to be reduced due to high side forces hence added resistance on the rudder due to sailing with a drift angle.

- sail forces were calculated based on the semi-empirical expressions based on a combination of CFD results from Li et al. (2012) and full-scale measurements (see Section 3.2).

- initial RPM is optimized for each given wind and sailing condition to a value that maximizes the net rotor power of the rotor itself (see Section 3.2.4)

- Thrust from the sails can never be greater than the resistance of the ferry. If so, the RPM of the rotor is reduced until this condition no longer is True.

- Rotor RPM can never be less than 0.

Resistance model:

- Resistance derived by assuming a propulsive efficiency of $\eta = 0.7$ from the speed-power prediction of the hull performed on one of the ferries in the preliminary design phase.

- ITTC's standard procedure for added resistance due to hull roughness (see Section 2.1.1)

- air resistance on the superstructure approximated with coefficients from Blendermann (1994) using ferry parameters

$$R_T = \frac{\eta_D \, P_D}{V_s} + R_{\Delta C_F} - (-R_{air}). \tag{6.1}$$

Route simulation:

- using weather data measurements from each of SINTEF's buoys separately in the route simulation

- the timeframe for the downtime in the sensor located at Ingdalen is also filtered out for the sensor at Munkholmen (referred to as Sensor Ingdalen and Sensor Munkholmen).

- the case is also performed when the data from the sensor at Munkholmen is not filtered out (referred to as Sensor Munkholmen Unfiltered).

- vessel heading calculated using azimuth angle using coordinates from the starting and stopping point of the ferries along the connection Flakk-Rørvik and Rørvik-Flakk.

Battery

- relationship between cycle life and DoD from Figure 4.2 is based on Kalogirou (2017)

- the aforementioned relationship is fitted by the 3rd order polynomial

$$f(x) = 10.0^{\left(-6.59126e-06x^3\right)+\left(0.0012884x^2\right)+\left(-0.0934556x\right)+6.29564}$$

- total battery capacity of 2.1 MWh = 2100 kWh

6.2 WASP model

The case study was performed using Python. Classes were made for the various resistance components and the rotor sail and its forces. The weather data was obtained from the publicly available measurements from each of the buoys (Observatory, a) (Observatory, b). The data was post-processed to filter any bad data or downtime from any of the buoys.

The vessel headings along the ferry connection are calculated as the azimuth angle using the longitude and latitude for each of the ferry wharves and are given in Table 6.3.

Table 6.3: Vessel headings used in the case, calculated as the azimuth angle between each of the ferry wharves.

Route	Start point (Lat, Long)	End point (Lat, Long)	Azimuth angle [deg]
Flakk-Rørvik	(63.451, 10.201)	(63.509, 10.139)	334.7
Rørvik-Flakk	(63.509, 10.139)	(63.451, 10.201)	154.7

Each of the modules in Python was combined in a main file that together calculates the power obtained from the rotor sails in addition to the required propeller power with and without the rotor sails. A simplification of the WASP model is illustrated in the Flowchart on the next page.
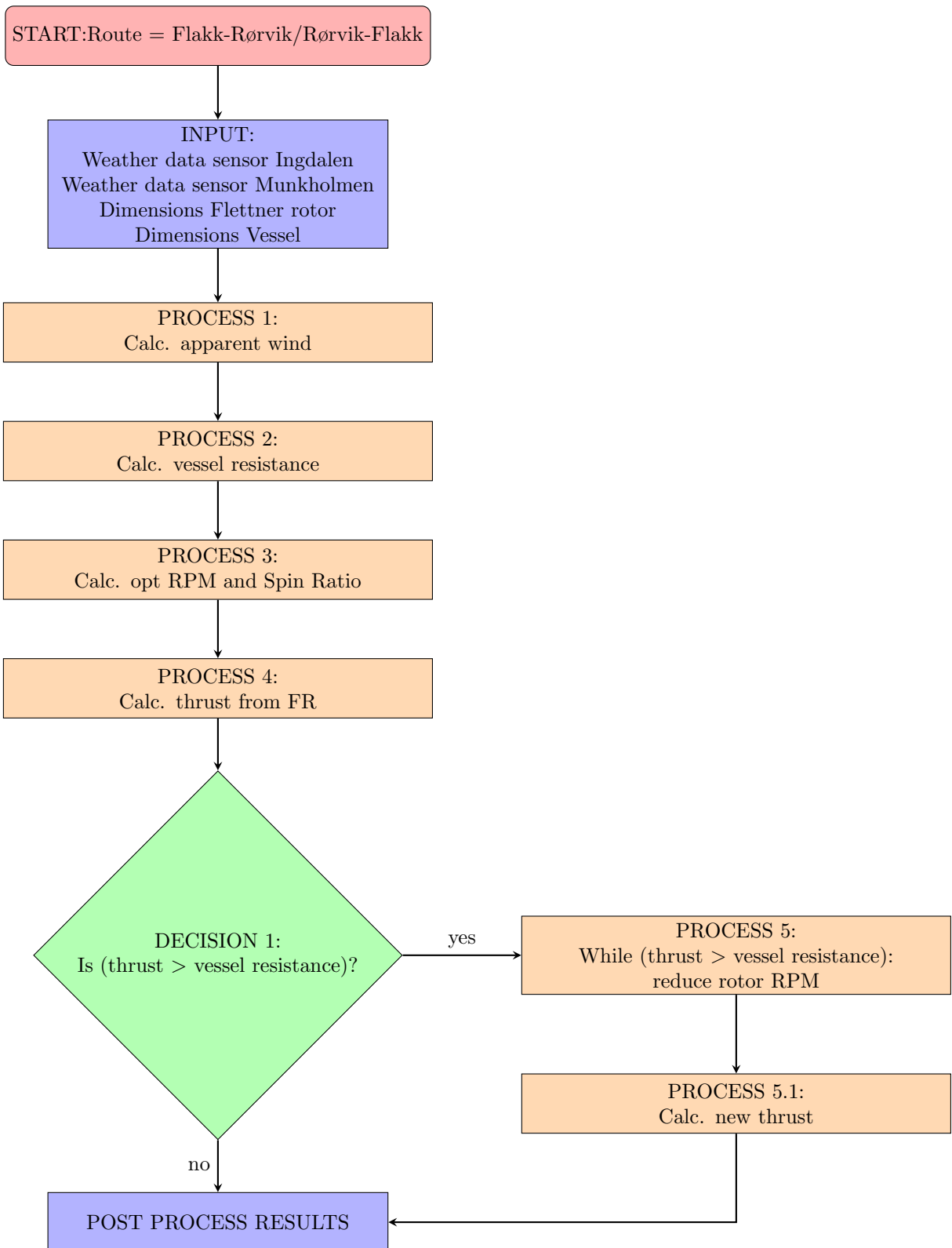
Chapter 7

Results

This section presents the results of the case study of power generation of Flettner rotors using weather data from sensors located at either side of the ferry connection *Flakk-Rørvik*. It is important to note that the route Rørvik-Flakk follows the same geographical direction as Flakk-Rørvik, with the vessel heading rotated by 180 degrees. Given that the power generation from the Flettner rotor is symmetrical around the axis at 180 degrees, the power generation along the Flakk-Rørvik route is treated as equivalent to that along the Rørvik-Flakk route. This assumption simplifies the analysis, considering the symmetry of the Flettner rotor's power generation.

The results presented are based on weather data where the timerange for the downtime for sensor Ingdalen also has been filtered out for the sensor at Munkholmen, but also where the full unfiltered dataset of wind measurements from Munkholmen has been included. The reason for filtering out the timerange for the downtime for Ingdalen in Munkholmen is to ensure a standarized evaluation by removing potential biases or variations introduced by the downtime. This allows a fair and comparable assessment of the results for the two sensor locations.

To evaluate the efficiency and effect of using Flettner rotors on the ferry, two KPIs were defined in the case objective. The first KPI was Saved Propeller Power, i.e., the amount of power saved in the ferry's propulsion system from the assistance provided by the Flettner rotors. As stated in the case objective, this is measured by looking at the reduction in power consumption in kW compared to the scenario without Flettner rotors. The second KPI was Change in Depth of Discharge of the Battery. This means to quantify the impact of the Flettner rotors on the overall battery energy consumption and usage. This is measured by comparing the DoD for the battery with and without the use of Flettner rotors.

NB: The results related to the resistance of the ferry, i.e., the propeller power consumption with and without Flettner rotors are made anonymous out of respect for the shipping operator. This measure has been implemented to safeguard sensitive information to prevent external parties to estimate the ferry's resistance.

7.1 Flettner rotor forces

The forces generated by the Flettner rotor depend on the apparent wind angle and apparent wind speed. The wind measurements from the sensors at Munkholmen and Ingdalen were used to simulate the wind speed and direction along the route of the ferries.

Figure 7.1 show the amount of thrust for one 24x4m Flettner rotor for a vessel speed, $V_s = 12.0$ kn and TWS =7.0 m/s. Figure 7.1a is the thrust as a function of TWA where

$$\text{TWA} = \text{TWA} - \text{vessel heading},$$

to keep 0° at the bow.

The maximum thrust is obtained when the true wind angle relative to the vessel is at angles of $\approx$ 90° and $\approx$ 270° relative to the bow at 0°. The corresponding thrust generation as a function of the apparent wind angle is seen in Figure 7.1b. The maximum amount of thrust of approximately 55 kN is generated at apparent wind angles of approximately 55 and 305°.
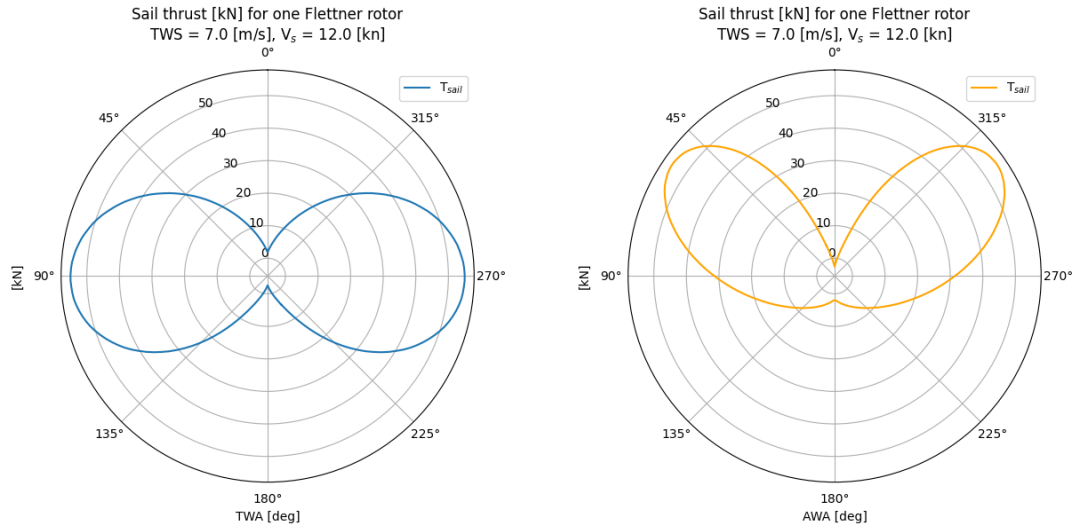
(a) Sail thrust as a function of true wind angle   **(b)** Sail thrust as a function of apparent wind angle

Figure 7.1: Sail thrust as a function of apparent and true wind angle for one Flettner rotor of size 24mx4m with maximum rotational speed equal to 225 [RPM]. Vessel speed, $V_s = 12.0$ [kn] and TWS= 7.0 [m/s].

7.1.1   Spin Ratio and Optimal RPM

The optimal spin ratio is seen in Figure 7.2b, and reaches a maximum at TWAs of 135° and 225°. For 90° where the FRs are seen to produce the most thrust, the SR is 4. From this it can be deducted that the FRs produce the most thrust for SRs between 3.5 and approximately 4.5 for beneficial TWAs.

The optimal rotational speed of the rotor is seen in Figure 7.2a, and reaches a maximum for TWAs between 45° and 90°. The rotational speed reaches a minimum when the TWAs are upwind and downwind of the bow.

(a) Optimal rotational speed in [RPM]

(b) Optimal spin ratio [-]
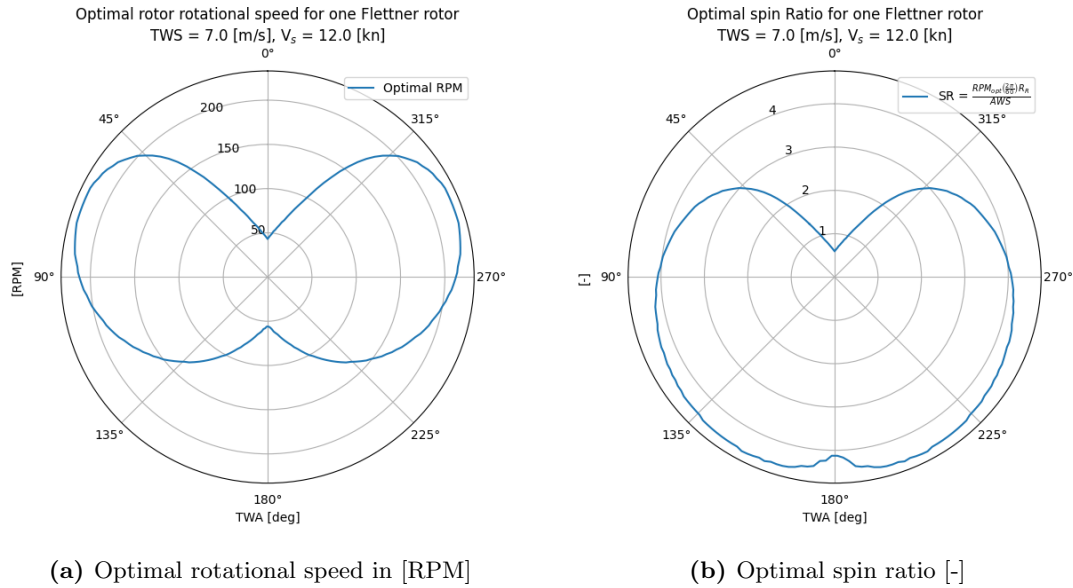
Figure 7.2: Optimal rotational speed in [RPM] and spin ratio [-] for one Flettner rotor of size 24mx4m with a maximum rotational speed equal to 225 [RPM]. Vessel speed, $V_s = 12.0$ [kn] and TWS= 7.0 [m/s].

7.2 Saved Propeller Power

7.2.1 Power produced by the FRs

Table 7.1 contains the average produced power by 2x FRs. To ensure an unbiased comparison of the results provided by the sensors, the downtime periods for the Ingdalen sensor have been systematically filtered out for both datasets. This data filtering ensures a standardized evaluation of the results for wind measurements across both sensor locations. The table highlights the impact of rotor dimensions on the average power production. By increasing the dimensions from the smallest rotor (4m×18m) to a taller configuration (4m×24m) increases the average power production with ≈27%, based on wind data from the Munkholmen sensor. With a further increase to rotors of dimensions 5m×30m, the average power production increases with ≈54% compared to the smallest one. The results based on the wind data from the Ingdalen sensor does not indicate the same average percentage increase in power generation as the wind data from the Munkholmen sensor. A possible explanation might be due to the higher wind speeds measured at Munkholmen. As discussed in Section 5.1.1, the sensor at Munkholmen is placed in a location that appears to benefit from the funnelling effect provided by the geometry and branches of the fjords that lead up to Trondheimsfjorden. A third weather data source should be assessed to get a reliable indication of the potential the Flettner Rotor's have for power generation in this case.

Results with unfiltered wind data from the sensor at Munkholmen is also added as the last row in Table 7.1. This is done to evaluate the how the weather during the "colder" months impact the average power generation of the Flettner rotors. The results indicate an average power increase of 18% by including the timeframe between 25th of November to 21st of February, which initially was filtered out due to the downtime of the sensor at Ingdalen.

Table 7.1: Comparison of average power produced by 2 Flettner rotors of different dimensions and max rotational speed based on sensor at Ingdalen and both filtered and unfiltered wind data from the sensor at Munkholmen.

Sensor	Rotor size		
	4m×18m, max rpm=225	4m×24m, max rpm=225	5m×30m, max rpm=180
Ingdalen	33.42 [kW]	41.58 [kW]	42.61 [kW]
Munkholmen filtered	46.43 [kW]	60.25 [kW]	70.99 [kW]
Munkholmen unfiltered	59.89 [kW]	73.62 [kW]	82.09 [kW]

Table 7.2 summarizes the average energy consumption saved on the total battery capacity by equipping the ferry with two FRs. The results in the table are based on wind data where the measurements from the Munkholmen sensor is both filtered and unfiltered for the timeframe of the downtime of the Ingdalen sensor.

The energy savings of equipping the ferry with two FRs a Figure 7.3 show the propeller power consumption per crossing by using two Flettner rotors of dimensions 4m×18m and 5m×30m as auxiliary propulsion. As indicated by the figures, equipping the ferry with two Flettner rotors reduces the frequency of maximum propeller power consumption from the blue to the green line. The values along the x-axis is blurred to uphold the confidentiality for the ferries of the ship operator. The amount of power saved in the ferry's total battery capacity system for various sizes of Flettner rotors are summarized in Table 7.2. All figures for the results illustrating the propeller power consumption with and without FRs are found in Appendix A.1.
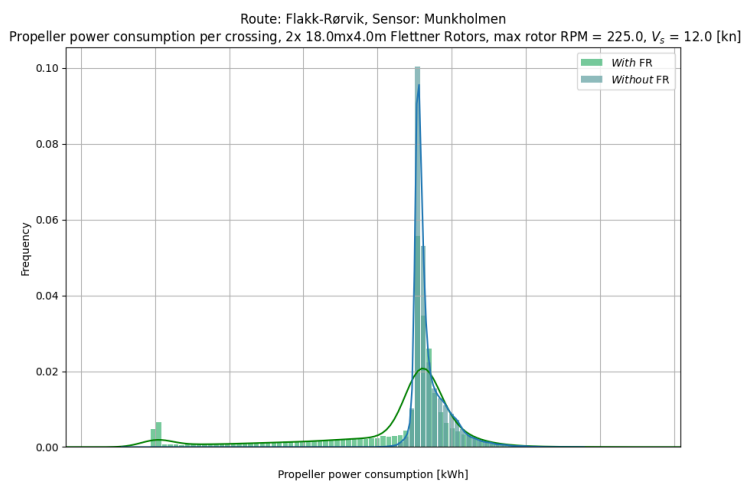
(a) 2× 4m×18m FRs
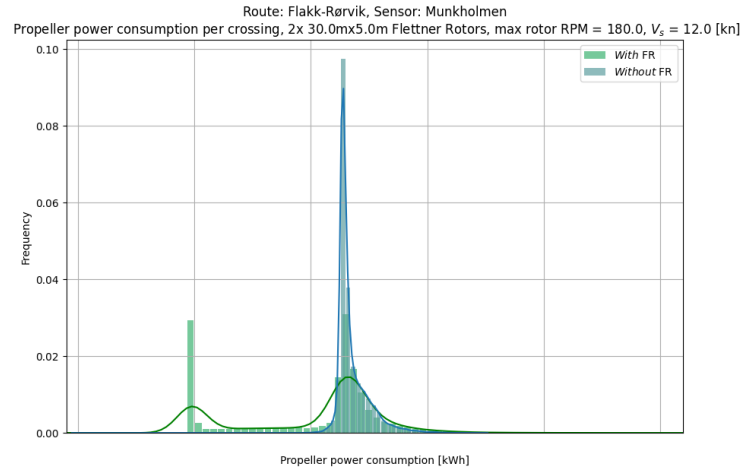
(b) 2× 5m×30m FRs

Figure 7.3: Propeller power consumption per crossing of 25 minutes for both 2× 4m×18m and 2× 5m×30m Flettner rotors.

Table 7.2: The average percentage power saved on the battery of 2100 kW by the Flettner rotors' power generation.

Sensor	Rotor size		
	4m×18m, max rpm=225	4m×24m, max rpm=225	5m×30m, max rpm=180
Ingdalen	1.591 [%]	1.980 [%]	2.029 [%]
Munkholmen filtered	2.211 [%]	2.869 [%]	3.380 [%]
Munkholmen unfiltered	2.835 [%]	3.505 [%]	3.909 [%]

Figure 7.4 show the power savings in percentage with two Flettner rotors for varying true wind speeds. The results shown in this figure indicate that the rotor should be turned off for true wind

speeds of 2 m/s and below, and also for true wind speed of 4 m/s in headwind.
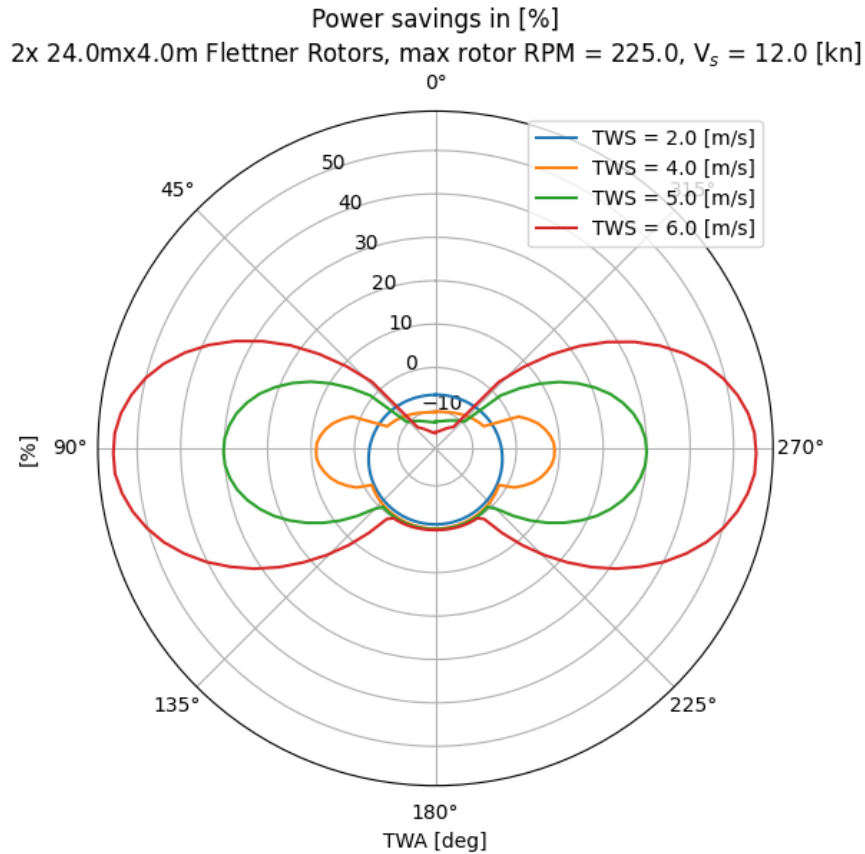
Figure 7.4: Power savings in percentage with two FRs of size 4m×24m for TWS = 2.0 m/s, 4.0 m/s and 6.0 m/s. Ship speed is constant at 12 kn.

7.3 Change in DoD of the Battery

The effect the Flettner rotors have on the battery's cycle life can be estimated by evaluating the derivative in the points of the battery's DoD with and without Flettner rotors. By calculating the derivative of the cycle life as a function of DoD, it is also possible to visualize how sensitive the cycle life is to changes in DoD.

Figure 7.5 shows the derivative of the battery's cycle life as a function of DoD. The derivative reveals how sensitive the cycle life is to changes in DoD, especially between 0 and 15-20%. Comparing with Figure 4.2 which show the cycle life as a function of DOD, the curve is steepest between these ranges and the cycle life experiences a significant reduction, declining from approximately 1E+06 to below 1E+05 at a DoD of 20%. The derivative in Figure 7.5 reflects this by the steep and almost "asymptotic" behaviour from -200 000 to -10 000. In Figure 7.5, the y-axis is limited to -60 000 to better visualize the points for the different DoDs. The full figure is seen in Appendix A.2.
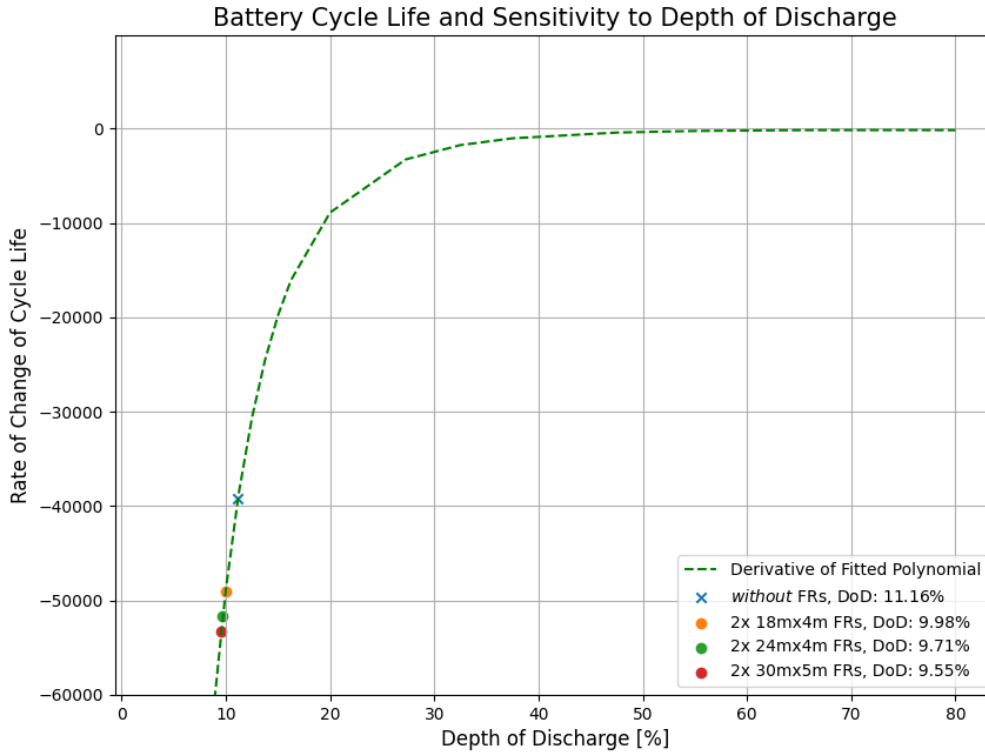
Figure 7.5: The derivative of the battery's cycle life as a function of DoD. The dots represents the DoD by equipping the ferry with two Flettner rotors of various sizes. The DoD is calculated based on the unfiltered data measured by the sensor at Munkholmen. The cross represents the DoD of the battery without Flettner rotors.

Table 7.3 provides a summary of the DoD for the battery per crossing, utilizing wind data both where the downtime at Ingdalen is also filtered out from Munkholmen, and when the Munkholmen data remains unfiltered. The DoD is also calculated by equipping the ferry with 2 Flettner rotors of various sizes to evaluate the impact of increasing the rotor dimensions. The table highlights that when including wind data from the winter months, accounting for the downtime at the Ingdalen sensor, the DoD reaches its minimum value of 9.98% for the smallest rotors of 4m×18m and 9.55% for the largest rotors of 5m×30m.

To get the change in DoD, the values in Table 7.3 for DoD with Flettner rotors are subtracted from the DoD without Flettner rotors, found in Table 7.4. The change in DoD for the various rotor sizes and both filtered and unfiltered wind data is seen in Table 7.5.

Table 7.3: Depth of discharge on the installed battery of 2100 kWh per crossing *with* 2 Flettner rotors of different dimensions and max rotational speed.

Sensor	Depth of Discharge		
	4m×18m, max rpm=225	4m×24m, max rpm=225	5m×30m, max rpm=180
Ingdalen	10.44 [%]	10.28 [%]	10.27 [%]
Munkholmen filtered	10.26 [%]	10.00 [%]	9.80 [%]
Munkholmen unfiltered	9.98 [%]	9.71 [%]	9.55 [%]

Table 7.4: Depth of discharge on the installed battery of 2100 kWh per crossing *without* 2 Flettner rotors.

Sensor	Depth of Discharge
Ingdalen	11.11 [%]
Munkholmen filtered	11.20 [%]
Munkholmen unfiltered	11.17 [%]

Table 7.5: The change in DoD per crossing by equipping the ferry with 2 Flettner rotors of different dimensions and max rotational speed.

Sensor	ΔDepth of Discharge		
	4m×18m, max rpm=225	4m×24m, max rpm=225	5m×30m, max rpm=180
Ingdalen	-0.663 [%]	-0.825 [%]	-0.845 [%]
Munkholmen filtered	-0.921 [%]	-1.195 [%]	-1.408 [%]
Munkholmen unfiltered	-1.181 [%]	-1.460 [%]	-1.628 [%]

The effect of the change in DoD can be seen by evaluating how many cycles that are saved by reducing the DoD with vs without Flettner rotors, e.g.,

$$f'(\text{DoD}_{\text{No FR}}) = f'(11.17\%) = -39\,202.26, \qquad f'(\text{DoD}_{\text{2xFR}}) = f'(9.98\%) = -49\,003.45.$$

The total cycles saved by the change of DoD is then found by

$$\text{Cycles Saved} = f'(\text{DoD}_{\text{2xFR}}) - f'(\text{DoD}_{\text{No FR}}). \tag{7.1}$$

By cycles saved, it is meant the amount of cycles the battery has gained on its life before the capacity diminishes below 80%, where it is said to no longer be of use.

Table 7.6 summarizes the cycles saved, representing the increase in the cycles of the battery and thus its increased longevity due to the changes in DoD. The results are based on the unfiltered data only from the sensor located at Munkholmen, and highlights how transitioning from the smallest configuration of 4m×18m to the largest of 5m×30m yields in approximately 30% more cycles saved. Specifically, the battery experiences an increase in longevity with the number of cycles saved increasing from 9 801 to 14 037.

Table 7.6: Cycles saved due to the change in DoD by the use of two FRs of various sizes based on the unfiltered wind data from the Munkholmen sensor.

Rotor Size	ΔDepth of Discharge	Cycles Saved
4m×18m, max rpm=225	-1.181 [%]	9801.18
4m×24m, max rpm=225	-1.460 [%]	12 414.61
5m×30m, max rpm=180	-1.628 [%]	14 037.10

7.4 Discussion

This section discusses the findings and assumptions of the case used to create the results.

One of assumption used when presenting the results were that the power generation along the Flakk-Rørvik route is treated as equivalent to that along the Rørvik-Flakk route. This is based on the principle that the Flettner rotor's performance characteristics are symmetrical around its axis. Assuming that the other conditions i.e., wind speed and direction are constant, the the direction of travel relative to the wind direction would not affect its ability to generate propulsion force.

However, upon closer evaluation of the sensor locations relative to the ferry route (see Figure 5.1), it becomes apparent that the sensors are situated closer to Flakk than to Rørvik. This discrepancy raises questions regarding the representativeness of the wind conditions captured by the sensors, particularly when the ferry sails further away from Flakk and closer to Rørvik. Since both sensors are relatively close to the shore, it is possible that the real wind conditions experienced by the ferry in open sea areas may not be fully captured.

For instance, the sensor at Ingdalen is approximately 1.2 km from the nearest shore and 3.3 km from the opposite shore at Stadsbygs. Similarly, the sensor at Munkholmen is located around 3.1 km from the nearest shore close to Byåsen and approximately 10.7 km from the shore on the opposite side of the fjord. This discrepancy suggests that the wind data collected by these sensors may not fully represent the wind conditions experienced by the ferry in open sea areas. Wind data measured closer to the ferry connection, particularly in open sea areas, may provide a more accurate representation of the actual wind conditions experienced by the ferry. Consequently, there may be reason to believe that the potential benefits of Flettner rotors could be greater than what the results were able to capture due to the constraints in the wind data caused by the sensor locations.

The decision to filter out the downtime from both sensors, despite continuous measurements being available from the Munkholmen sensor, was motivated by the need to establish an equal data basis for comparison. By analyzing the correlation between the power generated from the Flettner rotors using data from both sensors, it is possible to get an impression on the validity and robustness of the results. When comparing the average power generated by the two Flettner rotors (see Table 7.1) based on the wind data from the two sensors, it is seen that the calculations based on the wind data from the Munkholmen sensor consistently yielded higher values compared to those from the Ingdalen sensor. Even when filtering out the downtime period from the Ingdalen data in the Munkholmen sensor, the measurements based on the data from Munkholmen still indicated an average power generation approximately 33% greater than that calculated from Ingdalen's wind data. This discrepancy may be attributed to the geographical features of the fjord. The Munkholmen sensor, situated deeper within Trondheimsfjorden compared to the Ingdalen sensor near its inlet, likely benefits from the funneling effect of the fjord on wind speed and direction.

In evaluating the consistency of results between the two sensors, it's important to acknowledge the differences in wind data captured, particularly regarding wind speed and direction. The consistently higher power generation values from the Munkholmen sensor may be explained by the fact that the sensor measured a 12.3% higher mean wind speed than the sensor located at Ingdalen. As mentioned earlier, the power generated by the Flettner rotors depends on the wind speed to the power of three, hence a higher wind speed will result in higher power generation. Thus, the observation that the sensor located at Munkholmen resulted in higher power generation for equal timeframes seems reasonable.

While the Flettner rotor model provides valuable insights into potential energy savings, it's essential to recognize the simplifications and assumptions embedded within the model. One significant limitation is the disregard for the interaction between the sail and superstructure, as well as the additional resistance from drift and rudder angles associated with high side forces. From the paper of Tillig and Ringsberg (2020) it is highlighted that the interaction between the sails and the superstructure introduces additional complexity, altering the local inflow angle and velocity at the sails. This has the consequence that the there are even more factors affecting the operational conditions of the Flettner rotors, and that monitoring and control of each rotor individually is needed to optimize their performance and exploit their full potential.

Another point worth discussing is the simplifications in the battery modeling approach used in this analysis. The modeling of the battery is based only on the relationship between the DoD and the cycle life, which may not fully capture the complex interactions and dynamics involved. This simplification introduces limitations in the accuracy and predictive capability of the results, highlighting the need for further refinement and validation of the battery model.

Chapter 8

Conclusion

In conclusion, this study has explored the potential of using Flettner rotors as auxiliary propulsion on a battery-electric ferry operating in Trondheimsfjorden. Two main objectives were investigated, namely the saved propeller power and the amount of cycles saved by the change in DoD. The ferry was equipped with two Flettner rotors. The study investigated three different rotor size configurations based on technical information from Norsepower (2022). Two sensors located on either side of the ferry crossing provided wind data, however, one of the sensors had significant downtime between November 2022 until February 2023. The results from the sensor without downtime (Munkholmen unfiltered) is regraded as the most representative for the weather conditions as it includes continuous measurements for all months throughout a year, which is the timerange of the collected wind data.

A key finding emerges from the analysis of different rotor size configurations as it reveals an interesting trend in power generation efficiency with increasing rotor size. Moving from the smallest of 4m×18m to the medium-sized rotor of 4m×24m resulted in a substantial 19% increase in generated power. However, the incremental gain in power generation diminishes as rotor size further increases. Transitioning from the medium-sized rotor to the largest rotor of 4m×30m only yielded a 10.4% increase in generated power. This suggests that while scaling up rotor size does offer some benefits in power generation, the magnitude of these benefits diminishes as the rotor becomes larger. Consequently, there exists a point of diminishing returns in terms of power generation efficiency with increasing rotor size. This observation underscores the importance of carefully considering the trade-offs between rotor size, power generation capacity, and other factors such as installation space and operational costs in the design and optimization of wind-assisted propulsion systems.

The second key finding of this study is the reduction in Depth of Discharge (DoD) facilitated by the installation of Flettner rotors on the ferry. Across the three rotor size configurations examined, the DoD reductions were measured at 1.181% for the smallest rotor, 1.460% for the medium-sized rotor, and 1.628% for the largest rotor. Even though the reductions appear small, they translate into interesting benefits in terms of battery cycle savings, with the smallest rotor configuration yielding 9801 cycles saved, followed by 12 414 cycles saved for the medium-sized rotor, and 14 037 cycles saved for the largest rotor. The significant cycle savings achieved, despite relatively small percentage changes in depth of discharge (DoD), can be attributed to the logarithmic behavior of the relationship between DoD and battery cycle life. The logarithmic nature implies that small reductions in DoD can lead to disproportionately large increases in battery cycle life. For instance, as DoD decreases from 0-10%, the cycle life of the battery may decrease from 1 000 000 to below 400 000 (ref. Figure 4.2), showcasing the significant reduction in cycle life for relatively minor changes in DoD. This behavior underscores the sensitivity of the battery performance to variations in DoD, particularly at lower discharge levels.

8.1 Further Work

The analysis presented in this study offers insights into the potential benefits of integrating Flettner rotors on a battery-electric pendulum ferry. However, several key elements for further research emerge from the findings.

- To improve the reliability and accuracy of the results, future studies could consider incorporating wind data from multiple sources. This would provide a more comprehensive validation of the wind measurements and support or enhance the confidence in the results obtained. This also eliminates the vulnerability of the analysis for any potential downtime for one or more of the sensors.

- Developing a more sophisticated modeling approach to incorporate effects such as added resistance due to drift and high side forces and rudder angles into the analysis. This would enable a more comprehensive assessment of the performance and efficiency of Flettner rotor-assisted propulsion systems under varying environmental and operational scenarios.

- Develop a more comprehensive analysis of the battery life and potential savings in its lifetime with the implementation of Flettner rotors.

- Develop a cost analysis of the battery system to evaluate the overall economic benefits of integrating Flettner rotors.

Bibliography

W. Blendermann. Parameter identification of wind loads on ships. *Journal of Wind Engineering and Industrial Aerodynamics*, 51(3):339–351, 1994. ISSN 0167-6105. doi: https://doi.org/10.1016/0167-6105(94)90067-1. URL https://www.sciencedirect.com/science/article/pii/0167610594900671.

T. Chou, V. Kosmas, M. Acciaro, and K. Renken. A comeback of wind power in shipping: An economic and operational review on the wind-assisted ship propulsion technology. *Sustainability*, 13(4), 2021. ISSN 2071-1050. doi: 10.3390/su13041880. URL https://www.mdpi.com/2071-1050/13/4/1880.

G. DNV. Dnv gl handbook for maritime and offshore battery systems. Technical report, Technical Report, 2016.

J. Drapala, 2023. URL https://towardsdatascience.com/kernel-density-estimation-explained-step-by-step-7cc5b5bc4517.

L. A.-W. Ellingsen, G. Majeau-Bettez, B. Singh, A. K. Srivastava, L. O. Valøen, and A. H. Strømman. URL https://ntnuopen.ntnu.no/ntnu-xmlui/bitstream/handle/11250/2466860/Accepted%2Bmanuscript.pdf?sequence=3.

O. M. Faltinsen. *RESISTANCE AND PROPULSION*, page 12–77. Cambridge University Press, 2006. doi: 10.1017/CBO9780511546068.003.

B. Fosen, 2019. URL https://basto-fosen.no/nyhetsarkiv/verdens-storste-elektriske-bilferge-i-rutetrafikk-pa-oslofjorden.

S. Fox, 2014. URL https://www.greentechrenewables.com/article/how-does-depth-discharge-factor-grid-connected-battery-systems.

G. Green Shipping Programme, 2023. URL https://greenshippingprogramme.com/about-green-shipping-programme/.

H. Guldhammer and S. A. Harvald. Ship resistance-effect of form and principal dimensions.(revised). Technical report, Danish Technical Press, Danmark, Danmarks Tekniske Hojskole, kademisk Forlag, St. kannikestrade 8, DK 1169 Copenhagen, 1974.

J. Guo, Z. Li, and M. Pecht. A bayesian approach for li-ion battery capacity fade modeling and cycles to failure prognostics. *Journal of Power Sources*, 281:173–184, 2015. ISSN 0378-7753. doi: https://doi.org/10.1016/j.jpowsour.2015.01.164. URL https://www.sciencedirect.com/science/article/pii/S0378775315001925.

U. Hollenbach. Single and twin-screw vessels: Contribution towards estimating resistance and propulsion at preliminary design stage. 50:66–69, 01 1998.

Hydrosphere, 2023. URL https://hydrosphere.co.uk/products/mobilis-data-buoys/.

R. P. ITTC. Guidelines 7.5-04-01-01.2 'analysis of speed. *Power Trial Data*, 2014.

M. Kadivar, D. Tormey, and G. McGranaghan. A review on turbulent flow over rough surfaces: Fundamentals and theories. *International Journal of Thermofluids*, 10:100077, 2021. ISSN 2666-2027. doi: https://doi.org/10.1016/j.ijft.2021.100077. URL https://www.sciencedirect.com/science/article/pii/S266620272100015X.

S. Kalogirou. *McEvoy's handbook of photovoltaics: fundamentals and applications*. Academic Press, 2017.

M. Kaltschmitt, W. Streicher, and A. Wiese. *Renewable energy. Technology, economics and environment*. Jul 2007. doi: 10.1007/3-540-70949-5.

S. Karabelas, B. Koumroglou, C. Argyropoulos, and N. Markatos. High reynolds number turbulent flow past a rotating cylinder. *Applied Mathematical Modelling*, 36(1):379–398, 2012. ISSN 0307-904X. doi: https://doi.org/10.1016/j.apm.2011.07.032. URL https://www.sciencedirect.com/science/article/pii/S0307904X11004124.

K. Korei. Spinning metal sails could slash fuel consumption, emissions on cargo ships, 2017. URL https://www.science.org/content/article/spinning-metal-sails-could-slash-fuel-consumption-emissions-cargo-ships.

J. A. Kramer, S. Steen, and L. Savio. Drift forces-wingsails vs flettner rotors. *High performance marine vehicles*, 2016.

H. O. Kristensen, M. Lützen, et al. Prediction of resistance and propulsion power of ships. *Clean Shipping Currents*, 1(6):1–52, 2012.

K. Leidorf. URL https://www.leidorf.de/.

D.-Q. Li, M. Leer-Andersen, and B. Allenström. Performance and vortex formation of flettner rotors at high reynolds numbers. In *29th Symposium on Naval Hydrodynamics*, 2012.

R. Lu and J. W. Ringsberg. Ship energy performance study of three wind-assisted ship propulsion technologies including a parametric study of the flettner rotor technology. *Ships and Offshore Structures*, 15(3):249–258, 2020. doi: 10.1080/17445302.2019.1612544. URL https://doi.org/10.1080/17445302.2019.1612544.

MAN Energy Solutions. Basic principles of ship propulsion. *MAN Energy Solutions*, 2018.

MAN Energy Solutions. Batteries on board ocean-going vessels. Technical report, 2019. URL https://www.man-es.com/docs/default-source/marine/tools/batteries-on-board-ocean-going-vessels.pdf?sfvrsn=deaa76b8_14.

Marine Traffic. Lagatun. URL https://www.marinetraffic.com/en/ais/details/ships/shipid:5739728/mmsi:257057960/imo:9820398/vessel:LAGATUN.

K. Minsaas, S. Steen, and K. Koushan. Tmr4220 naval hydrodynamics compendium, 2016.

Norsepower. Norsepower brochure. 2022. URL https://www.norsepower.com/download/brochure.pdf.

S. O. Observatory, a. URL https://oceanlab.azure.sintef.no/d/aImXqWjnz/environmental-data3a-ingdalen?orgId=1.

S. O. Observatory, b. URL https://oceanlab.azure.sintef.no/d/Pd5SYHD7k/environmental-data-munkholmen?orgId=1&from=now-1y&to=now.

M. Rätsep, K. E. Parnell, T. Soomere, M. Kruusmaa, A. Ristolainen, and J. A. Tuhtan. Using spectrograms from underwater total pressure sensors to detect passing vessels in a coastal environment. *Journal of Atmospheric and Oceanic Technology*, 37(8):1353 – 1363, 2020. doi: https://doi.org/10.1175/JTECH-D-19-0192.1. URL https://journals.ametsoc.org/view/journals/atot/37/8/jtechD190192.xml.

H. Schneekluth and V. Bertram. *Ship design for efficiency and economy*, volume 218. Butterworth-Heinemann Oxford, 1998.

SINTEF OceanLab. Weather data summary. URL https://oceanlab.azure.sintef.no/d/Qhkm9GU7z/weather-summary?orgId=1&from=now-1y&to=now.

S. Steen. *Motstand og propulsjon - Propell- og foilteori*. Institutt for marin teknikk, 2011.

S. Steen, M. Bobo, G. Karafiath, M. Insel, R. Anzböck, J. Jang, N. Toki, D. Zhu, and W. Qiu. The specialist committee on powering performance prediction - final report and recommendations to the 25th ittc. In *Proceedings of 25th ITTC*, volume 2, pages 397–431, 2008. URL https://ittc.info/media/3485/volume2_1powering_perf_pred.pdf.

K. A. Striebel, J. Shim, E. J. Cairns, R. Kostecki, Y.-J. Lee, J. Reimer, T. J. Richardson, P. N. Ross, X. Song, and G. Zhuang. Diagnostic analysis of electrodes from high-power lithium-ion cells cycled under different conditions. *Journal of The Electrochemical Society*, 151(6):A857, 2004.

D. W. Taylor. The wetted surface of ships. *Transactions of the Society of Naval Architects and Marine Engineers*, 1, 1893.

the United States Library of Congress's Prints and Photographs. URL https://en.wikipedia.org/wiki/Rotor_ship#/media/File:Buckau_Flettner_Rotor_Ship_LOC_37764u.jpg.

F. Tillig and J. W. Ringsberg. A 4 dof simulation model developed for fuel consumption prediction of ships at sea. *Ships and Offshore Structures*, 14(sup1):112–120, 2019. doi: 10.1080/17445302.2018.1559912. URL https://doi.org/10.1080/17445302.2018.1559912.

F. Tillig and J. W. Ringsberg. Design, operation and analysis of wind-assisted cargo ships. *Ocean Engineering*, 211:107603, 2020. ISSN 0029-8018. doi: https://doi.org/10.1016/j.oceaneng.2020.107603. URL https://www.sciencedirect.com/science/article/pii/S0029801820306077.

F. Tillig, J. Ringsberg, W. Mao, and B. Ramne. A generic energy systems model for efficient ship design and operation. *Proceedings of the Institution of Mechanical Engineers, Part M: Journal of Engineering for the Maritime Environment*, 231(2):649–666, 2017. doi: 10.1177/1475090216680672. URL https://doi.org/10.1177/1475090216680672.

Tilnull, 2023. URL https://www.tilnull.no/om.

R. Townsin. The ittc correlation allowance: The evidence re-examined and supplemented. 1990.

Transocean Coatings. Estimation of surface areas, 2022. URL https://www.transocean-coatings.com/static/downloadcenter/2022/12/estimation-of-surface-areas-09dec2022.pdf.

VerLab. URL https://www.verlab.dcc.ufmg.br/old/projetos/roomba/batteries.

M. Waskom., 2023. URL https://seaborn.pydata.org/generated/seaborn.kdeplot.html.

M. L. Waskom. seaborn: statistical data visualization. *Journal of Open Source Software*, 6(60):3021, 2021. doi: 10.21105/joss.03021. URL https://doi.org/10.21105/joss.03021.

Q. Yao, C. Zhou, and C. Wang. Numerical study of the flow past a rotating cylinder at supercritical reynolds number. In *Proceedings of the 2016 4th International Conference on Mechanical Materials and Manufacturing Engineering*, pages 667–670. Atlantis Press, 2016/10. ISBN 978-94-6252-221-3. doi: 10.2991/mmme-16.2016.159. URL https://doi.org/10.2991/mmme-16.2016.159.

Appendix A

Results

A.1 Power produced by FRs

A.1.1 Ingdalen Filtered - excluding timeframe between 25th Nov - 21st Feb

Required propeller power
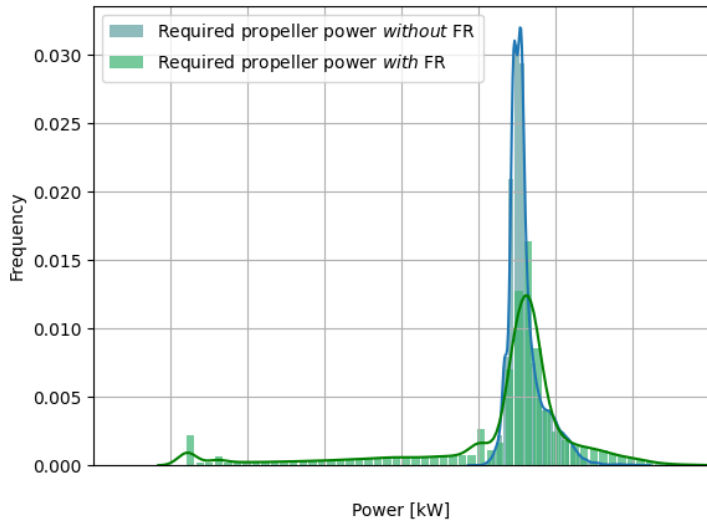
(a) Propeller power consumption
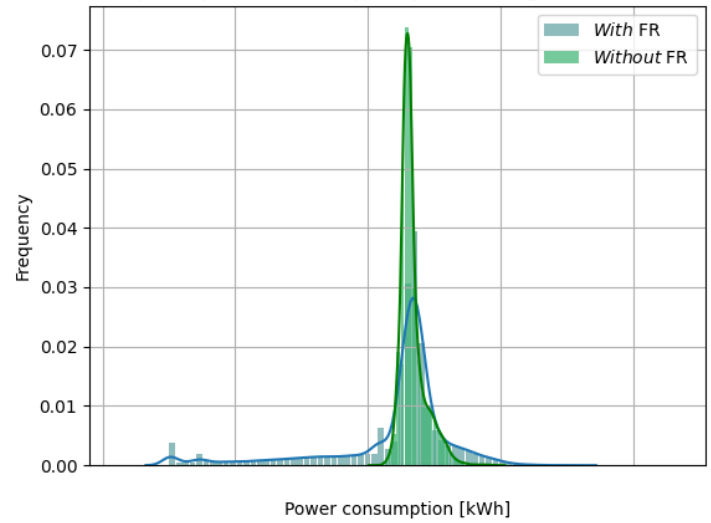
(b) Propeller power consumption per crossing

Figure A.1: 2× 4m×18m Flettner rotors.
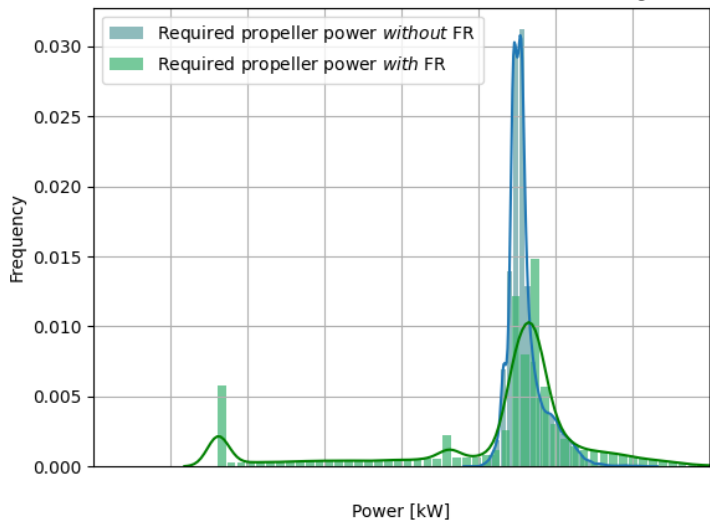
(a) Propeller power consumption
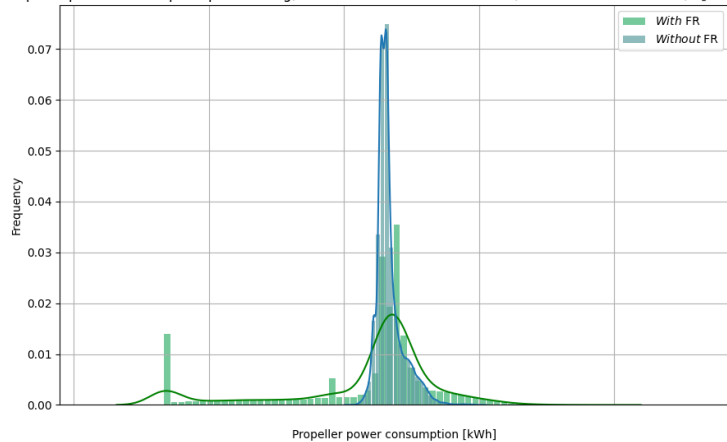
(b) Propeller power consumption per crossing

Figure A.2: $2\times$ 4m$\times$24m Flettner rotors.
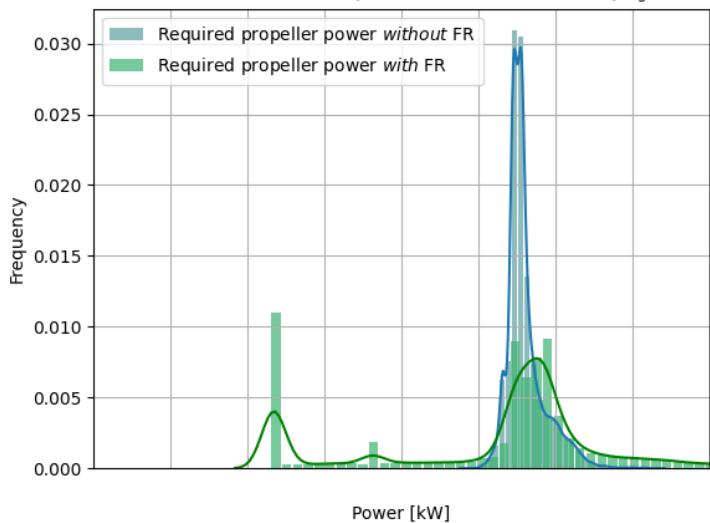
(a) Propeller power consumption
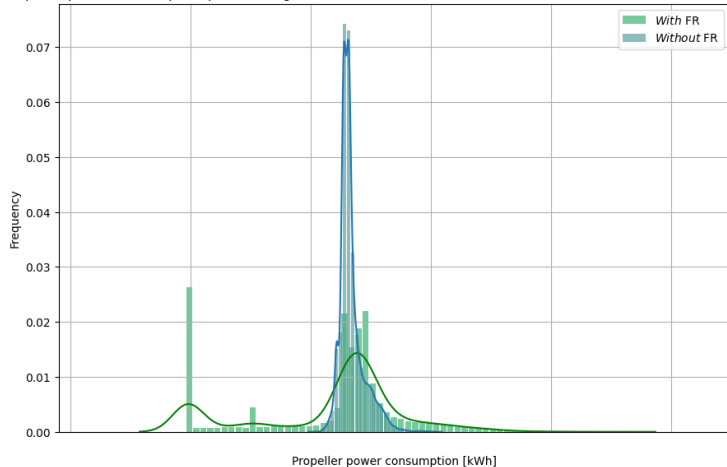
(b) Propeller power consumption per crossing

Figure A.3: $2\times$ 5m$\times$30m Flettner rotors.

A.1.2 Munkholmen Filtered - excluding timeframe between 25th Nov - 21st Feb

Required propeller power per crossing
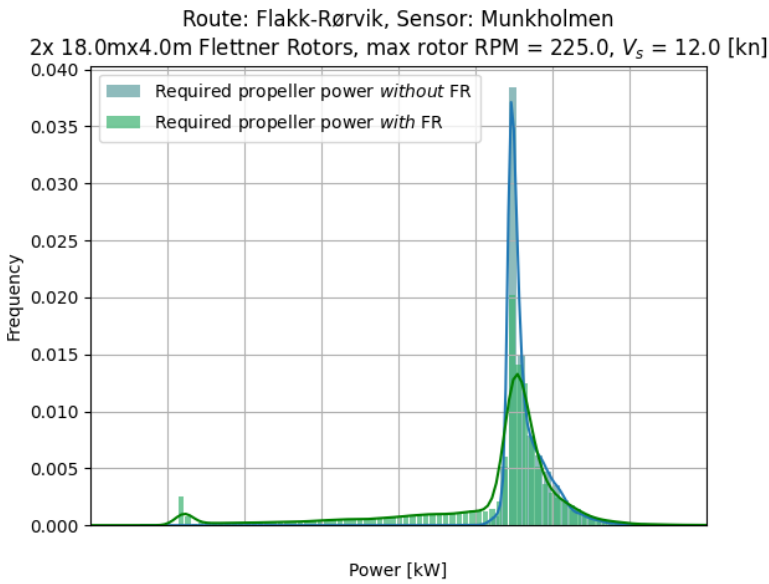
(a) Propeller power consumption
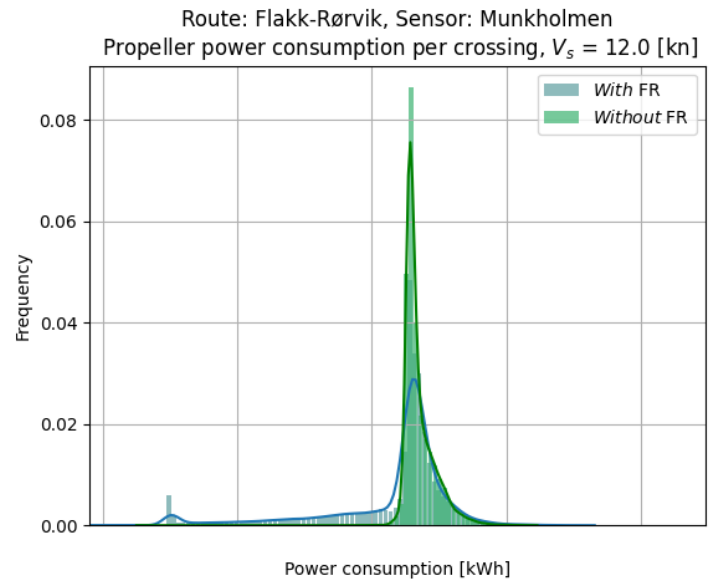
(b) Propeller power consumption per crossing

Figure A.4: 2× 4m×18m Flettner rotors.
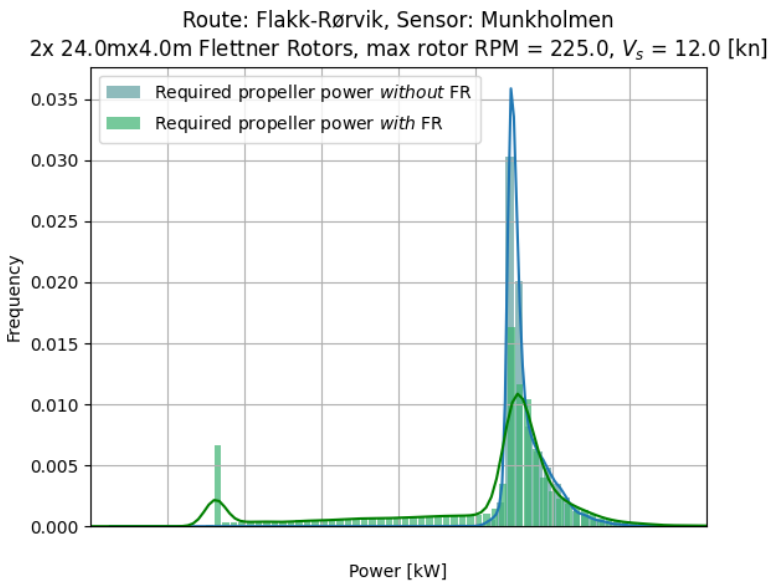
(a) Propeller power consumption
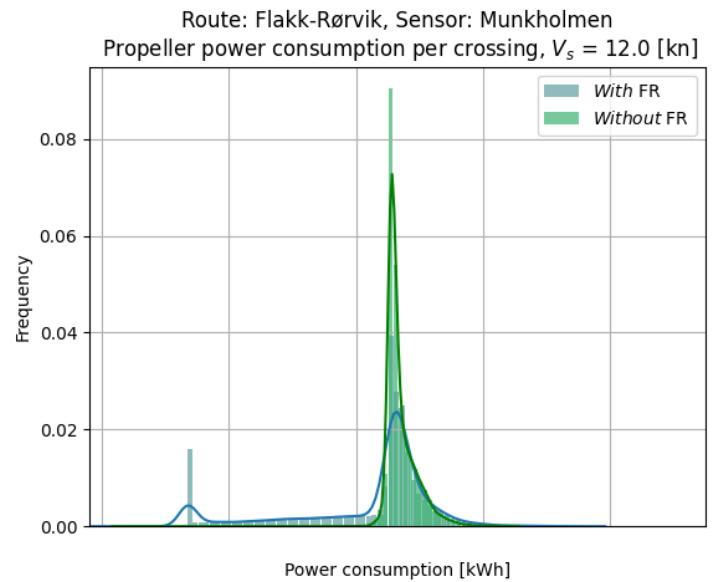
(b) Propeller power consumption per crossing

Figure A.5: 2× 4m×24m Flettner rotors.
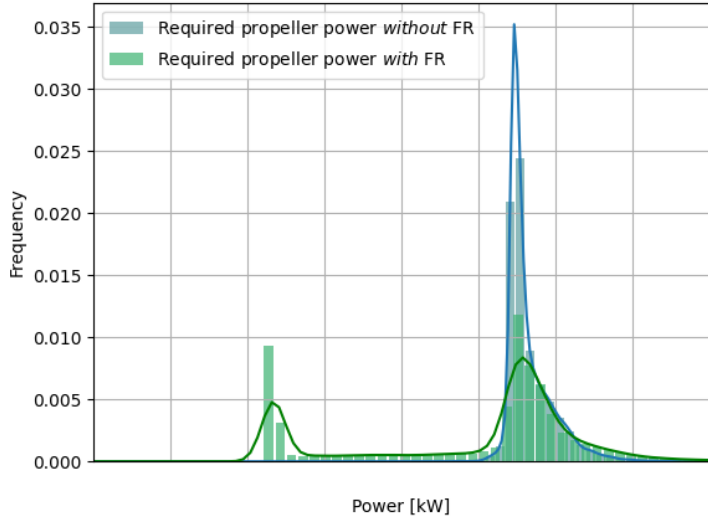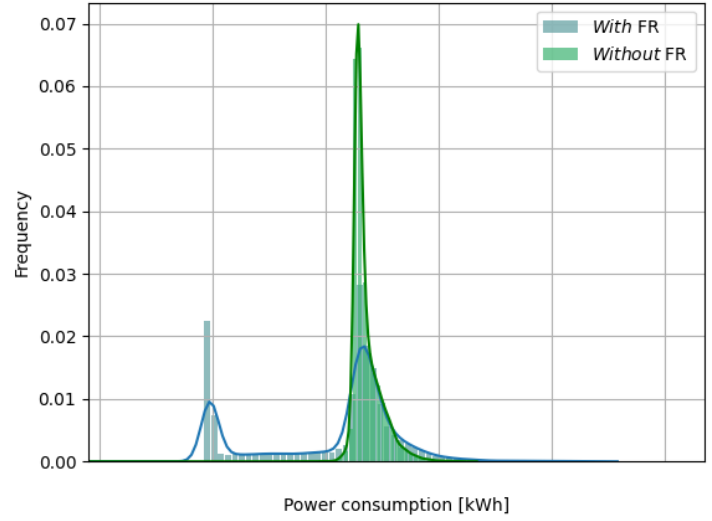
(a) Propeller power consumption   **(b)** Propeller power consumption per crossing

Figure A.6: $2\times$ 5m$\times$30m Flettner rotors.

A.1.3   Munkholmen Unfiltered - including timeframe between 25th Nov - 21st Feb

Required propeller power per crossing

(a) Propeller power consumption   **(b)** Propeller power consumption per crossing

Figure A.7: $2\times$ 4m$\times$18m Flettner rotors.

(a) Propeller power consumption

(b) Propeller power consumption per crossing

Figure A.8: 2× 4m×24m Flettner rotors.

(a) Propeller power consumption

(b) Propeller power consumption per crossing

Figure A.9: 2× 5m×30m Flettner rotors.

A.2 Cycle Life and Depth of Discharge
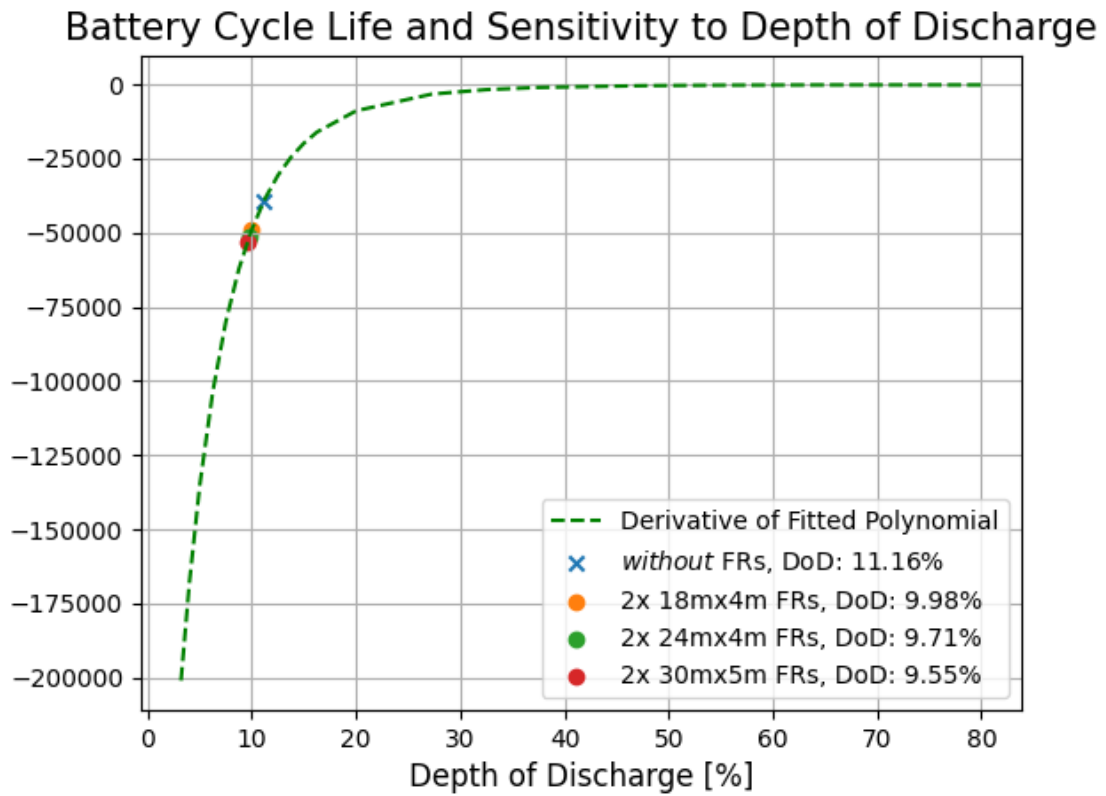
Figure A.10: Rate of change of cycle life for changing DoD. Derivative calculated from polyfit of curve from Kalogirou (2017).

Appendix B

Code

B.1 Polynomial fitting of curve for Cycle Life and DoD based on Kalogirou (2017)

```python
def read_csv_data(filename):
    xcoord = []
    ycoord = []
    fd = open(filename, "r")
    lines = fd.readlines()
    fd.close()
    printf("(reading file: %s)\n", filename)

    for line in lines:
        fields = line.strip().split()
        xcoord.append(float(fields[0]))
        ycoord.append(float(fields[1]))

    return [xcoord, ycoord]

def get_func(coefs, xi):
    exp_yi = (coefs[0] * xi * xi *xi) + (coefs[1] * xi * xi) + (coefs[2] * xi) +
    coefs[3]
    return pow(10.0, exp_yi)

def get_dy_dx(coefs, xi):
    dydu = get_func(coefs, xi)
    dudx = math.log(10.0) * ((3.0 * coefs[0] * xi * xi) + (2.0 * coefs[1] * xi) +
    coefs[2])
    dydx = dydu * dudx
    return dydx

def get_dy_dx_num(coefs, xi):
    dx = 1.0
    y1 = get_func(coefs, xi)
    y2 = get_func(coefs, xi + dx)
    return ((y2 - y1) / dx)

def make_fx(coefs, xcoord):
    ycoord = []
    for xi in xcoord:
        ycoord.append(get_func(coefs, xi))
    return ycoord

def make_df_dx(coefs, xcoord):
    ycoord = []
    for xi in xcoord:
        ycoord.append(get_dy_dx(coefs, xi))
    return ycoord
```

```
45  def make_df_dx_num ( coefs , xcoord ):
46      ycoord = []
47      for xi in xcoord :
48          ycoord . append ( get_dy_dx_num ( coefs , xi ))
49      return ycoord
50
51  def make_coefs (x , y ):
52      N = 4
53      A = np . zeros (( N,N ))
54      b = np . zeros ( N )
55
56      x1 = x [1];        b [0] = math . log10 ( y [1])
57      x2 = x [7];        b [1] = math . log10 ( y [7])
58      x3 = x [15];       b [2] = math . log10 ( y [15])
59      x4 = x [20];       b [3] = math . log10 ( y [20])
60
61      A [0 ,0] = ( x1 * x1 * x1 ); A [0 ,1] = ( x1 * x1 ); A [0 ,2] = x1 ; A [0 ,3] = 1.0
62      A [1 ,0] = ( x2 * x2 * x2 ); A [1 ,1] = ( x2 * x2 ); A [1 ,2] = x2 ; A [1 ,3] = 1.0
63      A [2 ,0] = ( x3 * x3 * x3 ); A [2 ,1] = ( x3 * x3 ); A [2 ,2] = x3 ; A [2 ,3] = 1.0
64      A [3 ,0] = ( x4 * x4 * x4 ); A [3 ,1] = ( x4 * x4 ); A [3 ,2] = x4 ; A [3 ,3] = 1.0
65
66      coefs = np . linalg . solve (A , b )
67      print ( "COEFS:" , coefs )
68
69      printf ( "f(x) = pow (10.0 , (( % g*x*x*x ) + (%g*x*x ) + (%g*x ) + %g ))\n" ,
70          coefs [0] , coefs [1] , coefs [2] , coefs [3])
71
72      print ( "Check1:" , x1 , b [0] - math . log10 ( get_func ( coefs , x1 )))
73      print ( "Check2:" , x2 , b [1] - math . log10 ( get_func ( coefs , x2 )))
74      print ( "Check3:" , x3 , b [2] - math . log10 ( get_func ( coefs , x3 )))
75      print ( "Check4:" , x4 , b [3] - math . log10 ( get_func ( coefs , x4 )))
76      return coefs
```

B.2 Frictional resistance class

```
1      import numpy as np
2
3  class FrictionalResistance ():
4      SEAWATER_DENSITY   = 1025.0
5      SEAWATER_VISCOSITY = 1.48E-03
6
7
8      def __init__ (
9              self ,
10             *,
11             ship_speed_kn ,
12             length_wl ,
13             draught ,
14             breadth ,
15             block_coeff ,
16             prismatic_coeff ,
17             wetted_surface
18     ) -> None :
19             self . ship_speed_kn   = ship_speed_kn
20             self . length_wl       = length_wl
21             self . draught         = draught
22             self . breadth         = breadth
23             self . block_coeff     = block_coeff
24             self . prismatic_coeff = prismatic_coeff
25             self . wetted_surface  = wetted_surface
26
27
28     def estimate_form_factor ( self ) -> float :
29         # method from MARINTEK 's formula ( p .11 motstand og prop )
30         phi = ( self . block_coeff / self . length_wl ) * np . sqrt (2.0* self . draught * self .
    breadth )
31         k   = 0.6* phi + 145.0* pow ( phi , 3.5)
32         #print ('form factor 1:', k )
33
```

```python
34              #D = np.sqrt(4.0/np.pi) * np.sqrt(2*self.draught*self.breadth)
35              #phi = self.block_coeff*self.prismatic_coeff * (D/101.0)
36              k2    = 0.6*phi + 75.0*pow(phi, 3.0)
37              #print('form factor 2:', k2)
38
39              return k2
40
41
42      def reynolds_number(self) -> float:
43          Re = (self.ship_speed_kn * 0.5144 * self.length_wl) / self.
    SEAWATER_VISCOSITY
44          return Re
45
46
47      def estimate_ITTC_friction_line(self) -> float:
48          Re = self.reynolds_number()
49          Cf = (0.075 / pow(np.log10(Re) - 2.0, 2.0))
50          return Cf
51
52
53      def estimate_hull_correction(self, *, hull_correction_method,
    hull_roughness_meter) -> float:
54          Re = self.reynolds_number()
55          Cf = self.estimate_ITTC_friction_line()
56
57          if hull_correction_method == 'ITTC':
58              delta_Cf = 0.044 * (pow((hull_roughness_meter/self.length_wl), 0.333) -
     10*pow(Re, -0.333)) + 0.000125
59          elif hull_correction_method == 'MARINTEK':
60              delta_Cf = ((110.0 * pow((hull_roughness_meter*pow(10, 6)*self.
    ship_speed_kn*0.5144), 0.21) - 403.0) * pow(Cf, 2))
61
62          return delta_Cf
63
64
65      def estimate_total_friction_coeff(self, *, hull_correction_method,
    hull_roughness_meter) -> float:
66          Cf = self.estimate_ITTC_friction_line()
67          delta_Cf = self.estimate_hull_correction(hull_correction_method=
    hull_correction_method, hull_roughness_meter=hull_roughness_meter)
68          #print('FUNC: estimate total friction coeff --- Cf ITTC:', Cf)
69          #print('FUNC: estimate total friction coeff --- delta Cf:', delta_Cf)
70
71          Cf = Cf + delta_Cf
72          #print('FUNC: estimate total friction coeff --- tot Cf:', Cf)
73
74          return Cf
75
76
77      def estimate_total_friction_coeff_form_factor(self, *, hull_correction_method,
    hull_roughness_meter) -> float:
78          k = self.estimate_form_factor()
79          Cf = self.estimate_total_friction_coeff(hull_correction_method=
    hull_correction_method, hull_roughness_meter=hull_roughness_meter)
80          #print('FUNC: estimate friction coeff --- form factor:', k)
81          #print('FUNC: estimate friction coeff --- total Cf (no form):', Cf)
82          Cf = (1.0 + k)*Cf
83          #print('FUNC: estimate friction coeff --- total Cf (yes form):', Cf)
84
85          return Cf
86
87
88      def estimate_friction_force_components(self, *, hull_correction_method,
    hull_roughness_meter) -> float:
89          Cf = self.estimate_ITTC_friction_line()
90          delta_cf = self.estimate_hull_correction(hull_correction_method=
    hull_correction_method, hull_roughness_meter=hull_roughness_meter)
91
92          Rf = 0.5 * self.SEAWATER_DENSITY * pow(self.ship_speed_kn*0.5144, 2.0) *
    self.wetted_surface * Cf
93          Rf_rough = 0.5 * self.SEAWATER_DENSITY * pow(self.ship_speed_kn*0.5144,
    2.0) * self.wetted_surface * delta_cf
94          #print('FUNC -- estimate friction force (ITTC line), Rf line:', Rf)
```

```
95        #print('FUNC -- estimate friction force (hull rough), Rf rough:', Rf_rough)
96
97        return Rf, Rf_rough
98
99
100
101    def estimate_total_friction_force(self, *, hull_correction_method,
       hull_roughness_meter) -> float:
102        Cf = self.estimate_total_friction_coeff(hull_correction_method=
       hull_correction_method, hull_roughness_meter=hull_roughness_meter)
103        Cf_k = self.estimate_total_friction_coeff_form_factor(
       hull_correction_method=hull_correction_method, hull_roughness_meter=
       hull_roughness_meter)
104
105        Rf = 0.5 * self.SEAWATER_DENSITY * pow(self.ship_speed_kn*0.5144, 2.0) *
       self.wetted_surface * Cf
106        Rf_k = 0.5 * self.SEAWATER_DENSITY * pow(self.ship_speed_kn*0.5144, 2.0) *
       self.wetted_surface * Cf_k
107        #print('FUNC -- estimate friction force (Cf+delta cf), Rf:', Rf)
108        #print('FUNC -- estimate friction force (total cf + k), Rf tot:', Rf_k)
109
110        return Rf, Rf_k
```

B.3 Hollenbach class and Hollenbach resistance coefficients

```
1      import numpy as np
2
3  # calculates the resicdual resistance R_R using Hollenbach's method for a given
       vessel
4  import empirical_models as emp
5  class Hollenbach():
6
7      G = 9.81
8      WATER_DENSITY = 1025.0
9
10     def __init__(
11             self,
12             *,
13             draught,
14             breadth,
15             length_pp,
16             length_wl,
17             draught_AP,
18             draught_FP,
19             block_coeff,
20             diameter_propeller,
21             amount_rudder,
22             amount_brackets,
23             amount_boss,
24             amount_thrusters,
25             hollenbach_coefficients_a,
26             hollenbach_coefficients_b,
27             #hollenbach_coefficients_c,
28             hollenbach_coefficients_d,
29             hollenbach_coefficients_e,
30             hollenbach_coefficients_f,
31             hollenbach_coefficients_g,
32             hollenbach_coefficients_h,
33             min_calc,
34             mean_calc
35     ) -> None:
36         self.draught = draught
37         self.breadth = breadth
38         self.length_pp   = length_pp
39         self.length_wl   = length_wl
40         self.draught_AP  = draught_AP
41         self.draught_FP  = draught_FP
42         self.block_coeff = block_coeff
43         self.diameter_propeller = diameter_propeller
```

```python
        self.amount_rudder       = amount_rudder
        self.amount_brackets     = amount_brackets
        self.amount_boss         = amount_boss
        self.amount_thrusters    = amount_thrusters
        self.hollenbach_coefficients_a = hollenbach_coefficients_a
        self.hollenbach_coefficients_b = hollenbach_coefficients_b
        #self.hollenbach_coefficients_c = hollenbach_coefficients_c
        self.hollenbach_coefficients_d = hollenbach_coefficients_d
        self.hollenbach_coefficients_e = hollenbach_coefficients_e
        self.hollenbach_coefficients_f = hollenbach_coefficients_f
        self.hollenbach_coefficients_g = hollenbach_coefficients_g
        self.hollenbach_coefficients_h = hollenbach_coefficients_h
        self.min_calc = min_calc
        self.mean_calc = mean_calc

    def min_froude_number(self) -> float:
        f1 = self.hollenbach_coefficients_f[0]
        f2 = self.hollenbach_coefficients_f[1]
        f3 = self.hollenbach_coefficients_f[2]

        value1 = f1
        value2 = f1 + (f2*(f3 - self.block_coeff))
        return min(value1, value2)

    def max_froude_number(self) -> float:
        g1 = self.hollenbach_coefficients_g[0]
        g2 = self.hollenbach_coefficients_g[1]
        g3 = self.hollenbach_coefficients_g[2]
        return (g1 + g2*self.block_coeff + g3*pow(self.block_coeff, 2))


    def chech_validity(self, *, vessel_speed_kn) -> bool:
        Fn = self.froude_number(vessel_speed_kn=vessel_speed_kn)
        FnMin = self.min_froude_number()
        FnMax = self.max_froude_number()

        if (FnMin < Fn < FnMax):
            print('Froude number is within limits, Hollenbach method is valid')
            return True
        else:
            print('
-------------------------------------------------------------')
            print('WARNING:')
            print('Froude number is outside limits, Hollenbach method is NOT valid'
)
            print('
-------------------------------------------------------------')
            return False

    def check_dimensions(self) -> None:
        '''
        if self.mean_calc == True:
            if 4.71 > (self.length_pp/self.breadth) or (self.length_pp/self.breadth
) > 7.11:
                print(f'ERROR: L_pp/B = {self.length_pp/self.breadth}, NOT within
    expected range')
            if 1.99 > (self.breadth/self.draught) or (self.breadth/self.draught) >
    4.00:
                print(f'ERROR: B/T = {self.breadth/self.draught}, NOT within
    expected range')
            if 1.00 > (self.length_wl/self.length_pp) or (self.length_wl/self.
length_pp) > 1.05:
                print(f'ERROR: L_os/L_pp = {self.length_wl/self.length_pp}, NOT
within expected range')
            if 1.00 > (self.length_wl/self.length_pp) or (self.length_wl/self.
length_pp) > 1.06:
                print(f'ERROR: L_wl/L_pp = {self.length_wl/self.length_pp}, NOT
within expected range')
            if 0.43 > (self.diameter_propeller/self.draught) or (self.
diameter_propeller/self.draught) > 0.84:
                print(f'ERROR: D/T = {self.diameter_propeller/self.draught}, NOT
within expected range')
        '''
```

```python
104
105            '''
106            print('-----------------------------------------------------')
107            print(f' L_pp/B    = {self.length_pp/self.breadth}')
108            print(f' B/T       = {self.breadth/self.draught}')
109            print(f' L_os/L_pp = {self.length_wl/self.length_pp}')
110            print(f' L_wl/L_pp = {self.length_wl/self.length_pp}')
111            print(f' D/T       = {self.diameter_propeller/self.draught}')
112            print('-----------------------------------------------------')
113            '''
114            return
115
116
117
118    def froude_number(self, *, vessel_speed_kn) -> float:
119        # assuming L_os = 102% x L_wl
120        L_os = self.length_wl*1.02
121        L_pp = self.length_pp
122
123        if (L_os/L_pp) < 1.0:
124            L_fn = L_os
125        elif (1.0 < (L_os/L_pp) < 1.1):
126            L_fn = L_pp + (2.0/3.0)*(L_os - L_pp)
127        elif 1.1 < (L_os/L_pp):
128            L_fn = 1.0667*L_pp
129        else:
130            print(f'ERROR: L_os/L_pp = {L_os/L_pp} is not within expected range')
131            print('L_fn = L_os')
132            L_fn = L_os
133
134        Fn = (vessel_speed_kn*0.5144) / np.sqrt((self.G*L_fn))
135        return Fn
136
137
138    def kL(self) -> float:
139        e1 = self.hollenbach_coefficients_e[0]
140        e2 = self.hollenbach_coefficients_e[1]
141
142        L_pp = self.length_pp
143        return (e1*pow(L_pp, e2))
144
145
146    def froude_number_critial(self) -> float:
147        d1 = self.hollenbach_coefficients_d[0]
148        d2 = self.hollenbach_coefficients_d[1]
149        d3 = self.hollenbach_coefficients_d[2]
150
151        Cb = self.block_coeff
152
153        FnKrit = d1 + (d2*Cb) + (d3*pow(Cb, 2))
154        return FnKrit
155
156
157    def residual_resistance_coeff_froude_critical(self, *, vessel_speed_kn) ->
       float:
158
159        Fn = self.froude_number(vessel_speed_kn=vessel_speed_kn)
160        FnKrit = self.froude_number_critial()
161        if FnKrit == 0.0:
162            return 1.0
163
164        if self.mean_calc==True:
165            c1 = Fn/FnKrit
166        elif self.min_calc==True:
167            c1 = 0.0
168
169        value1 = 1.0
170        value2 = pow(Fn/FnKrit, c1)
171
172
173        return max(value1, value2)
174
175
```

```
176
177     def residual_resistance_coeff_standard(self, *, vessel_speed_kn) -> float:
178         b11 = self.hollenbach_coefficients_b[0]
179         b12 = self.hollenbach_coefficients_b[1]
180         b13 = self.hollenbach_coefficients_b[2]
181
182         b21 = self.hollenbach_coefficients_b[3]
183         b22 = self.hollenbach_coefficients_b[4]
184         b23 = self.hollenbach_coefficients_b[5]
185
186         b31 = self.hollenbach_coefficients_b[6]
187         b32 = self.hollenbach_coefficients_b[7]
188         b33 = self.hollenbach_coefficients_b[8]
189
190         Fn = self.froude_number(vessel_speed_kn=vessel_speed_kn)
191         Cb = self.block_coeff
192
193         val1 = b11
194         val2 = b12*Fn
195         val3 = b13*pow(Fn, 2)
196         val4 = Cb*(b21 + (b22*Fn) + (b23*Fn*Fn))
197         val5 = pow(Cb, 2)*(b31 + (b32*Fn) + (b33*pow(Fn, 2)))
198
199
200         CR_std = b11 + (b12*Fn) + (b13*pow(Fn, 2)) + Cb*(b21 + (b22*Fn) + (b23*pow(
    Fn, 2))) + pow(Cb, 2)*(b31 + (b32*Fn) + (b33*pow(Fn, 2)))
201         return CR_std/10.0
202
203
204
205     def residual_resistance_coeff_hollenbach(self, vessel_speed_kn) -> float:
206         self.chech_validity(vessel_speed_kn=vessel_speed_kn)
207         self.check_dimensions()
208         # assuming L_os = 102% x L_wl
209         L_os = self.length_wl * 1.02
210
211         a1 = self.hollenbach_coefficients_a[0]
212         a2 = self.hollenbach_coefficients_a[1]
213         a3 = self.hollenbach_coefficients_a[2]
214         a4 = self.hollenbach_coefficients_a[3]
215         a5 = self.hollenbach_coefficients_a[4]
216         a6 = self.hollenbach_coefficients_a[5]
217         a7 = self.hollenbach_coefficients_a[6]
218         a8 = self.hollenbach_coefficients_a[7]
219         a9 = self.hollenbach_coefficients_a[8]
220         a10 = self.hollenbach_coefficients_a[9]
221
222         Cr_std  = self.residual_resistance_coeff_standard(vessel_speed_kn=
    vessel_speed_kn)
223         Cr_crit = self.residual_resistance_coeff_froude_critical(vessel_speed_kn=
    vessel_speed_kn)
224         kL = self.kL()
225
226         frac1 = (self.draught/self.breadth)
227         frac2 = (self.breadth/self.length_pp)
228         frac3 = (L_os/self.length_wl)
229         frac4 = (self.length_wl/self.length_pp)
230         frac5 = (1 + ((self.draught_AP - self.draught_FP)/self.length_pp))
231         frac6 = (self.diameter_propeller/self.draught)
232         frac7 = (1.0 + self.amount_rudder)
233         frac8 = (1.0 + self.amount_brackets)
234         frac9 = (1.0 + self.amount_boss)
235         frac10 = (1.0 + self.amount_thrusters)
236
237         Cr_Hollenbach = Cr_std * Cr_crit * kL * pow(frac1, a1) * pow(frac2, a2) *
    pow(frac3, a3) * pow(frac4, a4) * pow(frac5, a5) * pow(frac6, a6) * pow(frac7,
    a7) * pow(frac8, a8) * pow(frac9, a9) * pow(frac10, a10)
238         #print('FUNC residual_resistance_coeff: ', 'Cr_Hollenbach', Cr_Hollenbach)
239         return Cr_Hollenbach
240
241     def maximum_resistance(self, *, mean_total_resistance) -> float:
242         h1 = self.hollenbach_coefficients_h[0]
243         return (h1*mean_total_resistance)
```

```
244
245    def residual_resistance_force(self, *, vessel_speed_kn) -> float:
246        s = emp.wetted_surface_transocean(length_oa=self.length_wl, breadth=self.
       breadth, draught=self.draught)
247        Cr = self.residual_resistance_coeff(vessel_speed_kn=vessel_speed_kn)
248        R  = 0.5 * self.WATER_DENSITY * pow(vessel_speed_kn*0.5144, 2) * self.
       breadth * self.draught * Cr
249        R = R/s # NB: dividing on wetted surface!!
250
251
252        return R    # [N]
```

B.3.1   Hollenbach resistance coefficients for single-screw, design draft

```
1
2  def mean_resistance_coeffs_a() -> float:
3      # mean, single-screw, design draft
4      a1 = -0.3382
5      a2 = 0.8086
6      a3 = -6.0258
7      a4 = -3.5632
8      a5 = 9.4405
9      a6 = 0.0146
10     a7 = 0.0
11     a8 = 0.0
12     a9 = 0.0
13     a10 = 0.0
14
15     a_coeffs = [a1, a2, a3, a4, a5, a6, a7, a8, a9, a10]
16     return a_coeffs
17
18
19 def mean_resistance_coeffs_b(*, block_coeff) -> float:
20     # mean, single-screw, design draft
21     b11 = -0.57424
22     b12 = 13.3893
23     b13 = 90.5960
24
25     b21 = 4.6614
26     b22 = -39.721
27     b23 = -351.483
28
29     b31 = -1.14215
30     b32 = -12.3296
31     b33 = 459.254
32     if 0.49 <= block_coeff < 0.60:
33         b11 = -0.57424 - 25.0*pow((0.6 - block_coeff), 2.0)
34     elif block_coeff < 0.49:
35         b11 = -0.87674
36     b_coeffs = [b11, b12, b13, b21, b22, b23, b31, b32, b33]
37     return b_coeffs
38
39
40 def mean_resistance_coeffs_c(*, froude_number, froude_number_critical) -> float:
41     c1 = froude_number/froude_number_critical
42     return c1
43
44
45 def mean_resistance_coeffs_d() -> float:
46     # mean, single-screw, design draft
47     d1 = 0.854
48     d2 = -1.228
49     d3 = 0.497
50
51     d_coeffs = [d1, d2, d3]
52     return d_coeffs
53
54
55 def mean_resistance_coeffs_e() -> float:
56     # mean, single-screw, design draft
```

```python
    e1 = 2.1701
    e2 = -0.1602

    e_coeffs = [e1, e2]
    return e_coeffs

def mean_resistance_coeffs_f() -> float:
    # mean, single-screw, design draft
    f1 = 0.17
    f2 = 0.20
    f3 = 0.60

    f_coeffs = [f1, f2, f3]
    return f_coeffs

def mean_resistance_coeffs_g() -> float:
    # mean, single-screw, design draft
    g1 = 0.642
    g2 = -0.635
    g3 = 0.150

    g_coeffs = [g1, g2, g3]
    return g_coeffs

def mean_resistance_coeffs_h() -> float:
    # mean, single-screw, design draft
    h1 = 1.204
    return h1




def min_resistance_coeffs_a() -> float:
    # minimum, single-screw, design draft
    a1 = -0.3382
    a2 = 0.8086
    a3 = -6.0258
    a4 = -3.5632
    a5 = 0.0
    a6 = 0.0
    a7 = 0.0
    a8 = 0.0
    a9 = 0.0
    a10 = 0.0
    return [a1, a2, a3, a4, a5, a6, a7, a8, a9, a10]

def min_resistance_coeffs_b() -> float:
    # minimum, single-screw, design draft
    b11 = -0.91424
    b12 = 13.3893
    b13 = 90.5960

    b21 = 4.6614
    b22 = -39.721
    b23 = -351.483

    b31 = -1.14215
    b32 = -12.3296
    b33 = 459.254
    return [b11, b12, b13, b21, b22, b23, b31, b32, b33]


def min_resistance_coeffs_c() -> float:
    return 0.0


def min_resistance_coeffs_d() -> float:
    # minimum, single-screw, design draft
    d1 = 0.0
    d2 = 0.0
    d3 = 0.0
    return [d1, d2, d3]
```

```
130
131  def min_resistance_coeffs_e() -> float:
132      # minimum, single-screw, design draft
133      e1 = 0.0
134      e2 = 0.0
135      return [e1, e2]
136
137  def min_resistance_coeffs_f() -> float:
138      # minimum, single-screw, design draft
139      f1 = 0.14
140      f2 = 0.0
141      f3 = 0.0
142      return [f1, f2, f3]
143
144  def min_resistance_coeffs_g() -> float:
145      # minimum, single-screw, design draft
146      g1 = 0.952
147      g2 = -1.406
148      g3 = 0.643
149      return [g1, g2, g3]
150
151  def min_resistance_coeffs_h() -> float:
152      # minimum, single-screw, design draft
153      h1 = 0.0
154      return h1
```

B.4 Empirical equations

```
1      ''' DESCRIPTION OF FILE
2  Empirical models needed for estimation of the resistance.
3
4  form_factor:                          k   Form factor
5                                            Using MARINTEK's formula from p.11 '
      Motstand og Propulsjon' S.S
6  prismatic_coefficient:                Cp  Prismatic coefficient
7  wetted_surface_marin_grunnlag:        S   Wetted surface
8                                            Estimated with method from Marin Grunnlag (
      p.10-21)
9  wetted_surface_transocean:            S   Wetted surface
10                                            Estimated with method from Transocean
11                                            https://www.transocean-coatings.com/static/
      downloadcenter/2022/12/estimation-of-surface-areas-09dec2022.pdf
12  reynolds_number:                      Re  Reynolds number
13  frictional_resistance_coeff:          Cf  Friction resistance coefficient
14                                            Equation from p.16 'Motstand og Propulsjon'
       (S.S), with form factor correction (1+k)
15  '''
16  import numpy as np
17  import matplotlib.pyplot as plt
18
19
20
21  def form_factor(*, length_wl, breadth, draught, block_coeff) -> float:
22      phi = (block_coeff / length_wl) * np.sqrt(2.0 * draught * breadth)
23      k = 0.6*phi + 75.0*pow(phi, 3.0)
24      k = 0.6*phi + 145.0*pow(phi, 3.5)
25
26      return k
27
28
29  def form_factor2(*, length_pp, breadth, draught, prism_coeff) -> float:
30      # T_design
31      prism_coeff = 0.5569
32      L_cb = 50.50
33      C_stern = 0.0
34      C14 = 1 + 0.11*C_stern
35      Lr = length_pp * (1 - prism_coeff + 0.06*prism_coeff*(L_cb/(4*prism_coeff-1)))
36      k = 0.93 - 1.0 + 0.487118 # not finished
37
```

```python
38
39 def volume_displacement(*, block_coeff, length_wl, breadth, draught) -> float:
40     return (block_coeff * length_wl * breadth * draught)
41
42 def draught(*, block_coeff, length_wl, breadth, volume_displacement) -> float:
43     return (volume_displacement / (block_coeff * length_wl * breadth))
44
45
46 def midspan_area(*, midspan_coeff, breadth, draught) -> float:
47     return (midspan_coeff * breadth * draught)
48
49
50 def prismatic_coefficient(*, length_wl, breadth, draught, block_coeff) -> float:
51     # estimating the prismatic coefficient
52     # assuming the midspan-area to be 90% of the rectangle of size B*T - from my
       head
53     # adjusting assumption to be more accurate (tuning to fit CFD report) -->
       midspan-area 65% of the rectangle of size B*T
54     # 0.65 is an assumption made for the value of the midspan-coeff, C_M
55     #
       ---------------------------------------------------------------------------------
56     # Based on hull-shape factor, C_H, and Transocean experience for estimating
       wetted surface
57     # ferry has v-shaped hull --> Am  is typically 70% of the rectangle of size B*T
58     # cargo ship has u-shaped hull --> Am is typically 90% of the rectangle of size
        B*T
59     #
       ---------------------------------------------------------------------------------
60     displacement = volume_displacement(block_coeff=block_coeff, length_wl=length_wl
       , breadth=breadth, draught=draught)
61     midspan_coeff = 0.677 # from CFD report
62     midspan_coeff = 0.70  # typical value for v-shaped hull, Transocean Coatings
       (2022) https://www.scribd.com/document/613853232/estimation-of-surface-areas-09
       dec2022
63     midspan_coeff = 0.90  # typical value for u-shaped hull, Transocean Coatings
       (2022) https://www.scribd.com/document/613853232/estimation-of-surface-areas-09
       dec2022
64     cp = displacement / (midspan_coeff * breadth * draught * length_wl)
65     return cp, displacement
66
67
68 def wetted_surface_marin_grunnlag(*, length_wl, breadth, draught, block_coeff,
       prism_coeff) -> float:
69     # NB!! this method is actually Taylor (1893)!!
70     # this function assumes 3.5 < B/T < 4.0 for choice of 'k'
71     #if breadth/draught < 3.5 or breadth/draught > 4.0:
72         #print('WARNING: Estimation with this method may be unaccurate! B/T < 3.5
       or B/T > 4.0!')
73     displacement = block_coeff * length_wl * breadth * draught
74
75     midspan_coeff = block_coeff / prism_coeff
76     #print('cm', midspan_coeff)
77
78     # constant 'k' from figure 10-13 (page 10-21 marin grunnlag)
79     if 0.95 < midspan_coeff < 1.0:
80         k = 2.65
81     else:
82         k = 2.62
83
84     S = k * np.sqrt(displacement * length_wl)
85     return S
86
87
88 def wetted_surface_taylor(*, length_wl, breadth, draught, block_coeff, prism_coeff)
        -> float:
89     # this function assumes 1.0 < B/T < 5.0 for choice of 'k'
90     #if breadth/draught < 1.0 or breadth/draught > 5.0:
91         #print('WARNING: Estimation with this method may be unaccurate! B/T < 1.0
       or B/T > 5.0!')
92     displacement = block_coeff * length_wl * breadth * draught
93
```

```python
94      midspan_coeff = block_coeff / prism_coeff
95      #print('cm', midspan_coeff)
96

97
98      # values from figure from Taylor 1983 (Fig. 5.1 in thesis)
99      if 0.65 < midspan_coeff < 0.70:
100         if breadth/draught < 4.5:
101             k = 2.71
102         else:
103             k = 2.76
104     elif midspan_coeff > 0.70:
105         k = (2.64 + 2.67)/2.0
106

107
108     midspan_coeff = 0.68 # from @ T_max, CFD
109     midspan_coeff = 0.677 # @ T_design, CFD
110     k = 2.71 # NB HARDCODING
111     k = 2.8  # NB!! HARDCODING
112

113     S = k * np.sqrt(displacement * length_wl)
114     #print('FUNC wetted-surface-taylor, k', k, 'S', S, 'Cb', block_coeff)
115     return S
116

117
118 def wetted_surface_transocean(*, length_oa, breadth, draught) -> float:
119     # https://www.transocean-coatings.com/static/downloadcenter/2022/12/estimation-
        of-surface-areas-09dec2022.pdf
120     # Ch = hull shape factor
121     #     = 0.9 for large tankers
122     #     = 0.85 for bulk carriers
123     #     = 0.7 - 0.75 for smaller dry/general cargo vessels
124     Ch = 0.75
125     S = (2*draught) + (breadth * length_oa * Ch)
126     return S
127

128
129 def froude_number(*, ship_speed_kn, length_wl) -> float:
130     G = 9.81 # [m/s^2]
131     return ((ship_speed_kn * 0.5144) / np.sqrt(G * length_wl))
132

133
134 def reynolds_number(*, ship_speed_kn, lenght_wl, water_viscosity) -> float:
135     return ((ship_speed_kn * 0.5144 * lenght_wl) / water_viscosity)
136

137
138 def frictional_resistance_coeff(*, reynolds_number) -> float:
139     # cf without (1+k) calcs the friction along a line on a flat plate
140     cf = 0.075 / ((np.log10(reynolds_number) - 2.0)**2)
141     return cf
142

143

144
145 def frictional_resistance_force(*, ship_speed_kn, water_density, wetted_surface,
        form_factor, friction_resistance_coeff, hull_roughness_correction) -> float:
146     # the form factor takes the shape of the hull into account as cf = friction
        along a flat plate
147     CF = (1 + form_factor)*(friction_resistance_coeff + hull_roughness_correction)
148     return (0.5 * water_density * pow((ship_speed_kn * 0.5144), 2) * wetted_surface
         * CF)
149

150

151
152 def hull_roughness_correction_MARINTEK(*, hull_roughness_meter, ship_speed_kn,
        frictional_resistance_coeff) -> float:
153     # equation from page 13 'Motstand og Propulsjon' Sverre Steen
154     # NB!!! this equation also has to be corrected with the form coefficient (1+k)
155     #       this equation is uses the hull roughness in micro meter and not meter.
156     #       the hull roughness is therefore multiplied by 10^6
157     Cf = frictional_resistance_coeff
158     delta_Cf = ((110.0 * pow((hull_roughness_meter*pow(10, 6)*ship_speed_kn*0.5144)
        , 0.21) - 403.0) * pow(Cf, 2))
159     return delta_Cf
160
```

```
161
162
163 def hull_roughness_correction_ITTC(*, hull_roughness_meter, ship_length,
        reynolds_number) -> float:
164     # equation from https://ittc.info/media/3485/volume2_1powering_perf_pred.pdf
165     delta_cf = 0.044 * (pow((hull_roughness_meter/ship_length), 0.333) - 10*pow(
        reynolds_number, -0.333)) + 0.000125
166     return delta_cf
167
168
169
170 def dwt_displacement_ratio(*, length_oa) -> float:
171     # dwt-displacement ratio == dwt-displacement coefficient, Cd
172     # source 'Springer - Ship Design'
173     lengths = np.linspace(85.0, 120.0, 100)
174     dwt_displacement_ratios = np.linspace(0.16, 0.33, 100)
175     Cd = np.interp(length_oa, lengths, dwt_displacement_ratios)
176     return Cd
177
178
179 def prismatic_coeff(*, volume_displacement, midspan_area, length_pp) -> float:
180     return (volume_displacement / (midspan_area * length_pp))
```

B.5 Calculation of power generated by the Flettner rotors

```
1 import matplotlib.pyplot as plt
2 import wind_data_plot as wdp
3 import pandas as pd
4 import numpy as np
5 import seaborn as sns
6
7
8 from flettner_rotor3 import FlettnerRotor, RotorForces
9 from apparent_wind_data_2 import apparent_wind_dataframe,
      apparent_wind_dataframe_TWS
10 from vessel2 import Vessel2
11 from total_resistance_2_T_design import total_resistance_CFD
12 from resistance_components_2 import resistance_components
13 from propeller_equations import get_speed_power_prediction_data_Tdesign
14
15
16 # 1. FLETTNER ROTOR, 24x4 m --> R = 2.0 m
17 fr = FlettnerRotor(rotor_radius=2.0, rotor_height=24.0, max_rotor_rpm=225.0)
18 fr_area = fr.rotor_area(rotor_radius=fr.rotor_radius, rotor_height=fr.rotor_height)
19 fr_forces_ing = RotorForces(rotor_area=fr_area, rotor_height=fr.rotor_height,
      max_rotor_rpm=fr.max_rotor_rpm)
20
21 el_motor_nominal_power = 80E+03      # [W], (80 kW)
22
23
24 # 2. VESSEL
25 munken = Vessel2(length_oa=107.53, length_pp=101.0, length_wl=104.12, breadth
      =15.24, draught=3.41, max_height=26.34, height_deck_FR=13.0, block_coeff=0.36,
      midspan_coeff=0.68, prismatic_coeff=0.53, diameter_propeller=2.3)
26 vs_kn = 12.0
27 #vs_kn = 10.0
28 heading_FlRo = np.radians(334.7)
29 heading_RoFl = np.radians(154.7)
30
31 hull_roughness = 180E-06 # [m]
32
33 # crossing time Flakk-Rorvik and Rorvik-Flakk = 25 minutes
34 cross_time = 25.0/60.0   # [hours]
35
36 # 3. IMPORT WIND DATA
37 from read_wind_data import wind_data_munk, wind_data_ing
38
39 # 4. APPARENT WIND DATA - ship heading = Flakk -> Rorvik:
40 aw_munk_rad, aw_munk_deg = apparent_wind_dataframe(rotor_height=fr.rotor_height,
```

```python
          vessel_deck_height=munken.height_deck_FR, ship_speed_kn=vs_kn, ship_heading_rad
          =heading_FlRo, wind_data=wind_data_munk)
41 aw_ing_rad, aw_ing_deg    = apparent_wind_dataframe(rotor_height=fr.rotor_height,
          vessel_deck_height=munken.height_deck_FR, ship_speed_kn=vs_kn, ship_heading_rad
          =heading_FlRo, wind_data=wind_data_ing)


# 5. CALCULATE SAIL THRUST
# 5.1 Ingdalen
thrust_ing = []
RPM_ing    = []
SR_ing     = []
Rt_ing     = []

P_fr_ing   = []
P_prop_ing = []
P_req_ing  = []

P_cons_Ing = []
P_cons_prop_Ing = []
P_contribution_Ing = []

aws_ing = aw_ing_rad.iloc[:, 0]
awa_ing_rad = aw_ing_rad.iloc[:, 1]
awa_ing_deg = aw_ing_deg.iloc[:, 1]

for i in range(len(aw_ing_rad)):
    opt_RPM, sr = fr_forces_ing.calc_optimal_rotor_rpm(apparent_wind_speed=aws_ing[
    i], apparent_wind_angle_rad=awa_ing_rad[i])
    thrust = fr_forces_ing.calc_thrust_force(apparent_wind_speed=aws_ing[i],
    spin_ratio=sr, apparent_wind_angle_rad=awa_ing_rad[i])

    Rf_k, Rf_line, Rf_rough, Ra, Rr_mean, Rt = resistance_components(
    vessel_speed_kn=vs_kn, apparent_wind_speed=aws_ing[i], apparent_wind_angle_rad=
    awa_ing_rad[i], H_meter=hull_roughness, cb=munken.block_coeff)

    powerAft, powerFore, powerTotal = get_speed_power_prediction_data_Tdesign(
    vessel_speed_kn=vs_kn)
    rt_cfd = total_resistance_CFD(vessel_speed_kn=vs_kn,
    power_delivered_propeller_watt=powerTotal, propulsive_efficiency=0.7)

    rt_cfd = rt_cfd + Ra
    # thrust from 2 flettner rotors:
    thrust = thrust * 2.0


    while (thrust > rt_cfd):
        #print(f'Thrust = {thrust} is greater than resistance = {rt}, awa = {
    awa_ing_deg[i]} deg, aws = {aws_ing[i]} m/s, sr = {sr}, RPM = {opt_RPM}')
        opt_RPM = opt_RPM - 1.0
        sr = fr_forces_ing.calc_spin_ratio(apparent_wind_speed=aws_ing[i],
    rotor_rpm=opt_RPM)
        thrust = fr_forces_ing.calc_thrust_force(apparent_wind_speed=aws_ing[i],
    spin_ratio=sr, apparent_wind_angle_rad=awa_ing_rad[i])
        thrust = thrust*2.0
        #print(f'awa = {awa_ing_deg[i]} deg, aws = {aws_ing[i]} m/s, New thrust = {
    thrust}, new RPM = {opt_RPM}, new SR = {sr}')


    p_fr = thrust * vs_kn*0.5144 - 2*el_motor_nominal_power

    # power produced by rotor is less than power consumed by motor, rotor is
    stopped.
    if p_fr <= 0.0:
        opt_RPM = 0.0
        sr = fr_forces_ing.calc_spin_ratio(apparent_wind_speed=aws_ing[i],
    rotor_rpm=opt_RPM)
        thrust = fr_forces_ing.calc_thrust_force(apparent_wind_speed=aws_ing[i],
    spin_ratio=sr, apparent_wind_angle_rad=awa_ing_rad[i])
        thrust = thrust*2.0
        p_fr   = thrust * vs_kn*0.5144
```

```python
 97      p_pr = rt_cfd * vs_kn*0.5144
 98      p_req = p_pr - p_fr
 99
100      power_consumption      = p_req * cross_time
101      power_consumption_prop = p_pr  * cross_time
102
103      power_contribution     = p_fr * cross_time
104
105      thrust_ing.append(thrust/1000.0)      # [kN]
106      Rt_ing.append(rt_cfd/1000.0)          # [kN]
107
108      P_fr_ing.append(p_fr/1000.0)          # [kW]
109      P_prop_ing.append(p_pr/1000.0)        # [kW]
110      P_req_ing.append(p_req/1000.0)        # [kW]
111
112      P_cons_Ing.append(power_consumption/1000.0)          # [kWh]
113      P_cons_prop_Ing.append(power_consumption_prop/1000.0) # [kWh]
114
115      P_contribution_Ing.append(power_contribution/1000.0)  # [kWh]
116
117      RPM_ing.append(opt_RPM)
118      SR_ing.append(sr)
119
120
121  # 5.2 Munkholmen
122  thrust_munk = []
123  RPM_munk    = []
124  SR_munk     = []
125
126  Rt_munk     = []
127
128  P_fr_munk   = []
129  P_prop_munk = []
130  P_req_munk  = []
131
132  P_cons_Munk = []
133  P_cons_prop_Munk = []
134
135  P_contribution_Munk = []
136
137  aws_munk = aw_munk_rad.iloc[:, 0]
138  awa_munk_rad = aw_munk_rad.iloc[:, 1]
139  awa_munk_deg = aw_munk_deg.iloc[:, 1]
140
141  for i in range(len(aw_munk_rad)):
142      opt_RPM, sr = fr_forces_ing.calc_optimal_rotor_rpm(apparent_wind_speed=aws_munk
         [i], apparent_wind_angle_rad=awa_munk_rad[i])
143      thrust = fr_forces_ing.calc_thrust_force(apparent_wind_speed=aw_munk_rad.iloc[i
         , 0], spin_ratio=sr, apparent_wind_angle_rad=awa_munk_rad[i])
144
145      Rf_k, Rf_line, Rf_rough, Ra, Rr_mean, Rt = resistance_components(
         vessel_speed_kn=vs_kn, apparent_wind_speed=aws_munk[i], apparent_wind_angle_rad
         =awa_munk_rad[i], H_meter=hull_roughness, cb=munken.block_coeff)
146
147      powerAft, powerFore, powerTotal = get_speed_power_prediction_data_Tdesign(
         vessel_speed_kn=vs_kn)
148      rt_cfd = total_resistance_CFD(vessel_speed_kn=vs_kn,
         power_delivered_propeller_watt=powerTotal, propulsive_efficiency=0.7)
149
150      rt_cfd = rt_cfd + Ra
151      # thrust for 2 flettner rotors:
152
153      thrust = thrust * 2.0
154      while (thrust > rt_cfd):
155          #print(f'awa = {awa_munk_deg[i]} deg, aws = {aws_munk[i]} m/s: Thrust = {
             thrust} is greater than resistance = {rt},  sr = {sr}, RPM = {opt_RPM}')
156          opt_RPM = opt_RPM - 1.0
157          sr = fr_forces_ing.calc_spin_ratio(apparent_wind_speed=aws_munk[i],
             rotor_rpm=opt_RPM)
158          thrust = fr_forces_ing.calc_thrust_force(apparent_wind_speed=aws_munk[i],
             spin_ratio=sr, apparent_wind_angle_rad=awa_munk_rad[i])
159          thrust = thrust*2.0
160          print(f'awa = {awa_munk_deg[i]} deg, aws = {aws_munk[i]} m/s: New thrust =
```

```
      {thrust}, new RPM = {opt_RPM}, new SR = {sr}')
161         if opt_RPM < 0.0:
162             opt_RPM = 0.0
163             sr = fr_forces_ing.calc_spin_ratio(apparent_wind_speed=aws_munk[i],
      rotor_rpm=opt_RPM)
164             thrust = fr_forces_ing.calc_thrust_force(apparent_wind_speed=aws_munk[i
      ], spin_ratio=sr, apparent_wind_angle_rad=awa_munk_rad[i])
165             thrust = thrust*2.0
166             #print(f'awa = {awa_munk_deg[i]} deg, aws = {aws_munk[i]} m/s: New
      thrust = {thrust}, new RPM = {opt_RPM}, new SR = {sr}')
167             break
168
169     p_fr = thrust * vs_kn*0.5144 - 2*el_motor_nominal_power
170
171     # power produced by rotor is less than power consumed by motor, rotor is
      stopped. (net power = p_fr less than zero equals that the power produced by the
       rotor is less than power consumed by driving the rotor)
172     if p_fr <= 0.0:
173         opt_RPM = 0.0
174         sr = fr_forces_ing.calc_spin_ratio(apparent_wind_speed=aws_munk[i],
      rotor_rpm=opt_RPM)
175         thrust = fr_forces_ing.calc_thrust_force(apparent_wind_speed=aws_munk[i],
      spin_ratio=sr, apparent_wind_angle_rad=awa_munk_rad[i])
176         thrust = thrust*2.0
177         p_fr = thrust * vs_kn*0.5144
178
179     p_pr = rt_cfd * vs_kn*0.5144    # propeller power without FRs
180     p_req = p_pr - p_fr             # propeller power with FRs
181
182     power_consumption = p_req * cross_time              # required propeller power
      consumption with FRs per crossing
183     power_consumption_prop = p_pr * cross_time          # required propeller power
      consumtion without FRs per crossing
184     power_contribution = p_fr * cross_time              # power generated by FRs
      per crossing
185
186
187     thrust_munk.append(thrust/1000.0)        # [kN]
188     Rt_munk.append(rt_cfd/1000.0)           # [kN]
189
190
191     # calculated power generated and consumed for all wind conditions and times
192     P_fr_munk.append(p_fr/1000.0)           # [kW]
193     P_prop_munk.append(p_pr/1000.0)         # [kW]
194     P_req_munk.append(p_req/1000.0)         # [kW]
195
196     # power generated and consumed PER CROSSING
197     P_contribution_Munk.append(power_contribution/1000.0)        # [kWh], power
      generated by FRs per crossing
198     P_cons_Munk.append(power_consumption/1000.0)                 # [kWh], required
      propeller power with FRs per crossing
199     P_cons_prop_Munk.append(power_consumption_prop/1000.0)       # [kWh], required
      propeller power without FRs per crossing
200
201     RPM_munk.append(opt_RPM)
202     SR_munk.append(sr)
```

B.6 Blendermann air resistance

```
1  """ VARIABLE DEFINITIONS:
2
3  Estimating the air resistance of the ferry using
4  -> Blendermann's parameter identification  of wind loads on ships
5
6  Estimation is based on the semi-empirical loading functions proposed in the paper:
7  "Parameter identification of wind loads on ships"
8  https://www.sciencedirect.com/science/article/pii/0167610594900671
9
10 A_L   = lateral plane area (side arealet til fergen)
```

```python
11  A_F   = frontal projected area (front-arealet til fergen)
12  s_L   = lateral-plane centroid (tyngdepunkt) with respect to main section
13  s_H   = lateral-plane centroid (tyngdepunkt) above the waterline
14  L_oa  = length overall
15  H_M   = mean height
16        -> H_M = A_L/L_oa
17  eps   = apparent wind angle (eps = 0 in bow wind)
18  CX_AF = longitudinal force coefficient
19        -> Eq.(1)
20  CY    = side force coefficient
21        -> Eq.(1)
22  CN    = yawning-moment coeff
23        -> Eq.(2)
24  CK    = rolling-moment coeff
25        -> Eq.(2)
26  q     = dynamic pressure of apparent wind
27        -> q = rho/s*u^2
28  rho   = air density
29  u     = wind speed
30  CD_l  = longitudinal resistance coeff (long. = x-dir)
31        -> CD(eps = 0, pi)
32
33  # ----------------- values from Table 1
        ---------------------------------------------
34  CD_t    = lateral resistance coeff (lat. = y-dir)
35        -> CD(eps = pi/2) - value from Table 1
36  CD_l_Af = longitudinal resistance coeff with respect to the frontal projected area
        of the vessel
37        -> CD_l_Af = CD_l * (A_L/A_F) - value from Table 1
38  delta   = cross force parameter
39        -> value between 0 and 1 - value from Table 1
40  kappa   = rolling-moment factor
41        -> kappa = z_F / s_H - value from Table 1
42  #
        -------------------------------------------------------------------------------------

43
44  x_F   = yawning-moment lever arm
45        -> x_F = L_oa * (CN/CY)
46  z_F   = rolling-moment lever arm
47        -> z_F = H_M * (CK/CY)
48  """
49
50  import numpy as np
51  import matplotlib.pyplot as plt
52
53
54
55  class BlendermannSuperstructure():
56      # Estimating the air resistance of the different types of vessels using
57      # Blendermann's parameter identification  of wind loads on ships
58
59      AIR_DENSITY = 1.225  # [kg/m^3], air density
60
61      def __init__(
62              self,
63              *,
64              lateral_area,   # vessel's lateral area
65              frontal_area,   # vessel's frontal area
66              cd_l_af_0,      # vessel specific constant from Table 1, CD_l_Af for
        eps = 0
67              cd_l_af_pi ,    # vessel specific constant from Table 1, CD_l_Af for
        eps = pi
68              cd_t,           # vessel specific constant from Table 1
69              delta,          # vessel specific constant from Table 1
70              kappa           # vessel specific constant from Table 1
71      ) -> None:
72          self.lateral_area = lateral_area
73          self.frontal_area = frontal_area
74          self.cd_l_af_0   = cd_l_af_0
75          self.cd_l_af_pi  = cd_l_af_pi
76          self.cd_t        = cd_t
77          self.delta       = delta
```

```python
78          self.kappa        = kappa
79
80      def longitudinal_force_coeff(self, *, apparent_wind_angle_rad) -> float:
81          # eq.(13) in Blendermann paper
82          # function to calculate the longitudinal force coefficient with respect to
    frontal area, CX_AF
83          eps_rad = apparent_wind_angle_rad
84
85          AF    = self.frontal_area
86          AL    = self.lateral_area
87          CD_t  = self.cd_t
88          delta = self.delta
89
90          # linear interpolation of CD_l_Af for esp = 0 and eps = pi from Table 1 for
     a given app_wind_angle
91          #eps_values     = [0, np.pi]
92          #CD_l_AF_values = [self.cd_l_af_0, self.cd_l_af_pi]
93          #CD_l_AF        = np.interp(eps_rad, eps_values, CD_l_AF_values)
94
95          dCD     = (self.cd_l_af_pi - self.cd_l_af_0) / np.pi
96          CD_l_AF = self.cd_l_af_0 + dCD * eps_rad
97
98          CD_l    = CD_l_AF * (AF/AL)
99
100         sin2        = pow(np.sin(2.0*eps_rad), 2.0)
101         denominator = 1.0 - (delta/2.0)*(1.0 - (CD_l/CD_t))*sin2
102
103         CX_AF = - CD_l_AF * np.cos(eps_rad) / denominator
104
105         return CX_AF # [-]
106
107
108     def longitudinal_force(self, *, apparent_wind_angle_rad, apparent_wind_speed)
    -> float:
109         # eq. (1) in Blendermann paper
110         eps_rad = apparent_wind_angle_rad
111         CX_AF = self.longitudinal_force_coeff(apparent_wind_angle_rad=eps_rad)
112         rho = self.AIR_DENSITY
113         u = apparent_wind_speed
114         AF = self.frontal_area
115
116         q = 0.5 * rho * u*u
117
118         X = CX_AF * q * AF
119         return X  # [N]
120
121         # NB! X is a drag force. It is positive when pointing in negative x-
    direction.
122         # Must be multiplied with -1 to get a positive value for comparison
123         #return -1.0*X  # [N]
124
125     def side_force_coeff(self, *, apparent_wind_angle_rad) -> float:
126         eps_rad = apparent_wind_angle_rad
127
128         AF    = self.frontal_area
129         AL    = self.lateral_area
130         CD_t  = self.cd_t
131         delta = self.delta
132
133         dCD     = (self.cd_l_af_pi - self.cd_l_af_0) / np.pi
134         CD_l_AF = self.cd_l_af_0 + dCD * eps_rad
135
136         CD_l    = CD_l_AF * (AF/AL)
137
138         sin2        = pow(np.sin(2.0*eps_rad), 2.0)
139         denominator = 1.0 - (delta/2.0)*(1.0 - (CD_l/CD_t))*sin2
140
141         CY = (CD_t * np.sin(eps_rad)) / denominator
142
143         return CY
144
145     def side_force(self, *, apparent_wind_angle_rad, apparent_wind_speed) -> float:
146         # eq. (1) in Blendermann paper
```

```
147            eps_rad = apparent_wind_angle_rad
148            CY = self.side_force_coeff(apparent_wind_angle_rad=eps_rad)
149            rho = self.AIR_DENSITY
150            u = apparent_wind_speed
151            AL = self.lateral_area
152
153            q = rho * 0.5 * u*u
154
155            Y = CY * q * AL
156
157            return Y
```

B.7 Resistance calculation

```
1       """
2  Resistance components:
3  * Frictional resistance
4  * Air resistance
5  * Wave making resistance/Residual resistance
6  """
7
8  """ NB!! Comments to Hollenbach (mean, single-screw, design draft):
9  - min Cb = 0.60
10 - max Cb = 0.83
11 - munken Cb  = 0.358 < 0.60
12
13 - min L/B = 4.71
14 - max L/B = 7.11
15 - munken L/B = 6.62 < 7.11
16
17 - min B/T = 1.99
18 - max B/T = 4.00
19 - munken B/T = 4.47 > 4.00
20
21 --> since B/T > 4.00 and L/B is on the upper range of the valid range, upper value
        of Cb is used (Cb = 0.82) for a 'valid' Hollenbach calculation
22 """
23
24 from vessel2 import Vessel2, AreaVessel2
25
26 from class_frictional_resistance_3 import FrictionalResistance
27 import empirical_models as emp
28
29 from class_air_resistance import BlendermannSuperstructure
30
31 from hollenbach import Hollenbach
32 import hollenbach_resistance_coeffs_T_design as hrc
33
34 import numpy as np
35 # CFD: Lpp = 101.0 m, B = 15.24, D = 3.41
36 # PP and Marine Traffic: Lpp = 103.0 m, Lwl = 105.0, B = 16.0, D = 4.0
37 # MAN: Lpp = 0.97xLwl -> Lwl = Lpp/0.97 = 104.12 m
38
39 def froude_number(*, ship_speed_kn, length_wl) -> float:
40     G = 9.81 # [m/s^2]
41     return ((ship_speed_kn * 0.5144) / np.sqrt(G * length_wl))
42
43
44 def reynold_empirical(*, froude_number) -> float:
45     G = 9.81 # [m/s^2]
46     rnm = (6.0*froude_number*np.sqrt(6.0*G))/(1.1395)
47     return (rnm * 1E+06)
48
49 def Cfm(reynolds_number) -> float:
50     return (0.075 / ((np.log10(reynolds_number) - 2.0)**2.0))
51
52
53 def resistance_components(*, vessel_speed_kn, apparent_wind_speed,
        apparent_wind_angle_rad, H_meter, cb) -> float:
```

```
54
55     # Vessel:
56     # design draft: 3.41 m
57     munken = Vessel2(length_oa=107.53, length_pp=101.0, length_wl=104.12, breadth
       =15.24, draught=3.41, max_height=26.34, height_deck_FR=13.0, block_coeff=0.36,
       midspan_coeff=0.68, prismatic_coeff=0.56, diameter_propeller=2.3)
58     # max draft: 3.81 m
59     #munken = Vessel2(length_oa=107.53, length_pp=101.0, length_wl=104.12, breadth
       =15.89, draught=3.81, max_height=26.34, height_deck_FR=13.0, block_coeff=0.38,
       midspan_coeff=0.68, prismatic_coeff=0.56, diameter_propeller=2.3)
60
61     volume_disp = munken.volume_displacement()
62
63     area_vessel = AreaVessel2(length_oa=munken.length_oa, breadth=munken.breadth,
       height_wl_1deck=9.25, height_hotel=17.09, length_hotel=42.73)
64     area_fro = area_vessel.frontal_area_ferry()
65     area_lat = area_vessel.lateral_area_ferry()
66
67
68     # 1. Frictional resistance, Marin Grunnlag:
69     #S  = emp.wetted_surface_marin_grunnlag(length_wl=munken.length_wl, breadth=
       munken.breadth, draught=munken.draught, block_coeff=munken.block_coeff,
       prism_coeff=munken.prismatic_coeff)
70     S = emp.wetted_surface_taylor(length_wl=munken.length_wl, breadth=munken.
       breadth, draught=munken.draught, block_coeff=munken.block_coeff, prism_coeff=
       munken.prismatic_coeff)
71
72     munken_FR = FrictionalResistance(ship_speed_kn=vessel_speed_kn, length_wl=
       munken.length_wl, draught=munken.draught, breadth=munken.breadth, block_coeff=
       munken.block_coeff, prismatic_coeff=munken.prismatic_coeff, wetted_surface=S)
73
74     Rf_line, Rf_rough = munken_FR.estimate_friction_force_components(
       hull_correction_method='ITTC', hull_roughness_meter=H_meter) # ITTC line and
       hull roughness
75     Rf_line_rough, Rf_k = munken_FR.estimate_total_friction_force(
       hull_correction_method='ITTC', hull_roughness_meter=H_meter) # with and wo form
        factor
76
77     #cf, deltacf = munken_FR.estimate_friction_coeff(hull_correction_method='ITTC',
        hull_roughness_meter=H_meter)
78     #Rf, Rf_rough = munken_FR.estimate_friction_force(hull_correction_method='ITTC
       ', hull_correction_meter=H_meter)
79     #Rf_form = munken_FR.estimate_friction_force_form(hull_correction_method='ITTC
       ', hull_correction_meter=H_meter)
80
81     #print('debu resistance components, vs: ', vessel_speed_kn)
82     #print('resistance coeff', cf)
83     #print('Resistance Friction', Rf/1000.0, 'kN')
84
85     # 2. Air Resistance, Blendermann:
86     aws = apparent_wind_speed
87     awa = apparent_wind_angle_rad
88
89     ferry     = BlendermannSuperstructure(lateral_area=2125.80, frontal_area=325.3,
        cd_l_af_0=0.45, cd_l_af_pi=0.50, cd_t=0.90, delta=0.80, kappa=1.1) # ferry
       values from paper
90     munken_AR = BlendermannSuperstructure(lateral_area=area_lat, frontal_area=
       area_fro, cd_l_af_0=ferry.cd_l_af_0, cd_l_af_pi=ferry.cd_l_af_pi, cd_t=ferry.
       cd_t, delta=ferry.delta, kappa=ferry.kappa)
91     # X (Ra) is a drag force, and has a negative value when acting in the positive
       x-direction, as it is defined as positive in the negative x-direction
92     Ra = munken_AR.longitudinal_force(apparent_wind_angle_rad=awa,
       apparent_wind_speed=aws)
93     #print('Resistance Air:', Ra/1000.0, 'kN')
94
95
96     # 3. Wave Making Resistance/Residual Resistance, Hollenbach:
97     a_coeffs_mean = hrc.mean_resistance_coeffs_a()
98     b_coeffs_mean = hrc.mean_resistance_coeffs_b(block_coeff=cb)
99     d_coeffs_mean = hrc.mean_resistance_coeffs_d()
100    e_coeffs_mean = hrc.mean_resistance_coeffs_e()
101    f_coeffs_mean = hrc.mean_resistance_coeffs_f()
102    g_coeffs_mean = hrc.mean_resistance_coeffs_g()
```

```python
103     h_coeffs_mean = hrc.mean_resistance_coeffs_h()
104
105     WMR_mean = Hollenbach(draught=munken.draught, breadth=munken.breadth, length_pp
        =munken.length_pp, length_wl=munken.length_wl, draught_AP=munken.draught,
        draught_FP=munken.draught,
106                         block_coeff=cb, diameter_propeller=2.30, amount_rudder
        =1.0, amount_brackets=1.0, amount_boss=1.0, amount_thrusters=1.0,
        hollenbach_coefficients_a=a_coeffs_mean,
107                         hollenbach_coefficients_b=b_coeffs_mean,
        hollenbach_coefficients_d=d_coeffs_mean, hollenbach_coefficients_e=
        e_coeffs_mean,
108                         hollenbach_coefficients_f=f_coeffs_mean,
        hollenbach_coefficients_g=g_coeffs_mean, hollenbach_coefficients_h=
        h_coeffs_mean, min_calc=False, mean_calc=True)
109     Cr_mean = WMR_mean.residual_resistance_coeff(vessel_speed_kn=vessel_speed_kn)
110
111     '''
112     form_factor = emp.form_factor(length_wl=munken.length_wl, breadth=munken.
        breadth, draught=munken.draught, block_coeff=munken.block_coeff)
113     Fn = froude_number(ship_speed_kn=vessel_speed_kn, length_wl=munken.length_wl)
114     rnm = reynold_empirical(froude_number=Fn)
115
116     Cr = Cr_mean * (munken.breadth * munken.draught/S) - form_factor*Cfm(
        reynolds_number=rnm)
117     Rr_mean  = 0.5 * Hollenbach.WATER_DENSITY * pow(vessel_speed_kn*0.5144, 2) *
        munken.breadth * munken.draught * Cr
118     '''
119     Rr_mean = WMR_mean.residual_resistance_force(vessel_speed_kn=vessel_speed_kn,
        prism_coeff=munken.prismatic_coeff)
120     #print('Resistance Residual:', Rr_mean/1000.0, 'kN')
121
122     # debug:
123     #print('------ debug vs:', vessel_speed_kn, ' [kn], CB:', cb, ' --------')
124     #print('Frictional resistance:', Rf/1000.0, 'kN')
125     #print('Air resistance:', Ra/1000.0, 'kN')
126     #print('Residual resistance:', Rr_mean/1000.0, 'kN')
127     #print('--------------------------------------------------')
128
129     # TOTAL:
130     Rt = (Rf_k - Ra + Rr_mean) # NB: subtracting air resistance, since it is
        defined as a negative force in the positive x-direction
131
132     #print('--------------')
133     #print('Rt [kN]:', Rt)
134     #print('debug resistance components:')
135     #print('S:', S)
136     #print('Cf', cf)
137     #print('Rf:', Rf)
138
139     return Rf_k, Rf_line, Rf_rough, -Ra, Rr_mean, Rt # frictional resistance, air
        resistance, residual resistance
140
141
142
143 def total_resistance_CFD(*, vessel_speed_kn, power_delivered_propeller_watt,
        propulsive_efficiency) -> float:
144     P_D = power_delivered_propeller_watt # [W]
145     eta_D = propulsive_efficiency        # [-]
146     Vs = vessel_speed_kn * 0.5144        # [m/s]
147     Rt = (eta_D * P_D) / Vs              # [N]
148     return Rt
149
150
151 #print('Volume_disp', volume_disp)
152 #print('S', S, 'S2', S2)
153 #print('k', emp.form_factor(length_wl=munken.length_wl, breadth=munken.breadth,
        draught=munken.draught, block_coeff=munken.block_coeff))
```

B.8 Vessel

```python
# Vessel2 == Vessel, only that Vessel2 includes coefficients from CFD analysis

class Vessel2():
    #CB = x           # block_coeff, CFD (@ T_max)
    #CM = x           # midspan_coeff, CFD (@ T_max)
    #CP = x           # prismatic_coeff, CFD (@ T_max)

    CB = 0.36          # block_coeff, CFD (@ T_design)
    CM = x            # midspan_coeff, CFD (@ T_design)
    CP = x            # prismatic_coeff, CFD (@ T_design)

    def __init__(
            self,
            *,
            length_oa,
            length_pp,
            length_wl,
            breadth,
            draught,
            max_height,
            height_deck_FR,
            block_coeff,
            midspan_coeff,
            prismatic_coeff,
            diameter_propeller
    ) -> None:
            self.length_oa = length_oa
            self.length_pp = length_pp
            self.length_wl = length_wl
            self.breadth = breadth
            self.draught = draught
            self.max_height      = max_height
            self.height_deck_FR  = height_deck_FR
            self.block_coeff     = block_coeff
            self.midspan_coeff   = midspan_coeff
            self.prismatic_coeff = prismatic_coeff
            self.diameter_propeller = diameter_propeller

    def volume_displacement(self) -> float:
        return (self.block_coeff * self.length_wl * self.breadth * self.draught)



class AreaVessel2():
    def __init__(
            self,
            *,
            length_oa,
            breadth,
            height_wl_1deck, # height from waterline to first deck
            height_hotel,    # height of 'overhuset'
            length_hotel     # lateral length of 'overhuset'
    ) -> None:
            self.length_oa = length_oa
            self.breadth   = breadth
            self.height_wl_1deck = height_wl_1deck
            self.heigh_hotel     = height_hotel
            self.length_hotel    = length_hotel

    # get_lateral_area_ferry
    def lateral_area_ferry(self) -> float:
        # assuming area of ferry to be divided into a rectangle (hull) + triangle (
    hotel/overhuset)
        rect_L = self.length_oa
        rect_H = self.height_wl_1deck

        tri_L = self.length_hotel
        tri_H = self.heigh_hotel

        area_rect = rect_L * rect_H
        area_tri  = (1.0/2.0) * tri_L * tri_H
```

```python
73          #return (area_rect + area_tri)
74          return area_rect
75
76

77     # get_frontal_area_ferry
78     def frontal_area_ferry(self) -> float:
79          # assuming area of ferry to be divided into a rectangle (hull) + triangle
       (hotel/overhuset)
80          rect_L = self.breadth
81          rect_H = self.height_wl_1deck
82
83          tri_L = self.breadth
84          tri_H = self.heigh_hotel
85
86          area_rect = rect_L * rect_H
87          area_tri  = (1.0/2.0) * tri_L * tri_H
88
89          #return (area_rect + area_tri)
90          return area_rect
```

Appendix C

Modelling data

C.1 Hollenbach coefficients

	'mean' single-screw design draft	'mean' single-screw ballast draft	'mean' twin-screw	'minimum' single-screw design draft	'minimum' twin-screw
$a1$	-0.3382	-0.7139	-0.2748	-0.3382	-0.2748
$a2$	0.8086	0.2558	0.5747	0.8086	0.5747
$a3$	-6.0258	-1.1606	-6.7610	-6.0258	-6.7610
$a4$	-3.5632	0.4534	-4.3834	-3.5632	-4.3834
$a5$	9.4405	11.222	8.8158	0	0
$a6$	0.0146	0.4524	-0.1418	0	0
$a7$	0	0	-0.1258	0	0
$a8$	0	0	0.0481	0	0
$a9$	0	0	0.1699	0	0
$a10$	0	0	0.0728	0	0
b_{11}	-0.57424	-1.50162	-5.34750	-0.91424	3.27279
b_{12}	13.3893	12.9678	55.6532	13.3893	-44.1138
b_{13}	90.5960	-36.7985	-114.905	90.5960	171.692
b_{21}	4.6614	5.55536	19.2714	4.6614	-11.5012
b_{22}	-39.721	-45.8815	-192.388	-39.721	166.559
b_{23}	-351.483	121.820	388.333	-351.483	-644.456
b_{31}	-1.14215	-4.33571	-14.3571	-1.14215	12.4626
b_{32}	-12.3296	36.0782	142.738	-12.3296	-179.505
b_{33}	459.254	-85.3741	-254.762	459.254	680.921
c_1	$F_n/F_{n,\mathrm{krit}}$	$10C_B(F_n/F_{n,\mathrm{krit}}-1)$	$F_n/F_{n,\mathrm{krit}}$	0	0
d_1	0.854	0.032	0.897	0	0
d_2	-1.228	0.803	-1.457	0	0
d_3	0.497	-0.739	0.767	0	0
e_1	2.1701	1.9994	1.8319	0	0
e_2	-0.1602	-0.1446	-0.1237	0	0
f_1	0.17	0.15	0.16	0.17	0.14
f_2	0.20	0.10	0.24	0.20	0
f_3	0.60	0.50	0.60	0.60	0
g_1	0.642	0.42	0.50	0.614	0.952
g_2	-0.635	-0.20	0.66	-0.717	-1.406
g_3	0.150	0	0.50	0.261	0.643
h_1	1.204	1.194	1.206		
ship length L [m]	42.0...205.0	50.2...224.8	30.6...206.8	42.0...205.0	30.6...206.8
$L/\nabla^{1/3}$	4.49...6.01	5.45...7.05	4.41...7.27	4.49...6.01	4.41...7.27
C_B	0.60...0.83	0.56...0.79	0.51...0.78	0.60...0.83	0.51...0.78
L/B	4.71...7.11	4.95...6.62	3.96...7.13	4.71...7.11	3.96...7.13
B/T	1.99...4.00	2.97...6.12	2.31...6.11	1.99...4.00	2.31...6.11
L_{os}/L_{wl}	1.00...1.05	1.00...1.05	1.00...1.05	1.00...1.05	1.00...1.05
L_{wl}/L	1.00...1.06	0.95...1.00	1.00...1.07	1.00...1.06	1.00...1.07
D_P/T	0.43...0.84	0.66...1.09	0.50...0.86	0.43...0.84	0.50...0.86

Figure C.1: Coefficients for Hollenbach's method from Hollenbach (1998).